Catalysis to control targeted response in supramolecular systems

Piergentili, I.

DOI
10.4233/uuid:9b2da8bc-6b1b-4860-aeef-656809c86494

Publication date
2023

Document Version
Final published version

Citation (APA)
Piergentili, I. (2023). *Catalysis to control targeted response in supramolecular systems*. [Dissertation (TU Delft), Delft University of Technology]. https://doi.org/10.4233/uuid:9b2da8bc-6b1b-4860-aeef-656809c86494

Catalysis to control targeted response in supramolecular systems

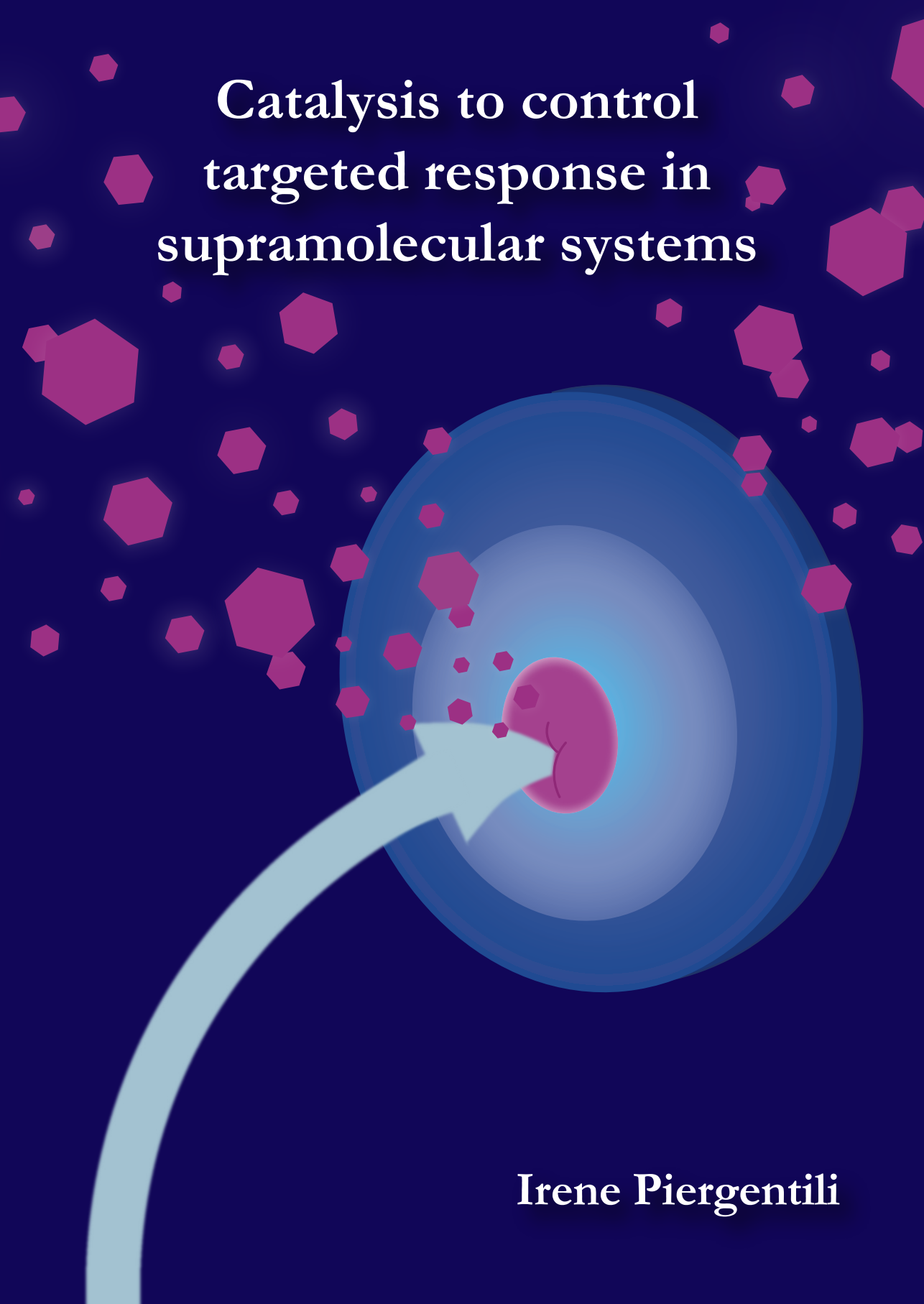

Irene Piergentili

Catalysis to control targeted response in supramolecular systems

Dissertation

for the purpose of obtaining the degree of doctor
at Delft University of Technology
by the authority of the Rector Magnificus, Prof.dr.ir. T.H.J.J. van der Hagen,
chair of the Board of Doctorates
to be defended publicly on

Thursday 28 September 2023 at 12.30 o'clock

by

Irene PIERGENTILI

Master of Science in Chemistry,
"Sapienza" University of Rome, Italy
Born in Rome, Italy

This dissertation has been approved by the promotors.

Composition of the doctoral committee:

Rector Magnificus	Chairperson
Dr. R. Eelkema	Delft University of Technology, promotor
Prof. dr. J.H.van Esch	Delft University of Technology, promotor
Independent members:	
Prof. dr. ir. T. Vermonden	Utrecht University
Dr. R. E. Kieltyka	Leiden University
Prof. dr. M. A. van der Veen	Delft University of Technology
Prof. dr. S.J. Picken	Delft University of Technology
Prof. dr. F.C. Grozema	Delft University of Technology, reserve member
Other members:	
Prof. F. Hollmann	Delft University of Technology

The research described in this dissertation was carried out in the Advanced Soft Matter (ASM) group, Department of Chemical Engineering, Faculty of Applied Science, Delft University of Technology. The research was funded by Netherlands Organisation for Scientific Research and the National Natural Science Foundation of China (NWO-NSFC joint project) and TU Delft.

ISBN: 978-94-6384-466-6
Printed by: Ipskamp printing, Enschede
Cover design: Irene Piergentili

Table of contents

Chapter 1

Introduction

Science originates from the need of humans to understand the natural phenomena that surround their daily life. Over the centuries, with the increasing knowledge of nature and its laws, the scientific community interest shifted towards learning how to control and exploit natural mechanisms for new discoveries. In particular, the fascination for biological systems brought enormous advances, not only in the medical field, but also in chemistry, physics and material science. In fact, many synthetic processes and artificial materials were developed taking inspiration from nature.[1,2]

Living cells are able to respond and adapt to environmental change through complex networks of chemical reactions. These processes also control cell organization, through assembly and disassembly of proteins, nucleic acids and cell membranes. Enzymes play a central role in metabolic pathways, using elemental compounds to synthesize biological precursors and products, then assembling these in biomacromolecules and biological structures. In addition, enzymes are responsible for breaking down these materials into the small molecules that fuel metabolic processes. Chemical and physical signals can trigger enzymatic activity to regulate chemical transformations necessary for cellular functions. Bond formation and bond breaking at the molecular level translate into conformational changes of the enzyme active sites to adjust the metabolic flux in response to changes in the environment.[3]

These synergic mechanisms, achieved in millions of years of evolution, inspired concepts such as organocatalysis, host-guest and supramolecular chemistry. More recently, characteristic cellular functions such as signal transduction, self-healing, self-replication and feedback control, were implemented in polymeric

and supramolecular systems.[4,5] Realizing materials with cell-like behavior can have a great impact for applications in drug delivery,[6,7] tissue engineering,[8] sensing[9] and even electronics and soft robotics.[10]

1.1 Stimuli responsive materials

Living systems adapt to their surrounding via signalling cascades controlled by specific receptors in the cellular membrane, which respond to temperature, light, sugars, steroids, peptides, gaseous molecules and other biomarkers.[11] In the last decades, many research groups have been focused on reproducing living cells adaptive behavior in man-made systems with the aim to obtain "smart" materials that sense and react to their environment.[12] These materials are usually based on polymers containing functionalities that are reactive towards one or more stimuli, producing a morphological change at the material level. Beside the well-studied pH and temperature stimuli, other exploited signals are mechanical stress, light, enzymes and redox changes.[13] Vesicles, micelles and hydrogels that respond to stimuli that are involved in cellular metabolism can have great potential as on-demand drug delivery and release systems. In particular, diseased cells have a different microenvironment than normal cells, expressing specific small molecules or enzymes, and changing pH, temperature and redox conditions.[14] Nanocarriers and platforms capable to respond to these internal stimuli can release drugs exclusively to the pathological areas, minimizing the side effects caused by the accumulation of often toxic drugs in healthy tissues.[15]

Hydrogen peroxide, superoxide anion, hydroxyl radical and singlet oxygen are collectively known as reactive oxygen species (ROS) and they are responsible for the regulation of redox processes in cellular metabolic pathways (Figure 1).[16] Hydrogen peroxide is the most common ROS and its concentration is usually below 0.7 μM in healthy cells, these levels increase up to 100-fold in diseased and tumor cells.[17] Such drastic change makes these oxidative species an ideal

trigger for drug delivery systems to achieve effective drug release specifically in pathological tissues. ROS-responsive materials are usually based on boron, sulfur and selenium chemistry, which are susceptible to oxidation, leading to chemical transformations that cause a physical change in the structure.[18] Part of the research presented in this thesis has been devoted to contribute to the field of ROS-sensitive materials for targeted drug delivery and release systems.

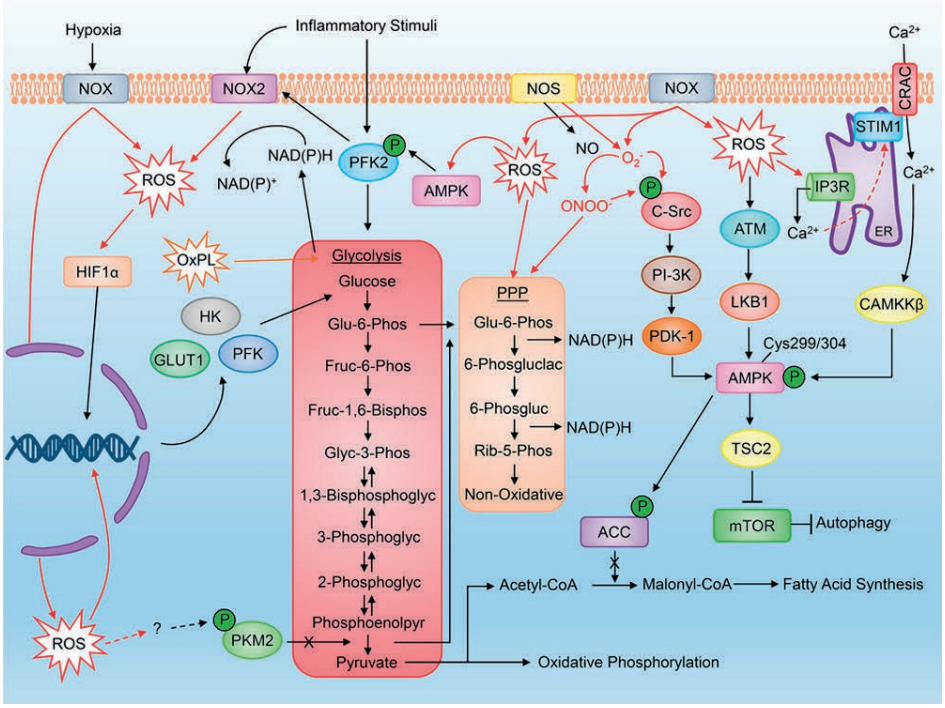

Figure 1. Reactive oxygen species (ROS) production and regulation of metabolic pathways in the cellular cytosol. Inflammatory stimuli associated with several pathologies and cancers activate this metabolism, altering the redox balance, reprinted from ref. 16.

1.2 Organocatalysis and enzyme catalysis in soft materials

Over the last half century organocatalysis has been developed into a powerful tool to accelerate and selectively control chemical reactions, culminating in the recognition of the development of asymmetric organocatalysis in the 2021 Nobel Prize in Chemistry.[19, 20] The use of small, purely organic molecules provides a simpler strategy compared to biocatalysis and an often less toxic one than transition metal catalysis. However, due to the solubility of reactants, reagents and products, only a limited number of organocatalyzed transformations have been successful in aqueous environment.[21] Beside performing organic synthesis in more environmental-friendly and safe solvent conditions, organocatalysis can be used to control reactions present in functional soft materials with a water-based matrix. In fact, polymeric micelles or supramolecular gels that self-assemble in aqueous conditions or crosslinked hydrogel that encapsulate large amounts of water are important platforms for several applications, especially in healthcare and nanomedicine. To date, there are few examples of the use of organocatalysis in water-based materials, using the catalyst as a tool to tune the formation and the mechanical properties of the material.[22,23] Most of these systems are based on hydrazone bond formation because its compatibility with water and the possibility of controlling bond formation and exchange by amine catalysts (e.g. aniline).[24,25] Organocatalyzed hydrazone chemistry have also been implemented in dynamic covalent networks for drug delivery purposes,[26, 27] but these developments concern more the preparation and the loading of the nanocarriers than the applicability in biological settings.

Despite their lower diffusive mobility and environmental resistance compared to organocatalysts, enzymes found larger application in material science.[28] This is not surprising if we think about the prominence that biocatalysis has in chemical and pharmaceutical industry nowadays.[29] The plethora of reactions that can be accelerated by enzymes explains the great appeal in realizing responsive

materials based on biochemical transformations. However, in most of these "smart" materials the enzyme plays mainly the role of signal, aiming to applications such as drug delivery, diagnostics and tissue regeneration that respond to these specific biomacromolecules.[30,31] Another approach is to use the enzyme as a nanoreactor encapsulated in the material to convert a first stimuli into a second one, which is either a much more reactive signal or the actual trigger designed for the responsive functionality.[32-34] Taking into account the excellent efficiency of enzymes and the easy use of organocatalysts, both types of catalysis offer incredible perspectives in making and controlling soft materials.

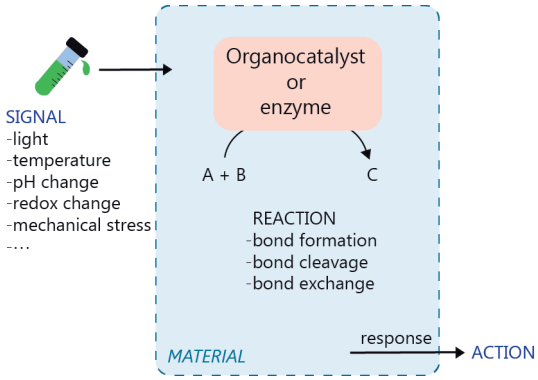

Figure 2. General concept of organocatalysis or enzyme catalysis embedded in signal-responsive materials.

1.3 Research aim

Materials with a pre-programmed response are the state of the art in material science and engineering. However, their implementation in the field of targeted biomedicine is still a challenge. Here, the development of responsive nanocarriers and platforms with life-like behavior can play an important role to reach clinical applications.

The aim of the research described in this thesis is to explore strategies to enable control over self-assembled materials that can interact with their environment. We investigated both natural (i.e. enzymes) and nature inspired (i.e. organocatalysts) catalysis to directly or indirectly activate chemical transformations that produce changes in the material properties. Eventually, these principles can be applied to realize drug delivery systems increasingly sensitive to biological cues.

1.4 Thesis outline

This thesis includes six chapters, covering theoretical background, experimental contributions and future perspectives of possible strategies to control soft materials for biomedical applications. After this first introductory chapter, chapter 2 describes how the introduction of a H_2O_2-responsive logic gate cascade mechanism in the hydrophobic domain of micelles allows hydrolytic degradation initiated by an oxidative stimulus. Chapter 3 builds on the second chapter by using organocatalysis to increase the disruption rate of micelles in presence of low concentrations of oxidant. Chapter 4 reports an oxidation-sensitive dipeptide able to form a supramolecular hydrogel in mildly acidic and neutral conditions. Here, the encapsulation of peroxyzymes in the gel matrix enables gel-sol transition with concentration of H_2O_2 almost 10 times lower than those required for uncatalyzed hydrogels. Chapter 5 introduces an organocatalysis-based method to form a supramolecular gel with potential virus inhibiting properties. Finally, the sixth chapter presents future perspectives in healthcare and drug delivery of the strategies developed in the previous chapters.

1.5 References

1. M. C. de la Torre and M. A. Sierra, *Angew. Chem. Int. Ed.*, 2004, **43**, 160-181.
2. T.-C. Tang, B. An, Y. Huang, S. Vasikaran, Y. Wang, X. Jiang, T. K. Lu and C. Zhong, *Nat. Rev. Mater.*, 2021, **6**, 332-350.
3. T. Traut, *Allosteric Regulatory Enzymes*, Springer US, Boston, 2008.
4. I. Insua and J. Montenegro, *Chem*, 2020, **6**, 1652-1682.
5. A. Sharko, D. Livitz, S. De Piccoli, K. J. M. Bishop and T. M. Hermans, *Chem. Rev.*, 2022, **122**, 11759-11777.
6. S. J. Buwalda, T. Vermonden and W. E. Hennink, *Biomacromolecules*, 2017, **18**, 316-330.
7. A. Zhang, K. Jung, A. Li, J. Liu and C. Boyer, *Prog. Polym. Sci.*, 2019, **99**, 101164.
8. H. W. Ooi, S. Hafeez, C. A. van Blitterswijk, L. Moroni and M. B. Baker, *Mater. Horiz.*, 2017, **4**, 1020-1040.
9. P. Scrimin and L. J. Prins, *Chem. Soc. Rev.*, 2011, **40**, 4488-4505.
10. L. Hu, Q. Zhang, X. Li and M. J. Serpe, *Mater. Horiz.*, 2019, **6**, 1774-1793.
11. D. L. Nelson, M. M. Cox and A. L. Lehninger, *Lehninger principles of biochemistry*, W.H. Freeman, New York, 2013.
12. A. Walther, *Adv. Mater.*, 2020, **32**, 1905111.
13. D. Roy, J. N. Cambre and B. S. Sumerlin, *Prog. Polym. Sci.*, 2010, **35**, 278-301.
14. V. P. Torchilin, in *Stimuli-responsive Drug Delivery Systems*, eds. A. Singh and M. M. Amiji, The Royal Society of Chemistry, London (UK), 2018, DOI: 10.1039/9781788013536-00001.
15. A. B. Cook and P. Decuzzi, *ACS Nano*, 2021, **15**, 2068-2098.

16. S. J. Forrester, D. S. Kikuchi, M. S. Hernandes, Q. Xu and K. K. Griendling, *Circ. Res.*, 2018, **122**, 877-902.

17. J. R. Stone, *Arch. Biochem. Biophys.*, 2004, **422**, 119-124.

18. C. Zhao, J. Chen, R. Zhong, D. S. Chen, J. Shi and J. Song, *Angew. Chem. Int. Ed.*, 2021, **60**, 9804-9827.

19. B. List, R. A. Lerner and C. F. Barbas, *J. Am. Chem. Soc.*, 2000, **122**, 2395-2396.

20. K. A. Ahrendt, C. J. Borths and D. W. C. MacMillan, *J. Am. Chem. Soc.*, 2000, **122**, 4243-4244.

21. M. P. van der Helm, B. Klemm and R. Eelkema, *Nat. Rev. Chem.*, 2019, **3**, 491-508.

22. F. Trausel, F. Versluis, C. Maity, J. M. Poolman, M. Lovrak, J. H. van Esch and R. Eelkema, *Acc. Chem. Res.*, 2016, **49**, 1440-1447.

23. M. P. van der Helm, C.-L. Wang, B. Fan, M. Macchione, E. Mendes and R. Eelkema, *Angew. Chem. Int. Ed.*, 2020, **59**, 20604-20611.

24. J. M. Poolman, J. Boekhoven, A. Besselink, A. G. L. Olive, J. H. van Esch and R. Eelkema, *Nat. Protoc.*, 2014, **9**, 977-988.

25. F. Trausel, C. Maity, J. M. Poolman, D. S. J. Kouwenberg, F. Versluis, J. H. van Esch and R. Eelkema, *Nat. Commun.*, 2017, **8**, 879.

26. R. P. Brinkhuis, F. de Graaf, M. B. Hansen, T. R. Visser, F. P. J. T. Rutjes and J. C. M. van Hest, *Polym. Chem.*, 2013, **4**, 1345-1350.

27. J. M. W. Chan, J. P. K. Tan, A. C. Engler, X. Ke, S. Gao, C. Yang, H. Sardon, Y. Y. Yang and J. L. Hedrick, *Macromolecules*, 2016, **49**, 2013-2021.

28. R. J. Williams, R. J. Mart and R. V. Ulijn, *Peptide Science*, 2010, **94**, 107-117.

29. E. L. Bell, W. Finnigan, S. P. France, A. P. Green, M. A. Hayes, L. J. Hepworth, S. L. Lovelock, H. Niikura, S. Osuna, E. Romero, K. S. Ryan, N. J. Turner and S. L. Flitsch, *Nat. Rev. Methods Primers*, 2021, **1**, 46.

30. R. V. Ulijn, *J. Mater. Chem.*, 2006, **16**, 2217-2225.

31. J. Mu, J. Lin, P. Huang and X. Chen, *Chem. Soc. Rev.*, 2018, **47**, 5554-5573.

32. B. L. Allen, J. D. Johnson and J. P. Walker, *ACS Nano*, 2011, **5**, 5263-5272.

33. A. Napoli, M. J. Boerakker, N. Tirelli, R. J. M. Nolte, N. A. J. M. Sommerdijk and J. A. Hubbell, *Langmuir*, 2004, **20**, 3487-3491.

34. M. Ikeda, T. Tanida, T. Yoshii, K. Kurotani, S. Onogi, K. Urayama and I. Hamachi, *Nat. Chem.*, 2014, **6**, 511-518.

Chapter 2

Thioanisole ester based logic gate cascade to control ROS-triggered micellar degradation

In certain tumor and diseased tissues, reactive oxygen species (ROS), such as H_2O_2, are produced in higher concentrations than in healthy cells. Drug delivery and release systems that respond selectively to the presence of ROS while maintaining their stability in "healthy" biological conditions, have great potential as on-site therapeutics. This study presents polymer micelles with 4-(methylthio)phenyl ester functionalities as a ROS-responsive reactivity switch. Oxidation of the thioether moieties triggers ester hydrolysis, exposing a hydrophilic carboxylate, leading to micellar disassembly. At 37 °C, the micelles fall apart on a timescale of days in the presence of 2.0 mM H_2O_2 and within hours at higher concentrations of H_2O_2 (60 – 600 mM). In the same time frame, the nanocarriers show no hydrolysis in oxidant-free physiological or mildly acidic conditions. This logic gate cascade behavior represents a step forward to realize drug delivery materials capable of selective response to a biomarker input.

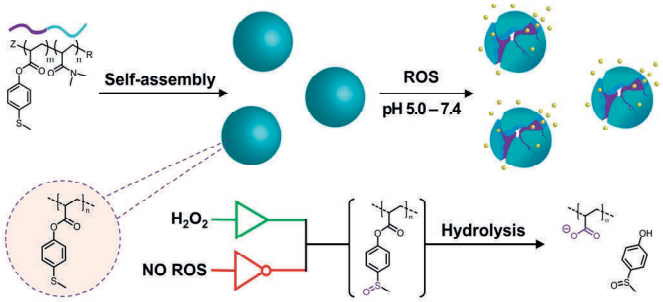

This chapter is published as:

I. Piergentili, P. R. Bouwmans, L. Reinalda, R. W. Lewis, B. Klemm, H. Liu, R. M. de Kruijff, A. G. Denkova and R. Eelkema, *Polym. Chem.*, 2022, **13**, 2383-2390.

2.1 Introduction

Smart materials that respond to external stimuli have emerged as an efficient platform to obtain targeted nanotherapeutics. Historically, amphiphilic block copolymers that spontaneously self-assemble in an aqueous environment are used as carriers to solubilize important, but poorly water soluble anti-inflammation and anti-cancer drugs in the bloodstream.[1] Still, these systems can suffer from nonspecific biodistribution and uncontrolled drug release, causing ineffective treatment or undesired side effects in the patient.[2] Therefore, the need for personalized therapeutics inspired researchers to study materials responsive to abnormal biological changes specifically caused by the diseased cells. Over the last decades, intelligent polymers have been developed to be responsive to several stimuli, like pH,[3] temperature,[4] and small molecule or biomacromolecular signals.[5]

Reactive oxygen species (ROS), such as hydrogen peroxide, regulate fundamental physiological processes in cells, including oxygen metabolism and signaling pathways.[6,7] However, in cancers and inflammatory,[6-8] cardiovascular[9] or neurodegenerative diseases,[10, 11] ROS are produced at a rate that natural antioxidant mechanisms, like enzymes (e.g. superoxide dismutase, catalase), cannot overcome.[12-14] Elevated intracellular H_2O_2 concentrations in diseased tissues are typically between 10 and 100 μM,[15,16] and can go up to 10 mM.[17] This change in the oxidative state of the cellular environment can be used as a trigger for selective local cargo release.[18-22] The pioneering work of Hubbell *et al.* in 2004 reported the first oxidation-sensitive polymeric vesicles for drug delivery purposes, degradable in 10 h in presence of 10 vol% H_2O_2.[23] Since then, the same group have applied that principle in several organic nanoparticles including micelles and vesicles.[24-26] Their responsiveness is based on the oxidation of hydrophobic thioethers to more hydrophilic sulfoxides and sulfones. Oxidation leads to more water-soluble polymeric materials, and therefore, less stable

micelles, allowing for the release of the incorporated cargo.[27] In most of these examples, exceedingly high concentrations of H_2O_2 (2.0-10 vol%) are required to disassemble the carrier within hours.

In contrast, boronate-based polymers have been extensively studied in the last 10 years because their sensitivity to H_2O_2 is in the sub-millimolar range.[28,29] Implementing boronic esters in a phenol-based polymeric backbone, Almutairi *et al.* reported in 2012 a cascade degradable nanoparticle sensitive to only 50 µM of H_2O_2.[30] This unique example of a nanocarrier sensitive to biologically relevant concentrations of H_2O_2 was, however, accompanied by poor control over cargo release (non-specific release and no significant effect over the release time scale when different concentrations of H_2O_2 are used). Various mechanisms of H_2O_2 triggered drug release based on the boronate cleavage methodology have been developed, including the degradation of polymeric backbones,[31] activation of prodrugs[32,33] and destruction of the amphiphilic block copolymer structure, usually by unmasking a more hydrophilic aliphatic acid (e.g. polyacrylic acid)[34-36]. In addition, boronic esters are also susceptible to hydrolysis and glycolysis at mildly acidic pH, forming diols and boronic acids.[37] The multi-responsiveness of boronates makes it a versatile moiety for biomedical materials, but can also pose a problem in terms of selectivity, causing off-target release. The need in the field of ROS-responsive materials resides currently in the design of systems with a cascade logic gate behavior, able to ensure specific and robust control over the performance of drug carriers.[38]

In this work, we present an oxidation-sensitive bond cleavage method that merges the responsivity of thioethers toward oxidation[39] with the tunability of ester hydrolysis through a reactivity switch. In the design of the system, we chose thioanisole type groups as our ROS-responsive moieties. First, we considered that the oxidation potential of aromatic thioethers is in the ideal range to undergo oxidation by H_2O_2.[20,40] The oxidation of aliphatic thioethers to sulfoxides or

sulfones has been extensively applied in polymeric materials to increase the hydrophilicity of the chain.[23, 41-44] An aromatic ring adjacent to the thioether group could enhance the nucleophilicity of the sulfur atom towards H_2O_2.[45] However, it is known that the oxidation of aromatic thioethers to the corresponding sulfoxide and sulfone is insufficient to achieve a desired solubility switch.[46] Instead, we decided to use sulfide oxidation to increase the hydrolytic lability of a nearby ester, thereby introducing a more effective solubility switch. Knowing that electron withdrawing groups on the aromatic ring of phenyl acetate esters increase the electrophilicity of the ester, our idea was to achieve a reactivity switch when the electron donating thioether is oxidized into a more electron withdrawing group, such as the corresponding sulfoxide or sulfone.[47-50] Therefore, H_2O_2-triggered thioether oxidation would activate the adjacent ester functionality towards hydrolysis.

We synthesized two amphiphilic block copolymers with different lengths of N,N-dimethylacrylamide as a hydrophilic block and 4-(methylthio) phenyl acrylates as a hydrophobic part of the chain. In aqueous environment, these macromolecules self-assemble into micelles with diameters between 30 and 50 nm, which is an appropriate size range for drug nanocarriers.[51] When H_2O_2 is added, the oxidation of sulfide to sulfoxide leads to the removal of 4-(methylsulfinyl)phenol **1** and 4-(methylsulfonyl)phenol **2** units through hydrolysis, turning the hydrophobic core into a more hydrophilic acrylate anion block and finally obtaining micellar disintegration (Figure 1). These ester-based polymeric micelles show great stability towards hydrolysis at neutral and acidic pH, demonstrating specific responsiveness towards oxidation by cascade logic behavior.

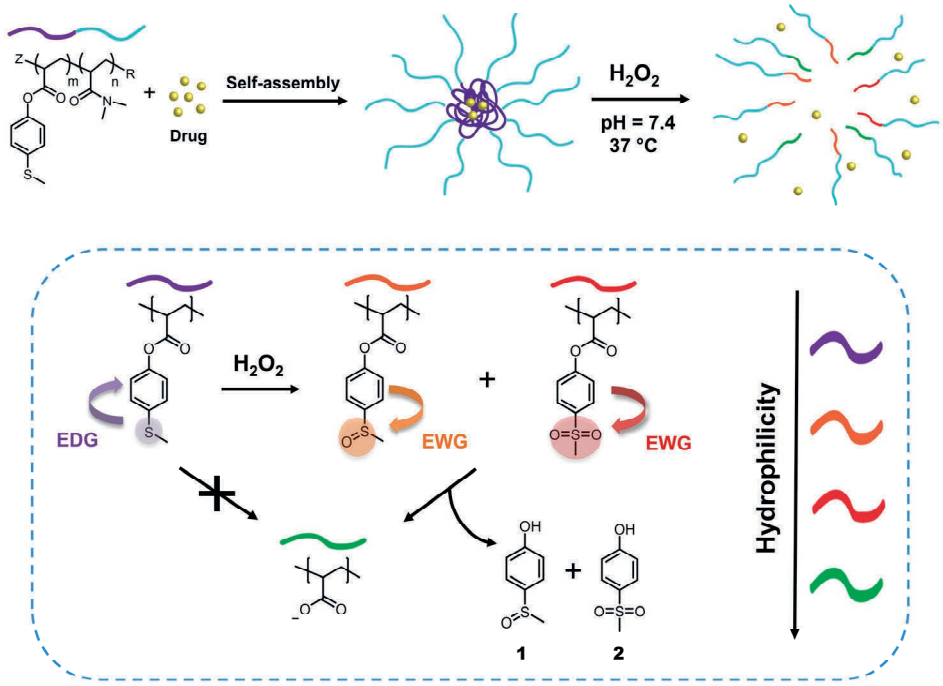

Figure 1. General concept: drug release from ROS-responsive micelles, triggered by the hydrolytic cleavage of ester bonds through switching from an electron donating (EDG) thioether group to electron withdrawing (EWG) sulfoxide and sulfone groups upon oxidation by H_2O_2.

2.2 Results and discussion

2.2.1 Synthesis and characterization of p(DMA$_n$-b-MTPA$_m$)

We synthesized the amphiphilic p(DMA$_n$-b-MTPA$_m$) block copolymers through sequential light-initiated RAFT polymerization (Scheme 1).[52] The choice of extending poly(N,N-dimethylacrylamide) macroDDMAT with 4-(methylthio) phenyl acrylate (MTPA) was due to the less successful chain extension when we attempted the opposite order. First, p(DMA) macroDDMAT was prepared using 2-(dodecylthiocarbonothioylthio)-2-methylpropionic acid (DDMAT) as the RAFT agent to obtain 130 and 102 DMA unit long polymeric chains (Table S1).

Then, the chain extension of hydrophilic macromolecular chain transfer agents p(DMA_{130}) macroDDMAT and p(DMA_{102}) macroDDMAT with MTPA (Table S2) produced PM16 and PM32. ^{1}H NMR spectra of the block copolymers in $CDCl_3$ (Figure S1) showed characteristic (broadened) signals of both DMA and MTPA, with the ratio of their integrations in line with what was expected from conversion data. In agreement with the ^{1}H NMR results, GPC traces (Figure S2) confirmed successful chain extension for both polymers through increase in molecular weight of a single peak. Thus, we obtained two block copolymers (Table 1), allowing investigation into the influence of varying hydrophobic block/hydrophilic block ratios on micelle formation and drug loading efficiency.[53]

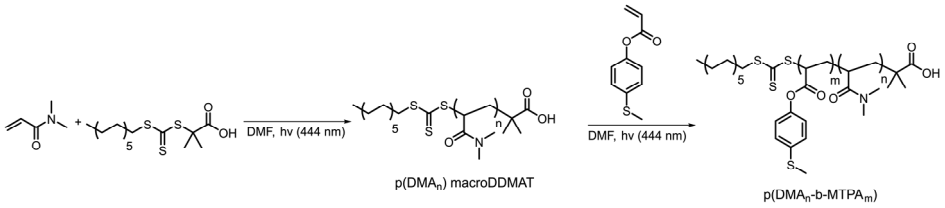

Scheme 1 Synthetic route for preparation of ROS-responsive p(DMA_n-b-$MTPA_m$) diblock copolymers via light initiated RAFT polymerization.

Table 1. Characterization of the block copolymers p(DMA_n-b-$MTPA_m$).

Code	Polymer	$M_{n,\,conv}$ (kDa)	$M_{n,\,GPC}$ (kDa)	Đ (M_w/M_n)
DMA130	p(DMA_{130})	13.2	13.0	1.13
DMA102	p(DMA_{102})	10.5	11.1	1.28
PM16	p(DMA_{130}-b-$MTPA_{16}$)	16.3	16.0	1.16
PM32	p(DMA_{102}-b-$MTPA_{32}$)	16.7	17.4	1.27

2.2.2 Preparation and characterization of p(DMA_n-b-$MTPA_m$) micelles

PM16 and PM32 micelles with a p(MTPA) core and a p(DMA) corona were prepared by a solvent evaporation method using THF. Addition of sodium phosphate buffer (PB, 100 mM, pH = 7.4) to the solubilized polymers led to

micellar dispersions of PM16 and PM32. The average hydrodynamic diameter (D_H) of the micelles at 1.0 mg/mL measured by DLS was 31.6 ± 0.5 and 42.4 ± 0.9 nm for PM16 and PM32, respectively (Table 2). With PM32 showing a larger D_H, the hydrodynamic size appeared to be correlate with the length of the hydrophobic block.[54] TEM images (Figure 3B and 3D) acquired from micellar dispersions at 1.0 mg/mL demonstrated the formation of spherical particles, ascribable to micelles. The particle analysis based on these TEM images gave an average diameter of 17.7 ± 3.1 nm for PM16 (Figure S5A) and 25.8 ± 3.1 nm for PM32 (Figure S5B). Cryo-EM analysis further confirmed the spherical morphology of both PM16 (Figure S6B) and PM32 (Figure S7C) micelles, with an average diameter of 10.4 ± 1.2 (Figure S6A) and 19.2 ± 2.3 nm (Figure S7A), respectively. Combined, these analyses demonstrated that both polymers formed micelles with the appropriate size range for nanotherapeutics,[55] and are thus possibly loadable with hydrophobic cargo.[56]

Table 2. Size of PM16 and PM32 micelles measured by DLS, TEM and Cryo-EM.

Polymer	D_H (nm)	D_{TEM} (nm)	$D_{Cryo\text{-}EM}$ (nm)
PM16	31.6 ± 0.5	17.7 ± 3.1	10.4 ± 1.2
PM32	42.4 ± 0.9	25.8 ± 3.1	19.2 ± 2.3

2.2.3 H_2O_2 induced oxidation and hydrolysis of p(DMA_n-b-$MTPA_m$) micelles

After characterization of the micelles, we wanted to test their response to H_2O_2. The oxidation of organic thioethers with H_2O_2 is notably slow and depends on the concentration of both reactants.[26,57] Thus, we chose to use a large excess of H_2O_2 (90 equivalents for PM16 and 46 for PM32) compared to the thioether units of the polymers to obtain an overview of the response times and behavior of these micelles. PM16 (6.7 mM thioether units at 6.8 mg/mL) and PM32 micelles (13 mM thioether units at 6.8 mg/mL) in PB/D_2O 9:1 were combined with 2.0 wt% H_2O_2 (600 mM) at 37 °C and studied by ^{1}H NMR spectroscopy (Figure 2C

and Figure S8 for PM16 and PM32, respectively). The micelles in aqueous media (bottom spectrum, Figure 2C) showed only the p(DMA_n) peaks, caused by the core-corona structure that is typical of polymeric micelles. However, almost immediately after the addition of H_2O_2, the ^1H NMR spectra revealed the release of **1** (^1H NMR spectrum reference in Supporting Information), confirming the oxidation and hydrolysis of the 4-(methylthio)phenyl ester functionalized core of the micelles (Figure 2A).

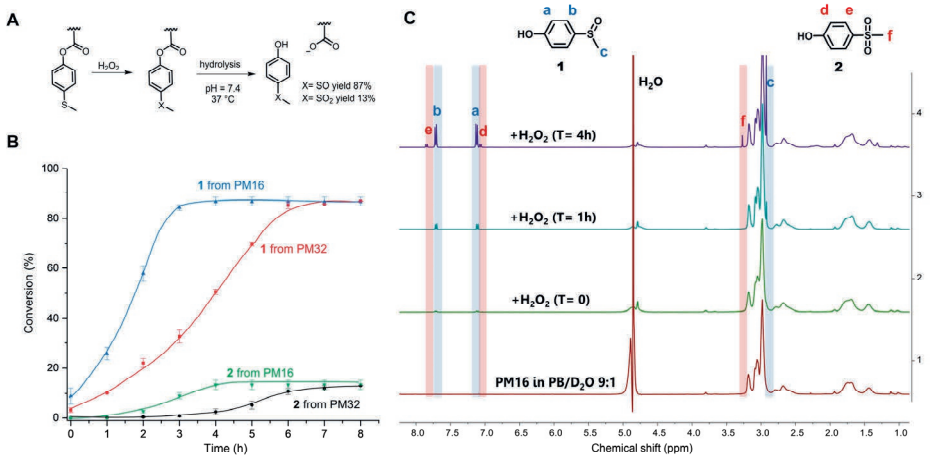

Figure 2. A) Scheme of H_2O_2-triggered solubility switch of 4-(methylthio) phenyl acrylate by oxidation induced hydrolysis leading to formation of hydrophilic acrylate anion and removal of **1** and **2** from the polymers. **B**) Conversion measured through ^1H NMR spectroscopy of **1** and **2** upon the addition of 2.0 wt% of H_2O_2 to PM16 and PM32 micellar solutions (6.8 mg/mL) in PB (100 mM, pH = 7.4) /D_2O 9:1 at 37 °C. The curves are drawn as a guide for the eye. **C**) ^1H NMR in PRESAT configuration of PM16 micelles after treatment with 2.0 wt% of H_2O_2 in PB (100 mM, pH = 7.4)/D_2O 9:1 at 37 °C.

Figure 2B shows the results of the combined ^1H NMR experiments for both polymeric micelles to give a comparative overview of the kinetics for different hydrophobic/hydrophilic block ratios. PM16 micelles exhibited 100% of degradation of the 4-(methylthio)phenyl ester moieties 3 h after addition of H_2O_2, converting to 87% of **1** and 13% of **2**. PM32 micelles reached the same outcome

after 6 h. It is worth noting that the release of these hydrolysis products followed sigmoidal curves. This effect was more significant for the release of **2**, which showed lag times of 2 h for PM16 and 4 h for PM32.

The conversion to 9% of **1** from PM16 and 3% from PM32 in the first ^{1}H NMR acquisition after the addition of H_2O_2 (~ 5 minutes) would suggest that as soon as the oxidation of the sulfide groups occurred, hydrolysis took place as well. This hypothesis is also supported by the absence of broad peaks related to the poly sulfoxide/sulfone in all the spectra acquired. In addition, both polymeric micelles resulted in the same distribution of sulfoxide and sulfone at the end of the degradation, which could be an indication that PM16 and PM32 followed a similar oxidation/hydrolysis mechanism. To asses this hypothesis, it is also interesting to note that PM32 required almost exactly 2 times as long to hydrolyze as PM16, matching the corresponding number of the 4-(methylthio)phenyl ester units to oxidize. At the same time, no clear dependence on hydrophilic block length is observed. Moreover, the formation of degradation products follows sigmoidal curves, which is in line with the fact that both oxidation of thioethers and ester hydrolysis inside polymer micelles in aqueous environment are known to be autocatalytic processes.[25,58] At the macromolecular level, when the hydrophobic core becomes more hydrophilic due to sulfur oxidation and ester hydrolysis, the micellar core turns into a more soluble matrix for H_2O_2. Thus, the increase of the local concentration of oxidant causes the acceleration of the reaction rate.[25,59] A clear indication of this phenomenon was the acceleration that we observed for the approximate complete release of **2** from PM32 in 2 h, after a 4 h long lag time. In fact, the significantly longer lag time for PM32 than PM16 can easily be explained considering the larger and less accessible hydrophobic core.

2.2.4 Stability of p(DMA$_n$-b-MTPA$_m$) micelles

To assess the stability of the micelles in non-oxidative physiological conditions (pH 7.4, 37 °C), we followed the hydrolysis rate for both PM16 and PM32 micelles by ^{1}H NMR for 144 h (6 days). We did observe the formation of a small amount of **1**, 1.0% for PM16 micelles and 0.7% for PM32 micelles after 6 days (Table 3). Furthermore, we investigated the hydrolytic stability of the ester functions in PM16 and in PM32 at pH 5.0 and 6.0 (37 °C), to analyze their behavior in acidic environments, which may occur in tissues or cells. Encouragingly, in all conditions both micelles were found to be hydrolytically stable, with ≤ 1.3% of **1** released in all cases after 6 days (Table 3). For all the experiments, the absence of the characteristic peaks of 4-(methylthio)phenol (reference spectrum in Supporting Information) showed that the 4-(methylthio)phenyl ester units do not directly hydrolyze. On the other hand, the release of **1** indicated background oxidation of the sulfide groups attached to the polymeric chain, enabling hydrolysis of the esters. This would demonstrate that the hydrolysis occurs exclusively after the oxidation of the thioether moiety. Nevertheless, such phenomenon can be considered negligible compared to the effect of the addition of H_2O_2 reported above, in which the hydrolysis of the pendent esters was complete within hours. Overall, we could confirm that PM16 and PM32 micelles are resistant to direct hydrolysis of 4-(methylthio)phenyl esters in environments with pH ranging from 5.0 to 7.4, demonstrating a unique response to oxidative stimulus.

Table 3. Oxidant-free release (%) of **1** from PM16 and PM32 micelles after 6 days at different pH.

pH	Release of 1 from PM16 (%)	Release of 1 from PM32 (%)
7.4	1.0	0.7
6.0	1.3	0.9
5.0	1.1	0.8

2.2.5 Morphological study of oxidation of p(DMA_n-b-$MTPA_m$) micelles

Having established the concept, we studied the morphological response of the micelles to various concentrations of H_2O_2. PM16 micelles (0.9 mM thioether units at 0.9 mg/mL) were exposed to concentrations of 2.0, 0.2 and 0.007 wt% of H_2O_2 (DLS, Figure 3A), corresponding respectively to 600, 60 and 2 mM. Upon addition of 2.0 wt% H_2O_2, we could not observe changes in Z-average diameter in the first hour (Figure 3A top, ■ red line). However, the scatter count dropped from 2.8 to 2.0 Mcps (Figure 3A bottom, ■ red line), indicating that the micelles started to dissociate. This value dropped to 1.0 Mcps within the next hour. After 4 h, the PM16 micelles reached a maximum Z-average diameter of 108 nm. The approximate 3-fold reduction in scatter count observed after H_2O_2 addition indicates degradation of the micelles due to oxidation induced hydrolysis. While the concurrent increase in Z-average diameter may be counterintuitive, it can be explained by a partial clustering of the hydrolyzed polymer chains. TEM images showed the presence of micelles before H_2O_2 addition (Figure 3B), and no significant structure could be detected 24 h after the addition of 2.0 wt% H_2O_2 (Figure S5C). This analysis supported the rapid disruption (within 4 hours) of the polymeric micelles after addition of 2.0 wt% H_2O_2, as showed in both DLS and ^{1}H NMR data. Z-average diameter and scatter count after 24 h (Figure 3A, ▲ blue line) of PM16 micelles triggered with 0.2 wt% H_2O_2 were similar to those observed for 2.0 wt% in the first 4 hours. Interestingly, this could be interpreted as ~6 fold reduction in rate of disassembly of the micelles when the concentration of H_2O_2 is 10 times lower.

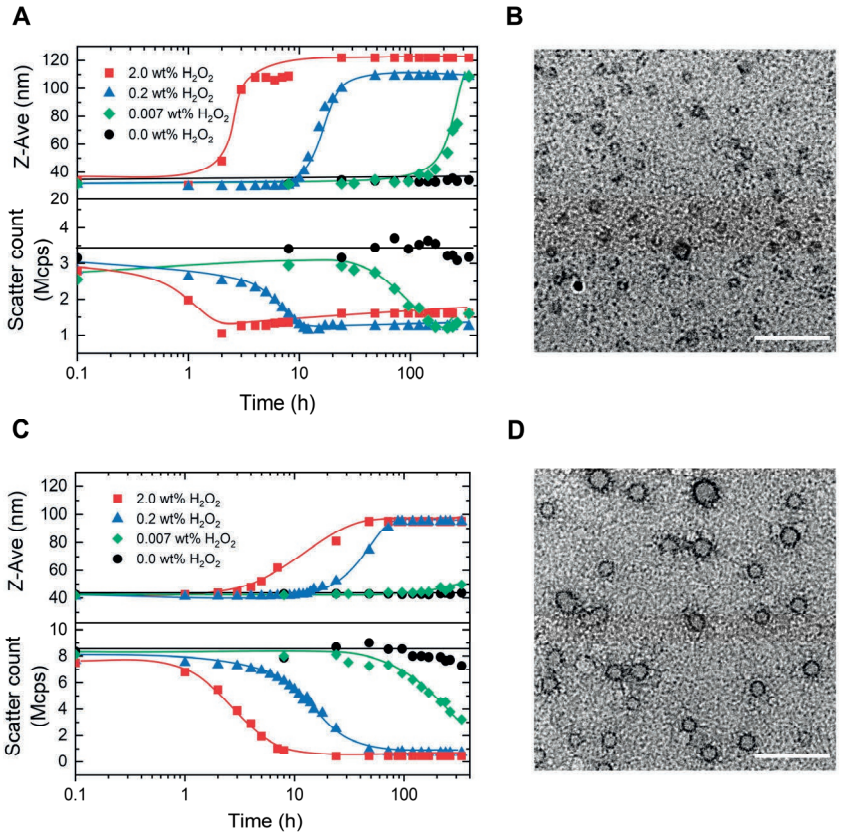

Figure 3. Morphological study of oxidation of PM16 and PM32 micelles. The curves are drawn as a guide for the eye. **A**) Z-average diameter (top) and scatter count (bottom) of PM16 micelles (0.9 mg/mL) measured by DLS at 37 °C for four concentrations of H_2O_2: 2.0 wt% (■ red line), 0.2 wt% (▲ blue line), 0.007 wt% (♦ green line) and 0.0 wt% (control ● black line). **B**) TEM image (Scale bar = 100 nm) of PM16 micelles at t=0, stained with 2.0 wt% uranyl acetate. **C**) Z-average diameter (top) and scatter count (bottom) of PM32 micelles (0.9 mg/mL) measured by DLS at 37 °C for four concentrations of H_2O_2: 2.0 wt% (■ red line), 0.2 wt% (▲ blue line), 0.007 wt% (♦ green line) and 0.0 wt% (control ● black line). **D**) TEM image (Scale bar = 100 nm) of PM32 micelles at t=0, stained with 2.0 wt% uranyl acetate.

Encouraged by these promising results, we decided to investigate whether the system is able to respond to concentrations of the oxidant approaching biologically relevant conditions (0.007 wt% (2 mM) of H_2O_2). Z-average diameter of PM16 micelles reached a maximum after 336 h (Figure 3A top, ♦ green line) and the scatter count decreased steadily from 48 h, getting to 1.2 Mcps at 168 h (Figure 3A bottom, ♦ green line). It is important to note that, in the absence of H_2O_2 the PM16 micelles remained stable at 32 – 34 nm and 3.2 – 3.7 Mcps for 336 h. These results demonstrate a sensitivity down to 0.007 wt% H_2O_2 and a considerable stability in the absence of an oxidative trigger.

Next, we repeated the same DLS study with PM32 micelles (1.8 mM thioether units at 0.9 mg/mL). These micelles had similar behavior to PM16 micelles, with a sigmoidal increase in Z-average diameter and a sigmoidal decrease in scatter count after H_2O_2 addition. Specifically, the Z-average diameter of PM32 micelles increased from 42 to ~90 nm (Figure 3C top), while the scatter count dropped from 8.0 to 1.0 Mcps (Figure 3C bottom). The lower plateau value of the scatter count was reached 7 and 48 h after the addition of 2.0 wt% H_2O_2 and 0.2 wt% H_2O_2, respectively. Showing that, similarly to PM16, PM32 micelles disrupted ~6 times slower when 10 times lower oxidant concentration was used. For 0.007 wt% (2.0 mM) H_2O_2, the scatter count dropped to 3.2 Mcps after 336 h (Figure 3C bottom, ♦ green line). Considering that here the ratio of thioether units/H_2O_2 was nearly 1, the low rate of micellar disruption is not surprising. Additionally, like for PM16 micelles, the scatter count remained relatively stable (7.3 – 8.5 Mcps) over 336 h without H_2O_2.

Curiously, the aggregates formed after the disruption of PM32 were apparently smaller than those obtained from PM16. With TEM images of PM32 micelles before (Figure 3D) and 24 h after the addition of 2.0 wt% H_2O_2 (Figure S5D), we could see the initial spherical micelles, but could not distinguish any particular structure after the H_2O_2 treatment. We therefore acquired Cryo-EM

images of PM32 micelles before (Figure S7C) and 24 h after (Figure S7D) the addition of 0.2 wt% H_2O_2. The particle analysis showed a relatively small increase in average diameter from 19.2 ± 2.3 (Figure S7A) to 28.9 ± 15.4 nm (Figure S7B), supporting the increase in size during PM32 micelles degradation. On the other hand, Cryo-EM images (Figure S6) of PM16 micelles before and 24 h after the addition of 0.2 wt% H_2O_2 exhibited the starting spherical and homogeneous micelles in non-oxidative conditions, but, similar to the TEM images, did not show any significant structure after the H_2O_2 addition. The low scatter count associated with the proposed larger aggregates indicates a very low abundance, explaining the result of Cryo-EM imaging. Despite of the uncertain characterization of the final structures, the Z-average diameter change and the decrease in scatter count of the micelles at different concentrations of H_2O_2 measured by DLS demonstrated the oxidation-triggered morphological change of both PM16 and PM32 micelles.

Interestingly, the DLS data not only agreed with the ^{1}H NMR results, but also followed similar sigmoidal trends, confirming the autocatalytic degradation of our micelles. We observed that micelles prepared from PM16 underwent a faster (2 – 4 times depending on the conditions and methods of measurements) disassembly than those from PM32. The greater H_2O_2 sensitivity observed for PM16 indicates that shorter 4-(methylthio)phenyl ester functionalized blocks allow for faster micellar degradation. In perspective, this opens the possibility of tuning the hydrophobic block length of p(DMA_n-b-$MTPA_m$) to precisely control drug release.

2.2.6 Assessment of Nile Red loading and release

To assess the suitability of p(DMA_n-b-$MTPA_m$) micelles as carriers for drug release, we chose Nile Red, a non-water soluble dye which is fluorescent exclusively in a hydrophobic environment. The fluorescence of Nile Red can be constant in presence of up to 5 vol% (~7.3 wt%) H_2O_2 over 170 h,[60] making it a good drug model for the time range and conditions of our experiments. First, we determined the drug loading (DL) and encapsulation efficiency (EE) of Nile Red using a known fluorescence method.[60] We obtained DL (2.0 – 4.0 μg/mg polymer) and EE (10 – 20%) (Table S3), comparable to other drug release systems reported in literature.[27]

We subsequently tested the Nile Red loaded p(DMA_n-b-$MTPA_m$) micelles for release of Nile Red under oxidative conditions. PM16 micelles led to a 90% Nile Red release within 3 and 13 h when 2.0 wt% and 0.2 wt% of H_2O_2 was respectively added (Figure 4, top). PM32 micelles released Nile Red on longer time scales (Figure 4, bottom part), getting to 90% within 5 h (2.0 wt% H_2O_2) and 21 h (0.2 wt% H_2O_2). These results showed, similarly to the ^{1}H NMR data, that PM16 micelles disassembled and released the cargo almost 2 times faster than PM32 micelles in presence of the same H_2O_2 concentration. We again would like to highlight that the Nile Red release curves presented sigmoidal shapes, in line with the data acquired with the previous techniques. Specifically the release profile from PM16 micelles at 0.2 wt% of H_2O_2 displayed a three stage profile, typical of polymeric drug delivery systems with a heterogeneous degradation mechanism.[61] This would position the p(DMA_n-b-$MTPA_m$) micelles as an oxidation-triggered alternative to the hydrolysis-degradable polymers commonly used for controlled drug release.[62] Interestingly, this behavior does not show any burst release,[63] increasing the relevance of the system for applications where burst release of cytotoxic drugs may cause excessive side effects.[62] We observed 10% release for PM32 micelles in a non-oxidative

environment and 3% for PM16 by 30 h. This would suggest only minor passive leakage of Nile Red from the micelles. However, such effect can be considered negligible when compared to the release rate obtained in presence of H_2O_2. Overall, the release profile shows a dependence on the type of polymer and on the concentration of H_2O_2, making this technology potentially tunable according to the required dosage and release time of the drug.

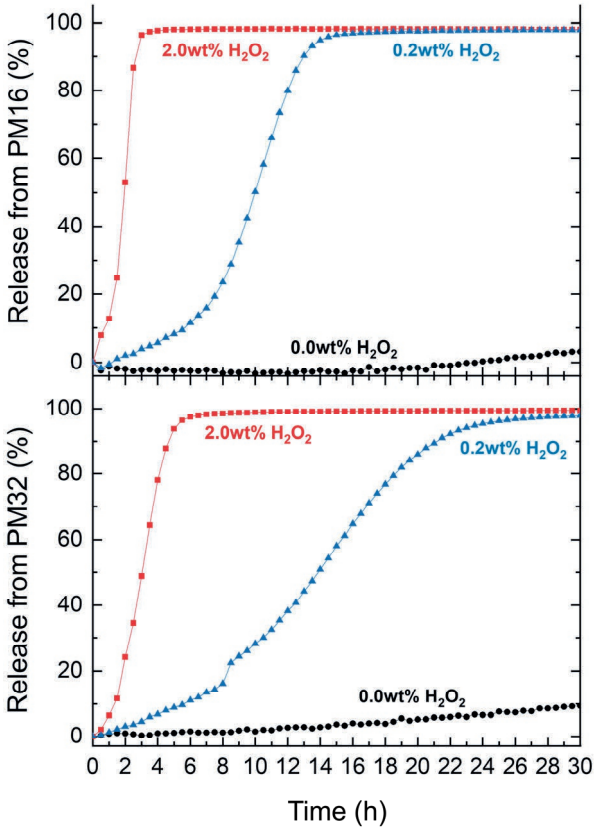

Figure 4. Nile Red release from PM16 (top) and PM32 (bottom) micellar dispersion (0.9 mg/mL) in PB (100 mM, pH =7.4) for three concentrations of H_2O_2 at 37 °C: 2.0 wt% (■ red line), 0.2 wt% (▲ blue line) and 0.0 wt% (control ● black line) measured by fluorescence spectroscopy (λ_{ex} = 540 ± 20 nm, λ_{em} = 620 ± 30 nm).

2.2.7 Cell viability assay of p(DMA_n-b-$MTPA_m$) micelles

We tested the cytotoxicity of PM16 and PM32 micelles on HeLa cells, by administering micellar dispersions in concentrations between 0.0 and 1.0 mg/mL, in line with the concentration used for the morphological study and Nile Red release. After 24 h of incubation, the WST-8 assay showed high cell viability for both polymers across all the applied concentrations, with no statistical difference compared to the controls (Figure S10).

2.3 Conclusion

In this work, we demonstrate selective ROS triggered breakdown of block copolymer micelles, and associated release of model cargo. The disruption mechanism is programmed into the material using a solubility switch in the hydrophobic block, based on a logic gate that increases the ester hydrolytic lability upon oxidation of a thioether phenyl moiety. In the absence of oxidants, such as H_2O_2, the micelles are stable for several days under neutral and mildly acidic buffered conditions (pH 5.0 – 7.4, 37 °C). Millimolar concentrations of H_2O_2 lead to micellar disintegration and cargo release on timescales of hours to days depending on the ROS concentration. Building on these encouraging results, our laboratory is currently investigating methods to further increase the ROS sensitivity of these micelles to concentrations typically present in cancerous tissue. Subsequently, studying the release of bioactive compounds and the stability of the polymers in blood plasma (specifically against esterase activity) will be necessary before in vivo evaluation. In perspective, the thioanisole ester-based logic gate could also be implemented as a linker in ROS-responsive prodrugs to achieve the release of the active compound directly controlled by the oxidation-induced ester hydrolysis.

2.4 References

1. M. L. Adams, Lavasanifar, A., Kwon, G.S., *J. Pharm. Sci.*, 2003, **92**, 1343-1355.
2. A. Zhang, K. Jung, A. Li, J. Liu and C. Boyer, *Prog. Polym. Sci.*, 2019, **99**, 101164.
3. K. Zhou, H. Liu, S. Zhang, X. Huang, Y. Wang, G. Huang, B. D. Sumer and J. Gao, *J. Am. Chem. Soc.*, 2012, **134**, 7803-7811.
4. E. M. Frazar, R. A. Shah, T. D. Dziubla and J. Z. Hilt, *J. Appl. Polym. Sci.*, 2020, **137**.
5. T. Miyata, N. Asami and T. Uragami, *Nature*, 1999, **399**, 766-769.
6. C. C. Winterbourn, *Nat. Chem. Biol.*, 2008, **4**, 278-286.
7. S. C. Gupta, D. Hevia, S. Patchva, B. Park, W. Koh and B. B. Aggarwal, *Antioxid. Redox Signaling*, 2012, **16**, 1295-1322.
8. L. M. Coussens, Werb Z., *Nature*, 2002, **420**, 860-867.
9. T. Wu, X. Chen, Y. Wang, H. Xiao, Y. Peng, L. Lin, W. Xia, M. Long, J. Tao and X. Shuai, *Nanomedicine*, 2018, **14**, 2215-2226.
10. K. J. Barnham, C. L. Masters and A. I. Bush, *Nat. Rev. Drug Discovery*, 2004, **3**, 205-214.
11. L. M. Sayre, G. Perry and M. A. Smith, *Chem. Res. Toxicol.*, 2008, **21**, 172-188.
12. S. Loft and H. E. Poulsen, *J. Mol. Med.*, 1996, **74**, 297-312.
13. P. D. Ray, B.-W. Huang and Y. Tsuji, *Cell. Signalling*, 2012, **24**, 981-990.
14. S. B. Nimse and D. Pal, *RSC Adv.*, 2015, **5**, 27986-28006.
15. C. T. Jordan, J. Z. Hilt and T. D. Dziubla, *J. Appl. Polym. Sci.*, 2019, 48647.
16. C. Tapeinos and A. Pandit, *Adv. Mater.*, 2016, **28**, 5553-5585.

17. H. Hagen, P. Marzenell, E. Jentzsch, F. Wenz, M. R. Veldwijk and A. Mokhir, *J. Med. Chem.*, 2012, **55**, 924-934.

18. C.-C. Song, F.-S. Du and Z.-C. Li, *J. Mater. Chem. B*, 2014, **2**, 3413-3426.

19. D. Trachootham, J. Alexandre and P. Huang, *Nat. Rev. Drug Discovery*, 2009, **8**, 579-591.

20. E. Lallana and N. Tirelli, *Macromol. Chem. Phys.*, 2013, **214**, 143-158.

21. C. Sun, L. Wang, B. Xianyu, T. Li, S. Gao and H. Xu, *Biomaterials*, 2019, **225**, 119514.

22. L. Wang, K. Zhu, W. Cao, C. Sun, C. Lu and H. Xu, *Polym. Chem.*, 2019, **10**, 2039-2046.

23. A. Napoli, M. Valentini, N. Tirelli, M. Muller and J. A. Hubbell, *Nat. Mater.*, 2004, **3**, 183-189.

24. D. Jeanmaire, J. Laliturai, A. Almalik, P. Carampin, d. A. Richard, E. Lallana, R. Evans, R. E. P. Winpenny and N. Tirelli, *Polym. Chem.*, 2014, **5**, 1393-1404.

25. V. V. Khutoryanskiy and N. Tirelli, *Pure Appl. Chem.*, 2008, **80**, 1703-1718.

26. F. El Mohtadi, R. d'Arcy, J. Burke, J. M. Rios De La Rosa, A. Gennari, R. Marotta, N. Francini, R. Donno and N. Tirelli, *Biomacromolecules*, 2020, **21**, 305-318.

27. P. Hu and N. Tirelli, *Bioconjug. Chem.*, 2012, **23**, 438-449.

28. K. E. Broaders, S. Grandhe and J. M. Frechet, *J. Am. Chem. Soc.*, 2011, **133**, 756-758.

29. K. Sato, M. Takahashi, M. Ito, E. Abe and J.-i. Anzai, *Langmuir*, 2014, **30**, 9247-9250.

30. C. de Gracia Lux, S. Joshi-Barr, T. Nguyen, E. Mahmoud, E. Schopf, N. Fomina and A. Almutairi, *J. Am. Chem. Soc.*, 2012, **134**, 15758-15764.

31. T. Zhang, X. Chen, C. Xiao, X. Zhuang and X. Chen, *Polym. Chem.*, 2017, **8**, 6209-6216.

32. C. Dong, Q. Zhou, J. Xiang, F. Liu, Z. Zhou and Y. Shen, *J. Controlled Release*, 2020, **321**, 529-539.

33. F.-Y. Qiu, M. Zhang, R. Ji, F.-S. Du and Z.-C. Li, *Macromol. Rapid Commun.*, 2015, **36**, 2012-2018.

34. X. Liu, J. Xiang, D. Zhu, L. Jiang, Z. Zhou, J. Tang, X. Liu, Y. Huang and Y. Shen, *Adv. Mater.*, 2016, **28**, 1743-1752.

35. S. Lv, Y. Wu, K. Cai, H. He, Y. Li, M. Lan, X. Chen, J. Cheng and L. Yin, *J. Am. Chem. Soc.*, 2018, **140**, 1235-1238.

36. E. Jäger, Humajová, J., Dölen, Y., Kučka, J., Jäger, A., Konefał, R., Pankrác, J., Pavlova, E., Heizer, T., Šefc, L., Hrubý, M., Figdor, C. G., Verdoes, M., *Adv. Healthcare Mater.*, 2021, 2100304.

37. A. Gennari, C. Gujral, E. Hohn, E. Lallana, F. Cellesi and N. Tirelli, *Bioconjug. Chem.*, 2017, **28**, 1391-1402.

38. F. El-Mohtadi, R. d'Arcy and N. Tirelli, *Macromol. Rapid Commun.*, 2019, **40**, 1800699.

39. E. Gardey, F. H. Sobotta, S. Quickert, T. Bruns, J. C. Brendel and A. Stallmach, *Macromol. Biosci.*, 2022, 2100482

40. P. Charlesworth, W. Lee and W. S. Jenks, *J. Phys. Chem.*, 1996, **100**, 15152-15155.

41. F. Cheng, T. Su, K. Luo, Y. Pu and B. He, *J. Mater. Chem. B*, 2019, **7**, 1005-1016.

42. M. Geven, R. d'Arcy, Z. Y. Turhan, F. El-Mohtadi, A. Alshamsan and N. Tirelli, *Eur. Polym. J.*, 2021, **149**, 110387.

43. W.-X. Wu, X.-L. Yang, B.-Y. Liu, Q.-F. Deng, M.-M. Xun, N. Wang and X.-Q. Yu, *RSC Adv.*, 2016, **6**, 11870-11879.

44. C. Brooker, R. d'Arcy, E. Mele and H. Willcock, *Soft Matter*, 2021, **17**, 3775-3783.

45. R. J. Mayer, T. Tokuyasu, P. Mayer, J. Gomar, S. Sabelle, B. Mennucci, H. Mayr and A. R. Ofial, *Angew. Chem. Int. Ed.*, 2017, **56**, 13279-13282.

46. C. D. Vo, G. Kilcher and N. Tirelli, *Macromol. Rapid Commun.*, 2009, **30**, 299-315.

47. W. Mabey and T. Mill, *J. Phys. Chem. Ref. Data*, 1978, **7**, 383-415.

48. R. Kakuchi and P. Theato, *Macromolecules*, 2012, **45**, 1331-1338.

49. B. J. Crielaard, C. J. Rijcken, L. Quan, S. van der Wal, I. Altintas, M. van der Pot, J. A. Kruijtzer, R. M. Liskamp, R. M. Schiffelers, C. F. van Nostrum, W. E. Hennink, D. Wang, T. Lammers and G. Storm, *Angew. Chem. Int. Ed. Engl.*, 2012, **51**, 7254-7258.

50. L. Li, Q. Wang, R. Lyu, L. Yu, S. Su, F.-S. Du and Z.-C. Li, *Polym. Chem.*, 2018, **9**, 4574-4584.

51. J. M. Caster, S. K. Yu, A. N. Patel, N. J. Newman, Z. J. Lee, S. B. Warner, K. T. Wagner, K. C. Roche, X. Tian, Y. Min and A. Z. Wang, *Nanomedicine*, 2017, **13**, 1673-1683.

52. D. J. Keddie, *Chem. Soc. Rev.*, 2014, **43**, 496-505.

53. Z. Ahmad, A. Shah, M. Siddiq and H.-B. Kraatz, *RSC Adv.*, 2014, **4**, 17028-17038.

54. M.-C. Jones and J.-C. Leroux, *Eur. J. Pharm. Biopharm.*, 1999, **48**, 101-111.

55. A. G. Denkova, H. Liu, Y. Men and R. Eelkema, *Adv. Therap.*, 2020, **3**, 1900177.

56. H. Cabral, Y. Matsumoto, K. Mizuno, Q. Chen, M. Murakami, M. Kimura, Y. Terada, M. R. Kano, K. Miyazono, M. Uesaka, N. Nishiyama and K. Kataoka, *Nat. Nanotechnol.*, 2011, **6**, 815-823.

57. M. Chen, Y. Jin, J. Li, Y. Zhang and X. Li, *Ind. Eng. Chem. Res.*, 2017, **56**, 7675-7684.

58. S. Fredenberg, M. Wahlgren, M. Reslow and A. Axelsson, *Int. J. Pharm.*, 2011, **415**, 34-52.

59. F. H. Sobotta, M. T. Kuchenbrod, F. V. Gruschwitz, G. Festag, P. Bellstedt, S. Hoeppener and J. C. Brendel, 2021, **60**, 24716-24723.

60. M. K. Gupta, T. A. Meyer, C. E. Nelson and C. L. Duvall, *J. Controlled Release*, 2012, **162**, 591-598.

61. T. G. Park, *Biomaterials*, 1995, **16**, 1123-1130.

62. N. Kamaly, B. Yameen, J. Wu and O. C. Farokhzad, *Chem. Rev.*, 2016, **116**, 2602-2663.

63. Z. Fan and H. Xu, *Polym. Rev.*, 2020, **60**, 114-143.

2.5 Supporting Information

2.5.1 Materials

All reagents were obtained from commercial suppliers (Sigma Aldrich, TCI Chemicals or Acros Organics) and used without further purification unless otherwise specified. Reference compounds 4-(methylthio)phenol and 4-(methylsulfonyl)phenol were purchased respectively from Sigma Aldrich and TCI. SDS of these compounds reports that chemical, physical, and toxicological properties have not been thoroughly investigated. 4-(methylthio)phenol: this substance/mixture contains no components considered to be either persistent, bioaccumulative and toxic (PBT), or very persistent and very bioaccumulative (vPvB) at levels of 0.1% or higher. Air and moisture sensitive reagents were transferred via syringe. All air and/or moisture sensitive reactions were carried out in oven-dried glassware under a positive pressure of argon gas with commercially available anhydrous solvents. Petroleum ether refers to the fraction boiling in the range 40 – 60 °C. Reactions were monitored by analytical thin-layer chromatography (TLC) on silica gel plates (Merck $60F_{254}$) and either visualized by UV light (254 nm) or by staining with a solution of $KMnO_4/K_2CO_3$/AcOH in water followed by heating. Flash chromatography was performed on 230-400 mesh silica gel (Sigma Aldrich). ^{1}H NMR and ^{13}C NMR spectra were recorded on an Agilent-400 MR DD2 (400 MHz and 101 MHz for ^{1}H and ^{13}C, respectively) spectrometer at 298 K. Chemical shifts are reported in ppm relative to the residual solvent peak, the multiplicity is reported as follows: s = singlet, d = doublet, t = triplet, q = quartet, m = multiplet, and J-couplings (*J*) are reported in Hertz (Hz). To suppress the water peak, PRESAT configuration (suppress one highest peak) was used. NMR spectra were processed by MNova NMR software (Mestrelab Research). Infrared spectra were recorded on a FT-IR Thermo Fisher Nicolet 6700 spectrophotometer and are reported in wavenumbers. GC-MS samples were analyzed using an Agilent 5977 GC/MSD

equipped with a Stabilwax MS column (oven temperature: 250 °C, flow: 2.5 mL/min). ESI-MS was performed using LTQ XL spectrometer equipped with Shimadzu HPLC setup operating at 0.2 mL/min flow rate with water/MeCN mobile phase containing 0.1 vol% formic acid and Discovery C18 column. Gel permeation chromatography (GPC) was performed on a Shimadzu system equipped with a LC-20AD liquid chromatograph and a RID-10A refractive index detector. Fluorescence release was measured in 96 well plates using a micro plate reader (Biotek Synergy H1). Fluorescence spectra of Nile Red loading were recorded with a fluorescence spectrometer Spex Fluorolog-3 equipped with a standard 90° setup. Dynamic light scattering (DLS) measurements were performed on a Malvern Zetasizer Nano-ZS equipped with a 4 mW laser operating at 633 nm. TEM and Cryo-EM measurements were performed on a Jeol JEM 1400 plus Transmission Electron Microscope with an operating voltage of 120 kV and a TVIPS F416 camera.

2.5.2 Synthesis

Synthesis of 4-(methylsulfinyl)phenol[1]

To 4-(methylthio)phenol (1.0 mmol) was added solution of 30% H_2O_2 (1.2 equiv., 0.04 g) and boric acid (10 mol%, 0.1 mmol, 0.006 g), and the mixture was stirred at room temperature for 30 min. The mixture was extracted with CH_2Cl_2 (5 × 10 mL) and the organic layers washed with brine (15 mL). The brine was extracted additional 5 times with CH_2Cl_2. The combined organics was dried over Na_2SO_4 and the solvent was removed through rotatory evaporation. The crude product was purified by flash chromatography over silica gel (methanol/ethyl acetate 2:98) and crystalized in ethyl acetate to obtain 4-(methylsulfinyl)phenol (62.0 mg, 0.40 mmol, 40% yield) as white crystals. ^{1}H NMR (400 MHz, $CDCl_3$): δ= 8.57 (s, 1H, OH), 7.51 (d, *J* = 8.5 Hz, 2H, Ar-H), 6.96 (d, *J* = 8.5 Hz, 2H, Ar-H), 2.76 (s, 3H, CH_3). ^{13}C NMR (101 MHz, $CDCl_3$): δ= 160.5 (C_q), 133.8 (C_q), 126.2 (CH, arom.), 116.9 (CH, arom.), 43.3 (CH_3).

MS (ESI+) *m/z*: $[M + H]^+$ calcd. for $C_7H_8O_2S$, 157.03, found 156.93. The spectroscopic data are in accordance with those reported in literature.[2]

Synthesis of 4-(methylthio)phenylacrylate

Triethylamine (Et_3N) (6.27 mL, 1.50 equiv.) was added dropwise to a solution of 4-(methylthio)phenol (4.20 g, 30.0 mmol, 1.00 equiv.) and acryloyl chloride (3.64 mL, 1.50 equiv.) in dry CH_2Cl_2 at 0 °C and stirred overnight for 16 hours, slowly increasing the temperature to 20 °C. The reaction mixture was diluted with CH_2Cl_2 (250 mL) and washed with water (500 mL) and brine (500 mL). The combined organic layers were dried over anhydrous Na_2SO_4 and the solvent was removed under reduced pressure. The crude product was purified by flash chromatography over silica gel (ethyl acetate/petroleum ether 1:9 to 1:4) to afford 4-(methylthio)phenylacrylate (MTPA) (4.30 g, 22.1 mmol, 74% yield) as a light yellow oil. ^{1}H NMR (400 MHz, $CDCl_3$, δ): 7.29 (d, J = 8.4 Hz, 2H, Ar-H), 7.07 (d, J = 8.4 Hz, 2H, Ar-H), 6.60 (d, J = 17.3 Hz, 1H, $CHCH_2$), 6.31 (dd, J = 17.3, 10.4 Hz, 1H, CH_2), 6.01 (d, J = 10.4 Hz, 1H, CH_2), 2.49 (s, 3H, CH_3). ^{13}C NMR (101 MHz, $CDCl_3$, δ): 164.7 (C=O), 148.4 (C_q), 135.9 (C_q), 132.8 (CH, arom.), 128.2 (CH, arom.), 128.0 ($CHCH_2$), 122.1 (CH_2CH), 16.6 (CH_3). EIMS *m/z* (%):196 (1.5), 195 (3.7), 194 (32) [M^+], 142 (5.3), 141 (8.8), 140 (100) [$M^+ - C_3H_2O$], 139 (6), 125 (20), 96 (3.8), 55 (34), 45 (3.4). The spectroscopic data are in accordance with those reported in the literature.[3]

Synthesis of p(DMA_n) macro-DDMAT

Specific conditions and data are shown in Table S1. N,N-dimethylacrylamide (DMA), which was filtered over basic alumina prior to use, and 2-(dodecylthiocarbonothioylthio)-2-methylpropionic acid (DDMAT) were dissolved in DMF and degassed for 15 minutes by bubbling argon gas. The resulting solution was stirred in a light reactor (444 nm), samples were taken regularly to follow the conversion with ^{1}H NMR. The reaction was stopped after 10 hours when the desired conversion was obtained. The reaction mixture was

diluted with DMF (10.0 mL) and precipitated three times in diethyl ether (500 mL). The precipitated product was dried in a vacuum oven at 50 °C for three hours to afford p(DMA_{102}) macroDDMAT (2.46 g) and p(DMA_{130}) macroDDMAT (3.37 g) as yellow solids.

Table S1 pDMA_n synthesis and characterization data.

	$[DDMAT]_0$ / $[DMA]_0$	DMA (mmol)	DMA (g)	DDMAT (mmol)	DDMAT (g)	DMF (mL)	Reaction time (h)	^{1}H NMR Conversion (%)
p(DMA_{102})	1/120	40	4.0	0.35	0.12	5.9	10	85
p(DMA_{130})	1/200	70	6.9	0.35	0.12	6.8	10	65

Synthesis of p(DMA_n-b-$MTPA_m$)

Specific conditions and data are shown in Table S2. Macro chain transfer agent p(DMA_n) macro-DDMAT and 4-(methylthio)phenyl acrylate were dissolved in DMF (1.0 mL) and degassed for 15 minutes by bubbling argon gas. The resulting solution was stirred in a light reactor (444 nm) for the given time. The reaction mixture was diluted with DMF (5.00 mL) and precipitated three times in diethyl ether (300 mL). The precipitated product was dried in a vacuum oven at 50 °C for three hours to afford p(DMA_{102}-b-$MTPA_{32}$) (0.54 g) and p(DMA_{130}-b-$MTPA_{16}$) (1.13 g) as white solids.

Table S2 p(DMA_n-b-$MTPA_m$) synthesis and characterization data.

	$[p(DMA_n)$ macro-DDMAT$]_0$ /$[MTPA]_0$	p(DMA_n) macro-DDMAT (mmol)	p(DMA_n) macro-DDMAT (g)	MTPA (mmol)	MTPA (g)	DMF (mL)	React. time (h)	^{1}H NMR Conversion (%)
p(DMA_{102}) b-$MTPA_{32}$	1/66	0.12	1.3	7.9	1.5	5.3	13	48
p(DMA_{130}) b-$MTPA_{16}$	1/25	0.10	1.3	2.4	0.46	6.8	6	64

2.5.3 Polymer Characterization

For all the polymers, ^{1}H NMR spectra were recorded in $CDCl_3$, and the molecular weight was measured through gel permeation chromatography (GPC) in DMF. p(DMA_n-b-$MTPA_m$) structures were derived by ^{1}H NMR as reported below.

Polymerization conversion (ρ) was calculated by monitoring reduction in the ^{1}H NMR integrals of the monomer unsaturated protons (∫M: 5.60 – 6.80 ppm for DMA, 6.12 – 6.55 ppm for MTPA) and aromatic protons in case of MTPA (7.32 ppm) relative to the proton (7.95 ppm) of the reaction solvent DMF. The ^{1}H NMR spectra to follow the polymerization conversion were taken in DMSO-d6. In the case of a copolymerization with both DMA and MTPA the conversion of both monomers was calculated according Equation S1.

$$\rho = \frac{\int M\,(t0) - \int M\,(t)}{\int M\,(t0)} \qquad \textbf{Equation S1}$$

For a polymerization containing z monomers, $M_{n,conv}$ was calculated according to Equation S2. Here $[Mx]_0$ is the initial concentration of monomer *x*, $[CTA]_0$ is the initial chain transfer agent (CTA) concentration and M_{Mx} and M_{CTA} are the monomer *x* and CTA molecular weights, respectively.

$$M_{n,conv} = \sum_{x=1}^{Z} \rho * \frac{[M]_0}{[CTA]_0} * M_{Mx} + M_{CTA} \qquad \textbf{Equation S2}$$

^{1}H NMR spectra of the block copolymers

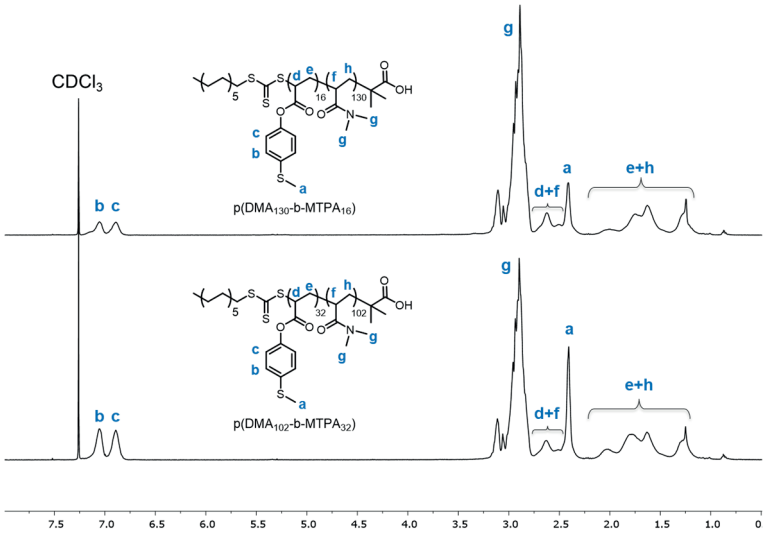

Figure S1. ^{1}H NMR stacked spectra of p(DMA$_{130}$-b-MTPA$_{16}$) (top) and poly(DMA$_{102}$-b-MTPA$_{32}$) (bottom) in $CDCl_3$.

GPC data of the block copolymers

The average molecular weight and dispersity Đ (M_w/M_n) of the synthesized polymers was measured using a Shimadzu GPC with DMF LiBr (25 mM) as eluent. The system was equipped with a Shimadzu CTO-20AC Column oven, a Shimadzu RID-10A refractive index detector, a Shimadzu SPD-20A UV-Vis detector, PL gel guard column (MIXED, 5 µm), 50 mm x 7.5 mm, and 1× Agilent PLGel (MIXED, 5 µm), 300 mm × 7.5 mm, providing an effective molar mass range of 200 to 2 x 10^6 g/mol. DMF LiBr (25 mM) was used as an eluent with a flow rate of 1.0 mL/min at 50 °C. The GPC columns were calibrated with low dispersity PMMA standards (Sigma Aldrich) ranging from 800 to 2.2 x 10^6 g/mol, and molar masses are reported as PMMA equivalents. A 3rd-order polynomial was used to fit the log Mp vs. time calibration curve for both systems, which was near linear across the molar mass ranges.

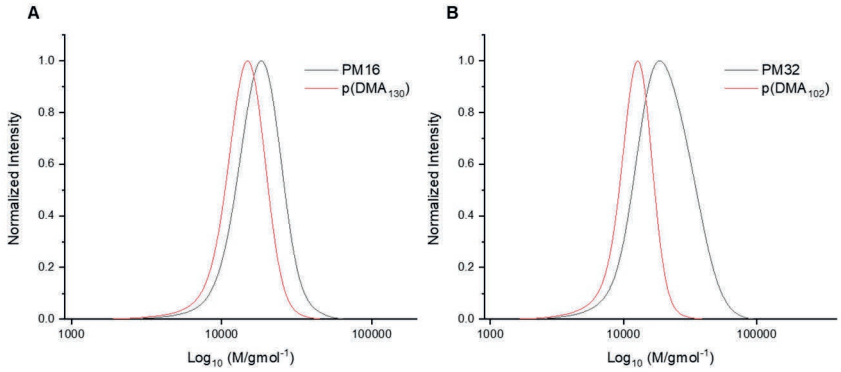

Figure S2. A) GPC traces of p(DMA_{130}) and the chain extended p(DMA_{130}-b-$MTPA_{16}$). B) GPC traces of p(DMA_{102}) and the chain extended p(DMA_{102}-b-$MTPA_{32}$).

2.5.4 Characterization of polymeric micelles

Preparation of the polymeric micelles

10 mg of p(DMA_m-b-$MTPA_n$) was dissolved in THF (0.25 mL), and sodium phosphate buffer (PB, 10 mL, 100 mM, pH = 7.4) was added slowly while vigorously stirring. The suspended micelles were left to stir for 18 hours in an open vial to evaporate the organic solvent.

DLS measurements of the polymeric micelles before and after H_2O_2 treatment

To 1.0 mL of a 1.0 mg/mL micellar dispersion of p(DMA_m-b-$MTPA_n$) prepared as previously described 66 µL of stock solutions of hydrogen peroxide in PB with variable concentration was added to yield a final H_2O_2 concentration of 0.0, 0.007, 0.2, 2.0 wt%. The size distribution and the scattering intensity at 37°C were followed by DLS as a function of time. The curves are drawn for the different data sets as a guide for the eye.

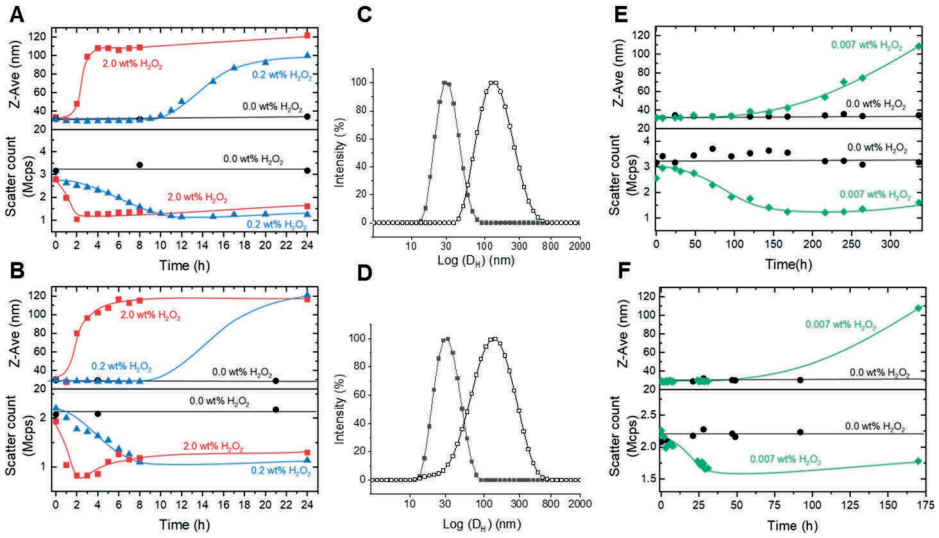

Figure S3. PM16 micelles in presence of different H_2O_2 concentrations at 37 °C. The curves are drawn as a guide for the eye. A) Z-Average size (top) and scatter count (bottom) distributions of PM16 micelles measured by DLS for three concentrations of H_2O_2: 2.0 wt% (■), 0.2 wt% (▲) and 0.0 wt% (control ●). B) Z-Average size (top) and scatter count (bottom) distributions of PM16 micelles (repeated with independent batch) measured by DLS for three concentrations of H_2O_2: 2.0 wt% (■), 0.2wt% (▲) and 0.0 wt% (control ●). C) Intensity plot measured by DLS of PM16 micelles before (■) and 24 h after (□) the addition of 2.0 wt% H_2O_2. D) Intensity plot measured by DLS of PM16 micelles before (■) and 24 h after (□) the addition of 0.2 wt% H_2O_2. E) Z-Average size (top) and scatter count (bottom) distributions of PM16 micelles measured by DLS after addition of 0.007 wt% (2 mM) H_2O_2 (♦) compared with control (●) over 336 h. F) Z-Average size (top) and scatter count (bottom) distributions of PM16 micelles (repeated with independent batch) measured by DLS after addition of 0.007 wt% (2 mM) H_2O_2 (♦) compared with control (●) over 170 h.

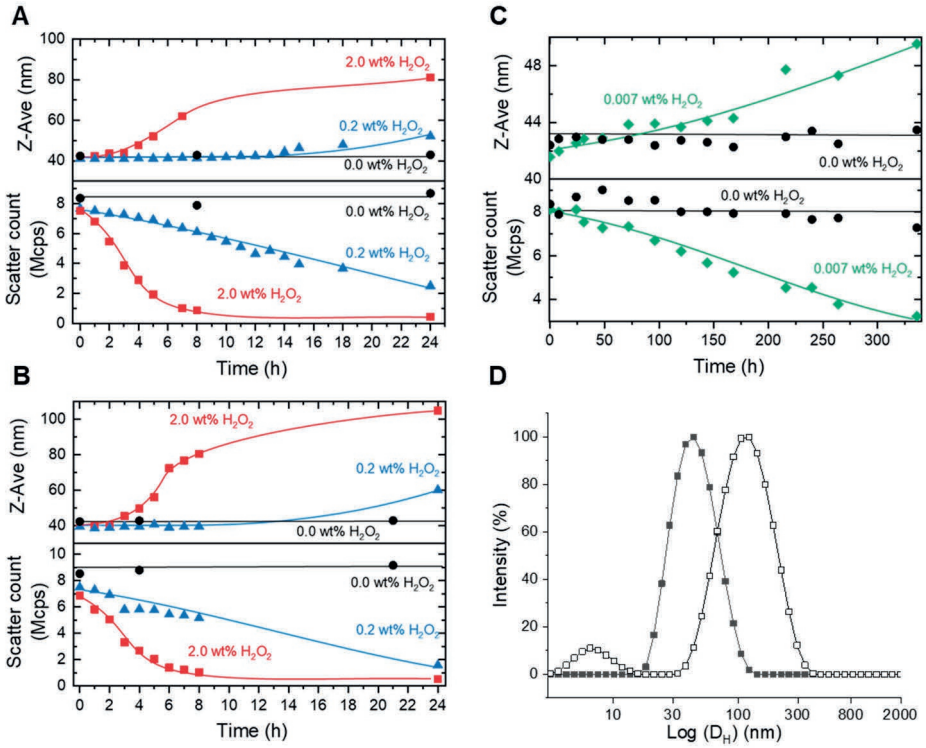

Figure S4. PM32 micelles in presence of different H_2O_2 concentrations at 37 °C. The curves are drawn as a guide for the eye. A) Z-Average size (top) and scatter count (bottom) distributions of PM32 micelles measured by DLS for three concentrations of H_2O_2: 2.0 wt% (■), 0.2 wt% (▲) and 0.0 wt% (control ●). B) Z-Average size (top) and scatter count (bottom) distributions of PM32 micelles (repeated with independent batch) measured by DLS for three concentrations of H_2O_2: 2.0 wt% (■), 0.2 wt% (▲) and 0.0 wt% (control ●). C) Z-Average size (top) and scatter count (bottom) distributions of PM32 micelles measured by DLS after addition of 0.007 wt% (2 mM) H_2O_2 (♦) compared with control (●) over 336 h. D) Intensity plot measured by DLS of PM32 micelles before (■) and 24 h after (□) the addition at of 2.0 wt% H_2O_2.

TEM images of the polymeric micelles before and after H_2O_2 treatment

To 1.0 mL of a 1.0 mg/mL micellar dispersion of p(DMA_m-b-$MTPA_n$) prepared as previously described was added 66 µL of stock solutions of H_2O_2 in phosphate buffer (100 mM, pH = 7.4) with variable concentration to yield a final H_2O_2 concentration of 0.0 and 2.0 wt%. After 24 hours the samples were prepared for TEM by adding 3.0 µL p(DMA_m-b-$MTPA_n$) micelles solution onto a Formvar/Carbon 400 mesh Cu grid. 3.0 µL uranyl acetate stain (2 wt% in H_2O) was pipetted on the grid, which was then washed with Milli-Q water and dried on filter paper 3 times. The grid was finally loaded on the TEM single tilt holder to acquire the pictures of the samples. For the statistical analysis of the micelles diameters, about 20 images were made of each of the samples. TEM images were analysed manually using ImageJ.[4]

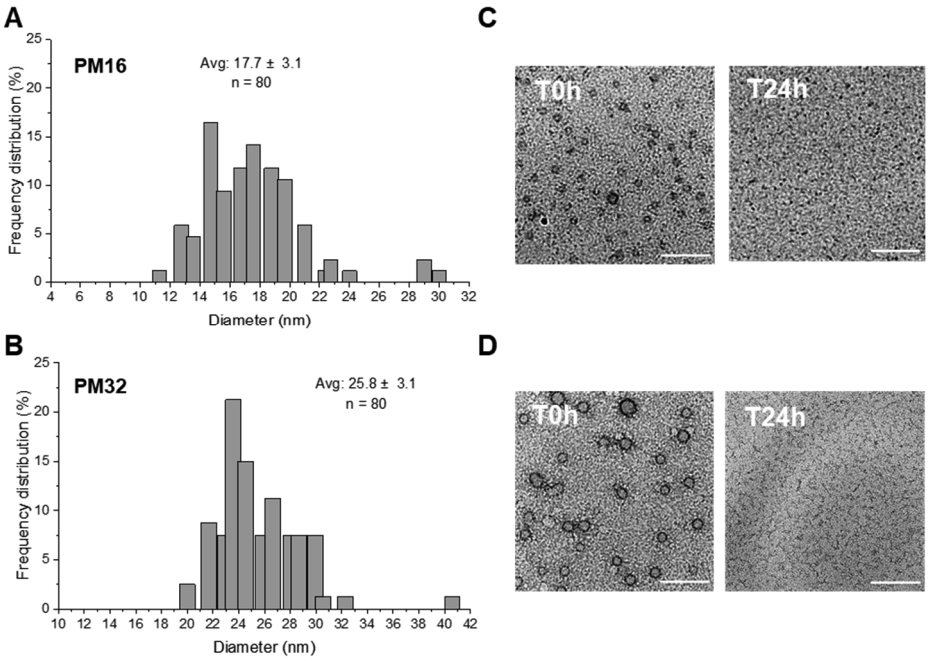

Figure S5 TEM images and particle analysis of PM16 and PM32 micelles stained with 2.0 wt% uranyl acetate. A) Normalized frequency distribution based on TEM images analysis of PM16 micelles. B) Normalized frequency distribution based on TEM images analysis of PM32 micelles. C) TEM images (Scale bar = 100 nm) of PM16 micelles before (left) and 24 h after (right) the addition of 2.0 wt% H_2O_2. D) TEM images (Scale bar = 100 nm) of PM32 micelles before (left) and 24 h after (right) the addition of 2.0 wt% H_2O_2.

Cryo-EM images of the polymeric micelles before and after H_2O_2 treatment

To two vials was added 2.0 mL each of a 1.0 mg/mL micellar dispersion of p(DMA_m-b-$MTPA_n$) prepared as previously described. To one of these vials, 132 µL of a stock solution of H_2O_2 in PB (100 mM, pH = 7.4) was added to reach final H_2O_2 concentration of 0.2 wt% to take Cryo-EM pictures after 24 hours. To the second vial, 132 µL of phosphate buffer (100 mM, pH = 7.4) was added to obtain the sample without H_2O_2. The samples were centrifuged (4000 rpm for 15

minutes) using 10 kDa filters and concentrated to 20 mg/mL afterwards. The concentrated in 100 µL volume was washed with additional 100 µL H_2O, obtaining a final concentration of 10 mg/mL. Cryo-TEM images were obtained by adding 4 µL of the 10 mg/mL micellar solution onto a Quantifoil 1.2/1.3 200 mesh Cu grid. The drop was blotted for four seconds with filter paper to obtain a thin layer on the grid, and vitrified by rapid immersion in liquid ethane (Leica EM GP version 16222032). The grid was finally inserted into a cryo-holder (Gatan model 626) and then transferred to the Jeol JEM 1400 plus TEM. For the statistical analysis of the micelles diameters, about 20 images were made of each of the samples. Cryo-EM images were analyzed manually using ImageJ.

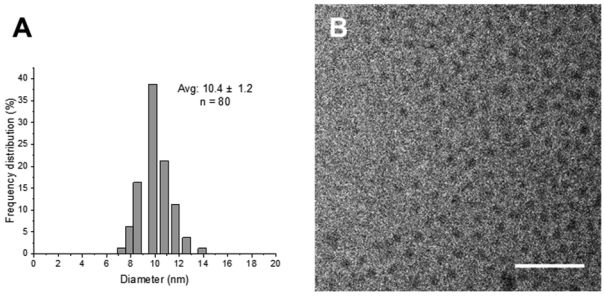

Figure S6 Cryo-EM images and particle analysis of PM16 micelles A) Normalized frequency distribution based on Cryo-EM images analysis of PM16 micelles. B) Cryo-EM image (Scale bar = 100 nm) of PM16 micelles.

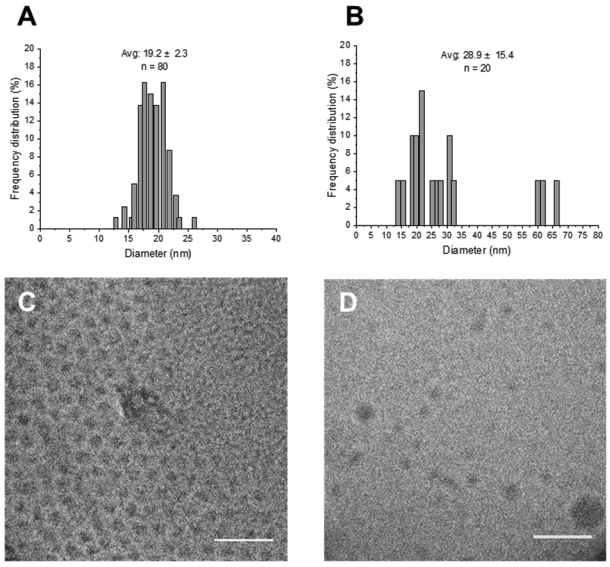

Figure S7 Cryo-EM images and particle analysis of PM32 micelles before and 24 h after the addition of 0.2 wt% H_2O_2. A) Normalized frequency distribution based on Cryo-EM images analysis of PM32 micelles. B) Normalized frequency distribution based on Cryo-EM images analysis of PM32 micelles 24 h after the addition of 0.2 wt% H_2O_2. C) Cryo-EM image (Scale bar = 100 nm) of PM32 micelles. D) Cryo-EM image (Scale bar = 100 nm) of PM32 micelles 24 h after the addition of 0.2 wt% H_2O_2.

2.5.5 ^{1}H NMR study of p(DMA$_n$-b-MTPA$_m$) micelles before and after H_2O_2 treatment

To 0.5 ml of p(DMA$_m$-b-MTPA$_n$) micelles (8.0 mg/mL) in a NMR tube was added 55 µL D_2O and 33 µL H_2O_2 (30 wt%). NMR tubes were kept at 37 °C during all the experiments. The first ^{1}H NMR spectrum was taken right after the addition of H_2O_2 (t=0) and, subsequently, a measurement is taken every hour until no change in conversion was detected. The conversion (%) of **1** and **2** was measured calculating the percentage of the integral of the respective aromatic peaks at 7.64 and 7.77 ppm for each time point against the total integral value obtained at the end of the acquisitions. The peak between 2.87 and 3.24 ppm corresponding to the protons of p(DMA$_n$) was used as reference.

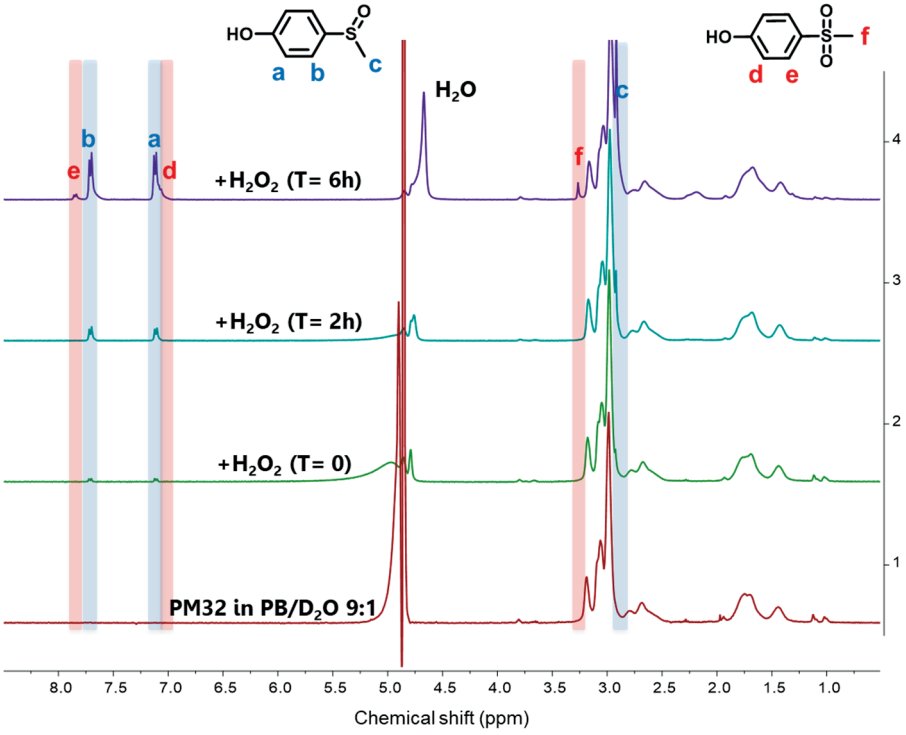

Figure S8. ^{1}H NMR of PM32 micelles after treatment with 2.0 wt% of H_2O_2 in PB (100 mM, pH = 7.4) at 37 °C.

^{1}H NMR study of p(DMA$_n$-b-MTPA$_m$) micelles at different pH

p(DMA$_m$-b-MTPA$_n$) micelles (8.0 mg/mL) were prepared separately in PB (100 mM) with different pH: 5.0, 6.0, 7.4. From each micellar dispersion, 0.5 mL were added in a NMR tube together with 55 µL D_2O and 33 µL of the appropriate phosphate buffer at 37 °C. ^{1}H NMR measurements were taken every 24 h for 6 days. The conversion (%) of **1** was measured calculating the percentage of the difference between the integral of the peak in the aromatic region at 7.64 ppm for each time point and the integral of the same region at t=0, divided by the expected integral for the complete removal of **1**. The peak between 2.87 and 3.24 ppm corresponding to the protons of p(DMA$_n$) was used as reference.

2.5.6 Cargo load and release of p(DMA$_n$-b-MTPA$_m$) micelles

Determination of micelle loading with Nile Red

A Nile Red solution in THF (20 µL, 1.0 mg/mL) was added to the previously prepared micellar dispersions of p(DMA$_m$-b-MTPA$_n$) (1.0 mL, 1.0 mg/mL) and incubated in the dark in an open vial to evaporate the organic solvent. The nonencapsulated payload was removed through centrifugation (5000 rpm, 10 minutes) and 900 µL DMF was added to 100 µL of the Nile Red-loaded micellar dispersions. The fluorescence of the solution was measured at an excitation wavelength of 540 ± 20 nm and emission wavelength 620 ± 30 nm and compared to the calibration curve of known concentrations Nile Red in PB (100 mM, pH = 7.4)/ DMF 1:9 (Figure S9), to determine the Nile Red loading per mg of polymer. Drug loading (DL) and encapsulation efficiency (EE) were calculated as follows (Equations S3 and S4, respectively).

$$\mathrm{DL(w/w)} = \frac{\text{amount of loaded drug}}{\text{amount of polymer}} \quad \textbf{Equation S3}$$

$$\mathrm{EE(w/w\%)} = \frac{\text{actual amount of loaded drug}}{\text{theoretical amount of loaded drug}} \quad \textbf{Equation S4}$$

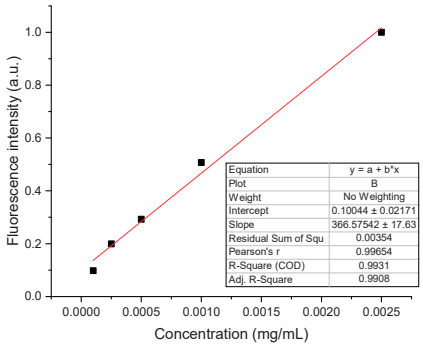

Figure S9. Nile Red calibration curve in phosphate buffer (100 mM, pH = 7.4)/ DMF 1:9.

Table S3. Properties of PM16 and PM32 micellar dispersions (1.0 mg/mL). The average hydrodynamic diameter (DH) is determined with DLS. The drug loading (DL) and encapsulation efficiency (EE) of Nile Red in the micelles were determined with fluorescence spectroscopy.

Polymer	D_H [unloaded] (nm)	DL (µg/mg polymer)	EE (%)
PM16	31.6 ± 0.5	2.4	12
PM32	42.4 ± 0.9	3.6	18

H_2O_2-triggered release of Nile Red from p(DMA_n-b-$MTPA_m$) micelles

A Nile Red solution in THF (20 µL, 1.0 mg/mL) was added to the previously prepared micellar dispersions (1.0 mL, 1.0 mg/mL) and incubated in the dark in an open vial to evaporate the organic solvent. The micellar dispersions were divided over three vials for each polymer and hydrogen peroxide solution was added to a final concentration of 0, 0.2 and 2.0 wt% for each series. The fluorescence of the solution was measured on a Synergy H1 (Biotek) microplate reader at 37 °C, using an excitation wavelength of 540 ± 20 nm and emission wavelength 620 ± 30 nm. The release percentage for each sample at specific time point was determined by subtracting the fluorescent value (F_t) from that of the

sample before the addition of H_2O_2 (F_{t0}), and the percent fluorescence remaining was determined by normalization to the same value (F_{t0}).

2.5.7 Cell viability assay on p(DMA_n-b-$MTPA_m$) micelles

HeLa cells in DMEM culture medium supplemented with 10% fetal bovine serum (Gibco, life technologies™) and 1% Penicillin/Streptomycin (100x, Biowest) under humidified normoxic (95% air, 5% CO_2) were plated at 2000 cells/well (suspended in 200 µL cell culture medium) in a 96-well plate and incubated at 37 °C. After 3 days, 20 µL of both PM16 and PM32 micelles (0.0-11 mg/mL) in PBS (phosphate buffer saline, pH = 7.4) was added to each well, to reach final micelles concentrations in the range (0.0-1000 µg /mL). After 24 hours, the micellar solutions were removed, the cells were washed with PBS for three times, and 200 µL of fresh culture medium was added. The cells have been allowed to grow for an additional 3 days, then their cytotoxicity was evaluated using the WST-8 assay (Cell Counting Kit-8, Dojindo Laboratories, Tebu-Bio). For this test, 10 µL of CCK-8 reagent was added to each well and incubated for 3 hours, then the absorbance at 450 nm was measured using a microplate scanning spectrophotometer (PowerWave XSTM, Bio-Tek). The surviving fraction (SF) of the Hela Cells was calculated according equation S5.

$$SF = \frac{Abs(450)_{sample} - Abs(450)_{blank}}{Abs(450)_{control} - Abs(450)_{blank}} \quad \textbf{Equation S5}$$

$Abs(450)_{sample}$ is the absorbance at 450 nm for cell incubated with p(DMA_n-b-$MTPA_m$) micelles;

$Abs(450)_{control}$ is the absorbance at 450 nm for cell incubated with 10 µL of PBS;

$Abs(450)_{blank}$ is the absorbance at 450 nm for vials without addition of CCK-8 reagent.

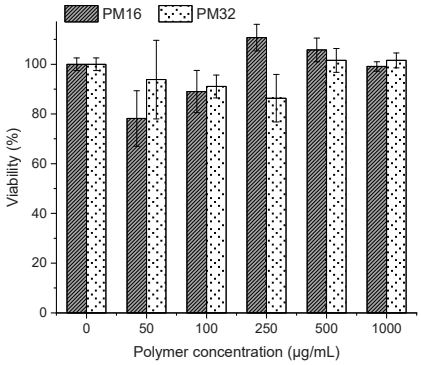

Figure S10. PM16 and PM32 cytocompatibility in HeLa cells cultured in DMEM culture medium. Cells were treated with micellar dispersions between 0.0 and 1.0 mg/mL in phosphate buffered saline (PBS) (20 uL/220 uL well). After 24 h cell viability was measured by WST-8 assay.

2.5.8 Supplementary references

1 A. Rostami and J. Akradi, *Tetrahedron Lett.*, 2010, **51**, 3501.

2 F. Secci, A. Frongia and P. P. Piras, *Tetrahedron Lett.*, 2014, **55**, 603.

3 R. Kakuchi and P. Theato, *Macromolecules*, 2012, **45**, 1331.

4 C. A. Schneider, W. S. Rasband and K. W. Eliceiri, *Nat. Methods*, 2012, **9**, 671.

2.5.9 Spectra overview

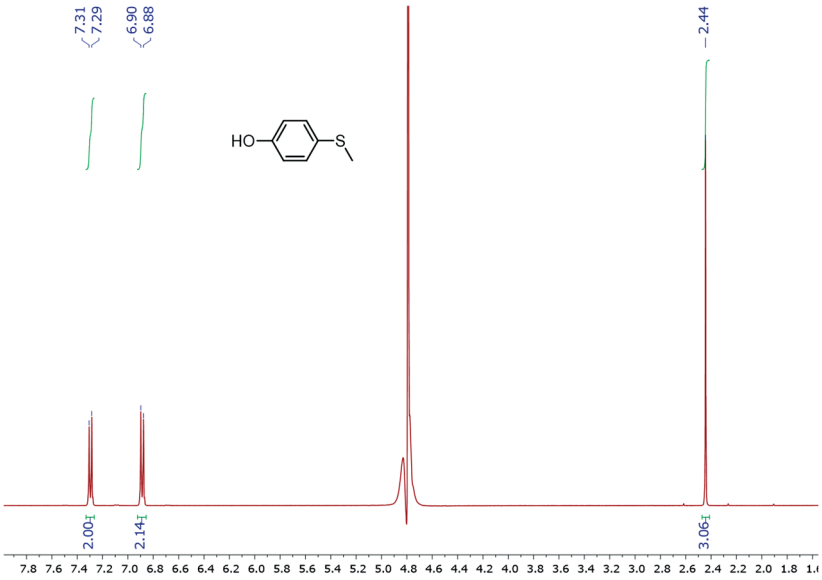

^{1}H NMR spectrum (400 MHz) of 4-(methylthio)phenol in PB (100 mM, pH=7.4)/D_2O 9:1.

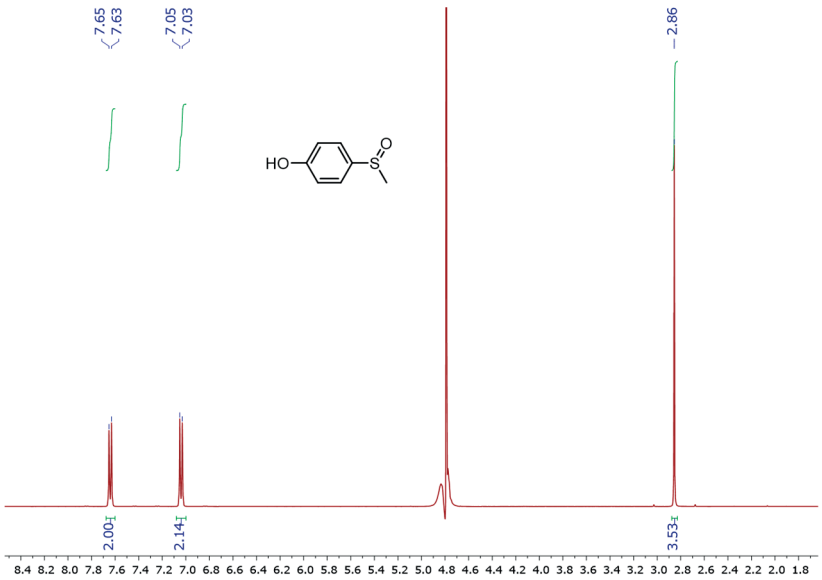

^{1}H NMR spectrum (400 MHz) of 4-(methylsulfinyl)phenol in PB (100 mM, pH=7.4)/D_2O 9:1.

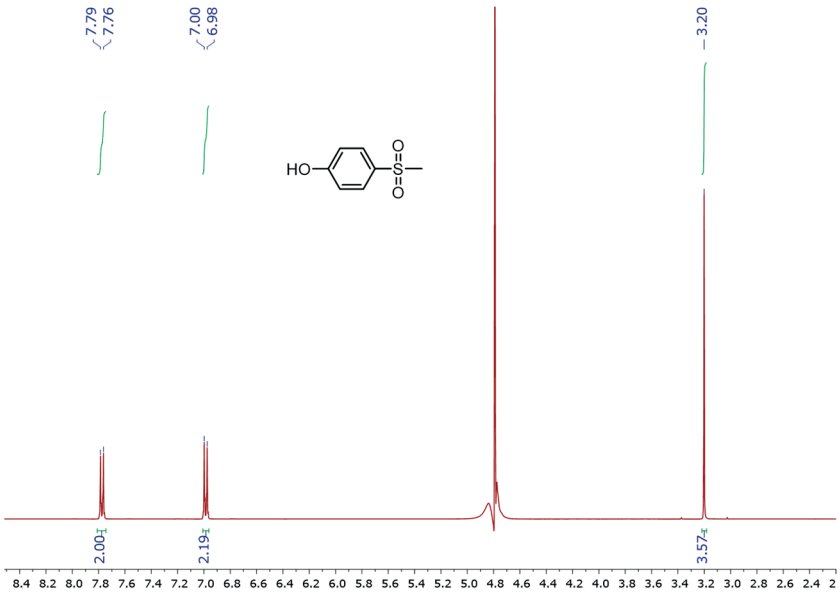

^{1}H NMR spectrum (400 MHz) of 4-(methylsulfonyl)phenol in PB (100 mM, pH=7.4)/D_2O 9:1.

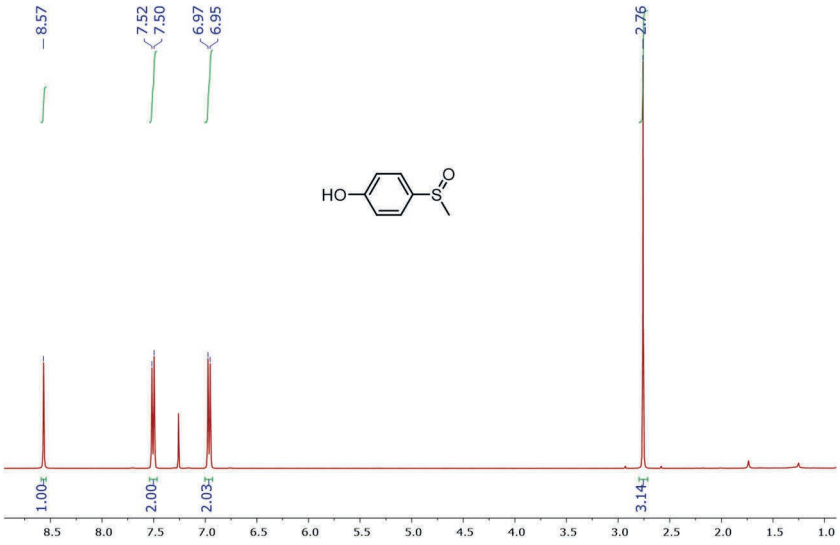

^{1}H NMR spectrum (400 MHz) of 4-(methylsulfinyl)phenol in $CDCl_3$.

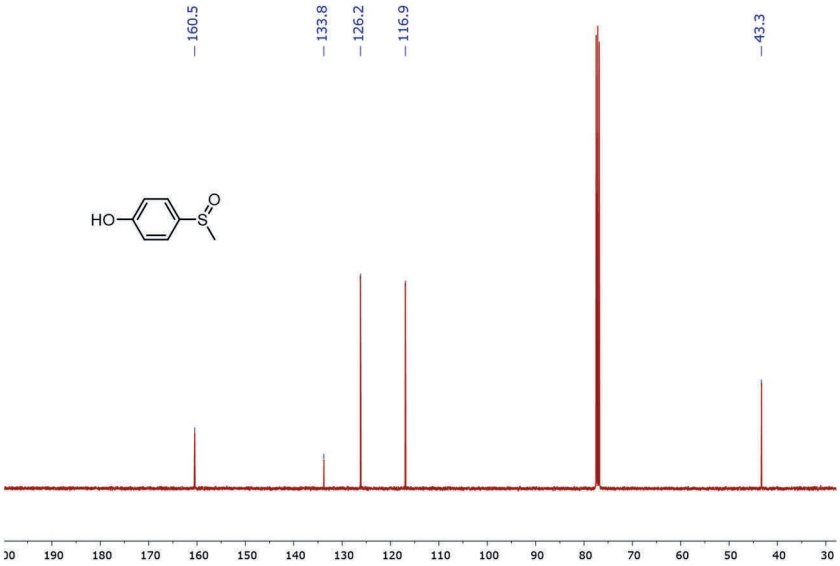

^{13}C NMR spectrum (101 MHz) of 4-(methylsulfinyl)phenol in $CDCl_3$.

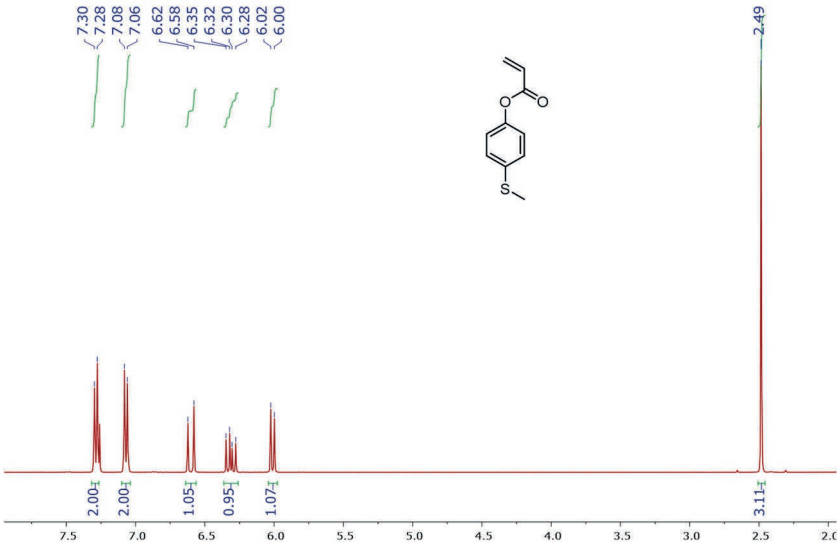

^{1}H NMR spectrum (400 MHz) of 4-(methylthio)phenyl acrylate in $CDCl_3$.

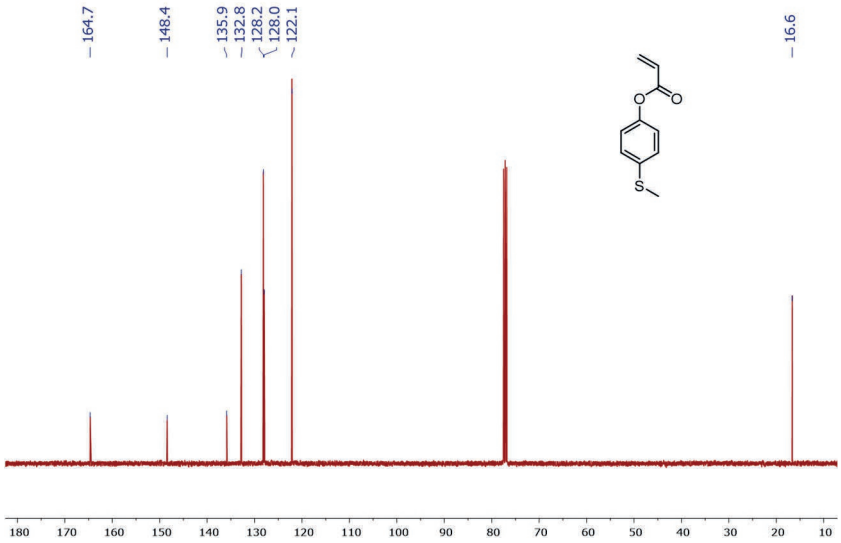

^{13}C NMR spectrum (101 MHz) of 4-(methylthio)phenyl acrylate in $CDCl_3$.

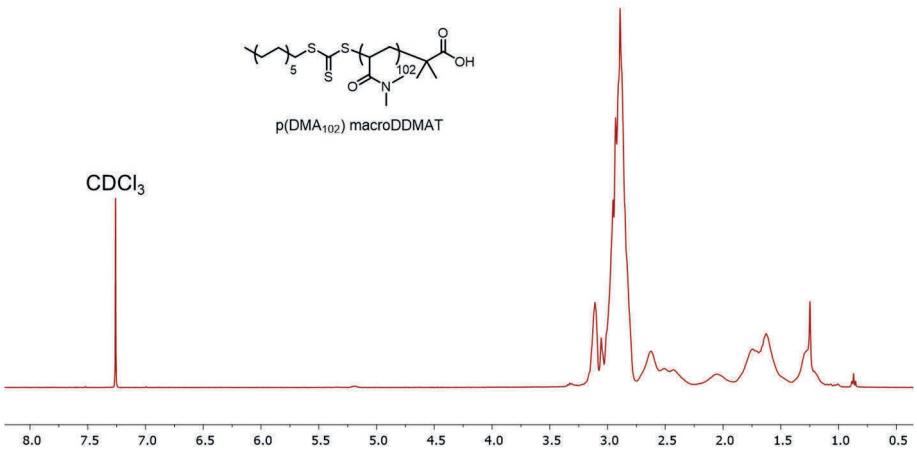

^{1}H NMR spectrum (400 MHz) of p(DMA_{102}) macroDDMAT in $CDCl_3$.

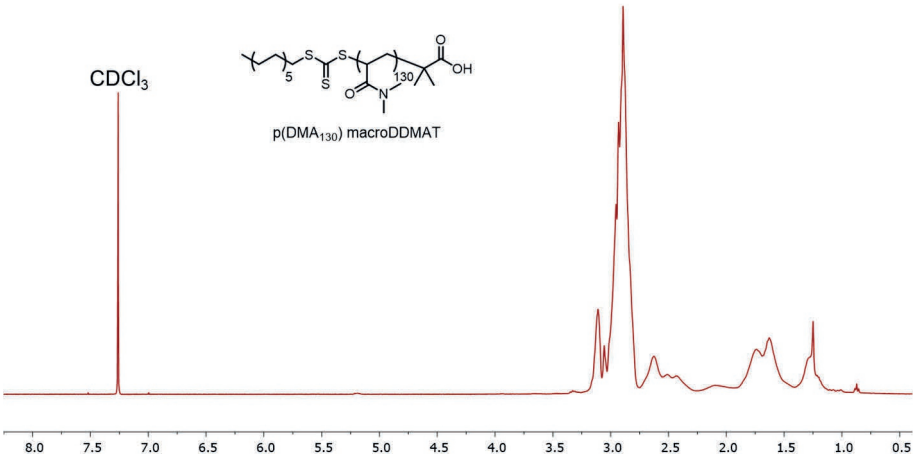

^{1}H NMR spectrum (400 MHz) of p(DMA_{130}) macroDDMAT in $CDCl_3$.

Chapter 3

Enhancing trigger sensitivity of nanocarriers through organocatalytic oxidant activation

The redox balance in tumor and diseased cells is often compromised, leading to overproduction of reactive oxygen species (ROS). Many ROS-responsive nanocarriers based on sulfur oxidation have been reported with the goal of achieving controlled delivery at the tumor. However, these materials often lack responsiveness to the tumor environment. In nature, enzymatic turnover is often used to amplify response to low concentration signals. Analogously, we use organocatalysis to achieve an enhanced response of oxidation-triggered thioether based nanocarriers. Using block copolymer micelles that can disassemble through thioether oxidation followed by ester hydrolysis, this work shows how an *in situ* formed imine oxidation catalyst can enhance disassembly kinetics at millimolar hydrogen peroxide concentration. In presence of organocatalysis, Nile Red loaded micelles release their cargo twice as fast as under uncatalyzed conditions. This work demonstrates that organocatalysis can be a valuable strategy to increase the responsiveness of biomarker triggered delivery systems.

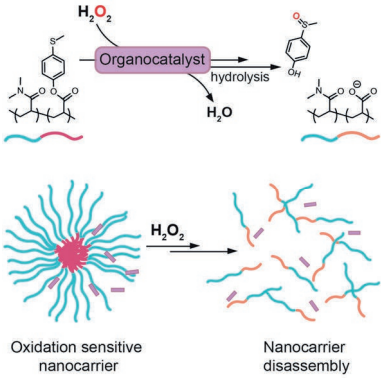

This chapter is based on:

I. Piergentili, M. Cai, B. Klemm, B. Xu, S. Luo, R. Eelkema, *Cell Reports Physical Science,* 2023.

3.1 Introduction

Oxidative stress is an imbalance of the reactive oxygen species (ROS) generated in metabolic pathways.[1-5] Such imbalance can be found in inflamed tissue and the tumor microenvironment. There is a great interest in materials able to respond to oxidative species such as H_2O_2, to target therapeutics to these tissues. Based on this concept, several examples of ROS-responsive materials have been reported, using redox-sensitive elements ranging from sulfur or selenium to boron.[6-12] Building on the work of Hubbel and coworkers on the use of polythioether based nanocarriers for targeted drug delivery in 2004,[10] the conversion of hydrophobic thioethers to hydrophilic sulfoxide upon reaction with H_2O_2 has been employed extensively to trigger the disassembly of polymeric structures.[13-15] Most of the thioether-bearing systems that have been tested with submillimolar concentrations of H_2O_2 show response times of many days and even weeks to achieve thioether oxidation and nanocarrier destruction, which limits their applicability in biologically relevant conditions (50 – 100 μM).[16-18] Due to the slow oxidation kinetics of thioethers with H_2O_2, even slightly reducing these timescales, while maintaining material stability and encapsulation efficiency, can be very challenging. In nature, biochemical signals are often present in micromolar concentrations or lower. Cells commonly use enzymes and enzymatic cascades to amplify these signals by catalytic turnover. Such strategies can be useful to couple targeted drug delivery to the presence of biomarker signals.[19-21] Low molecular weight organocatalysts could prove highly useful for this purpose as they are generally easy to make and use, and often far less toxic than their transition metal based counterparts.[22] Still, outside the realm of (enantioselective) synthesis of small molecule targets, organocatalysis is only sparingly applied, for instance to promote bond formation in polymer synthesis[23-26] or in dynamic covalent networks.[27,28] Here, we propose the use of organocatalysis to increase the sensitivity of nanocarriers to ROS, enabling

sulfur functionalized surfactants to respond to low concentrations of H_2O_2 at reduced timescale.[29,30] Despite many successful examples of organocatalysis to accelerate the oxidation of small molecule thioethers with H_2O_2,[31-35] application of organocatalysis to augment nanocarrier response has been greatly overlooked.

We recently reported block copolymer micelles that are able to degrade in presence of H_2O_2 through the oxidation-triggered hydrolysis of their thioanisole ester based micellar core.[36] The conversion of a thioether into a more electron withdrawing group such as a sulfoxide triggers the hydrolysis of the adjacent ester, unmasking the acrylate anion on the polymer backbone (Figure 1). This solubility change in aqueous environment leads to the disassembly of the micelles. This logic gate behavior enables the use of these micelles as nanocarriers for targeted delivery and release systems. In this oxidation-hydrolysis cascade, the slow oxidation[37] is the rate limiting step. For this reason, high concentrations of H_2O_2 are often needed to achieve a material response on an hour timescale.[38] We found that these micelles fully disintegrate within 2 hours when elevated concentrations of H_2O_2 (600 mM) were used. This timescale extended to 168 h for 2 mM of H_2O_2 (2.2 eq. relative to the estimated thioether units on the polymer). Similar to other thioether based nanocarrier systems, such high concentrations of H_2O_2 have limited clinical relevance, posing an incentive to develop methods that will allow the acceleration of thioether oxidation at lower concentration.

In the context of enhancing the response of ROS-triggered nanocarriers, we found the prospect of using a simple organocatalyst highly appealing. For this purpose, we had to develop an organocatalyst for the oxidation of thioethers with hydrogen peroxide. In the 1950's, Emmons studied the synthesis and stability of oxaziridines as alternative to organic peroxides,[39] and subsequently many other researchers started to employ this oxidant as a catalyst in sulfoxidations.[40-43] In 1994 the Page group reported the oxidation of alkyl aryl sulfides, using a

stoichiometric amount of imine to activate H_2O_2.[44] The need of extra activating agents or bases for *in situ* generation of oxaziridine in these methods discouraged its application for oxidation under mild conditions.[45] Still, based on previous work from our group,[46] we chose to investigate a two-component imine catalyst that spontaneously forms from a mixture of $PhCOCF_3$ and primary amines. $PhCOCF_3$ can form an imine by reaction with amines, activating H_2O_2, likely through an oxaziridine-like intermediate. This species is more electrophilic than H_2O_2 alone due to the electron withdrawing ketone, and it is effective even in neutral conditions, which will be important for use in biological environments. We considered the use of water-soluble amines to increase the solubility of the hydrophobic $PhCOCF_3$. The latter was found as the most promising ketone for the imine formation due to the strongly electron withdrawing CF_3 group. We included -*t*Bu functionalized amines in our study considering that the presence of tert-butyl groups adjacent to the nitrogen was shown to be important to ensure heterocycle stability.[39]

Based on these considerations, we here present a cooperative ketone/amine catalyst to oxidize the thioether based hydrophobic block of block copolymer surfactants in presence of H_2O_2 (Figure 1), leading to improved micelle disassembly rates. This approach constitutes a step forward to obtain oxidation triggered drug delivery and release systems able to respond to H_2O_2 levels approaching the concentrations produced by in tumors and diseased tissue.

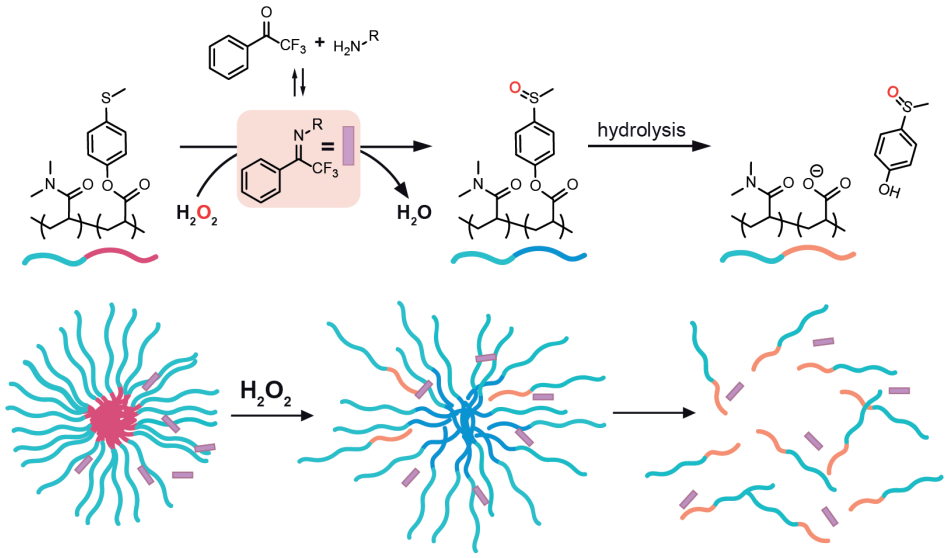

Figure 1. General concept of *in situ* imine formation used to catalyze the oxidation of PM16 micelles with H_2O_2. The conversion of thioether moieties to sulfoxides triggers the hydrolysis of the hydrophobic domain of the amphiphilic polymer, leading to disassembly of the micelles.

3.2 Results and discussion

3.2.1 Screening of ketone/amine catalysis for the oxidation of thioether ester molecular model

Based on its efficient α-hydroxylation of β-ketocarbonyls,[46] we investigated combined ketone/amine catalysis to activate H_2O_2 for thioether oxidation. We first chose 4-(methylthio)phenyl acetate **1** (Figure 2A) as molecular model of the ROS-responsive moiety of the thioanisole-ester based block copolymer micelles. We then screened conditions for the oxidation of **1** with 1.5 eq. of H_2O_2 using different catalysts and solvents (Figure 2C). $PhCOCF_3$ (**3**) was selected as ketone catalyst because of the strongly electrophilic carbonyl group and its proven catalytic activity towards thioether oxidation.[47] Our experiments showed that ketone **3** was indeed fundamental to achieve the oxidation of **1** into the

corresponding sulfoxide **2** (Figure 2C, entry 2 and 3). When **3** was used with amine **A1** as catalytic system in the oxidation of **1** with H_2O_2 in tert-butanol (^{t}BuOH), we obtained 85% yield of **2** in 3h (Figure 2C, entry 1). Under the same conditions, substituting **A1** with **A2** and **A3** led to yields of 65% (Figure 2C, entry 6) and 71% (Figure 2C, entry 7), respectively. Entries 8-11 report a decrease in the yields of **2** when the oxidation of **1** with H_2O_2 in presence of **3**/**A1** was carried in other solvents. The effect of the solvent can indeed be decisive in sulfoxidation reactions,[48] and ^{t}BuOH provided the best outcome in our case. The use of 2.0 eq. of H_2O_2 in the standard conditions afforded only 47% yield of **2**, caused by substantial overoxidation to the corresponding sulfone. The oxidation to sulfone of the thioether units on the block copolymer would possibly accelerate the hydrolysis of the ester and consequently the ROS-triggered micellar disassembly. However, our ultimate objective is to achieve a response of the thioanisole ester based micelles to very low H_2O_2 concentrations, therefore increasing the ratio of H_2O_2 to thioether was considered counterproductive to the aim of this work.

Once confirmed that the standard conditions provide the best performance for the oxidation of **1**, we pursued to follow the consumption of **1** by GC (Figure 2B, orange) over time. We found that the reaction reached completion after 5 hours. This result was similar when 0.5 mL buffer (0.1 M phosphate buffered saline (PBS), pH = 6.95) was added (Figure 2B, blue), demonstrating that the presence of aqueous buffer does affect the oxidation kinetics. In contrast, the absence of **3** drastically decreased the rate of sulfoxidation (Figure 2B, red), meaning that the presence of the ketone was fundamental to our system.

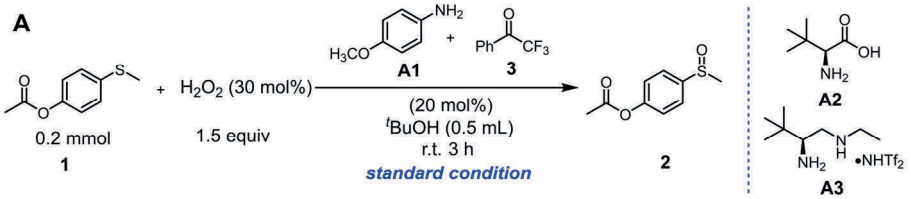

B

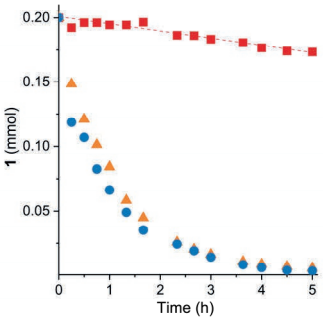

C

Entry	Variations from standard conditions[a]	Yield[b] (%)
1	none	85
2	without **3**	n.r.
3	acetone instead of **3**	n.r.
4	without H_2O_2	n.r.
5	without amine **A1**	20
6	**A2** instead of **A1**[c]	65
7	**A3** instead of **A1**[c]	71
8	PhMe/DCE instead of ^{t}BuOH	54
9	HFIP instead of ^{t}BuOH	73
10	EtOH/MeOH (4:1) instead of ^{t}BuOH	65
11	3 mL ^{t}BuOH[d]	80
12	2 equiv. of H_2O_2	47

Figure 2. A) Left: Scheme of the standard reaction conditions used to test ketone/amine catalysis on the oxidation of 4-(methylthio)phenyl acetate **1**. Right: Additional amino catalysts used in the study. B) Kinetic order plots for: standard condition (orange ▲), standard condition with the addition of 0.5 mL buffer (0.1 M PBS, pH = 6.95) (blue ●), standard condition without the addition of **3** (red ■). C) Obtained yield of **2** varying the standard condition. [a] Reactions were performed with **1** (0.2 mmol), **A1** (20 mol%), **3** (20 mol%), and H_2O_2 (30% wt.%, 0.3 mmol) in 0.5 mL tBuOH at room temperature in air for 3 h. [b] The yield was determined by GC analysis using n-dodecane as an internal standard (n.r. = no reaction). [c] The reactions were performed in toluene/dichloroethane (v/v 1:1). [d] The reaction was conducted for 8 hours.

Despite the superior results obtained for the sulfoxidation of **1** using **A1** as amino catalyst, the acute toxicity of p-anisidine **A1** discouraged us to employ it for drug delivery purposes. Therefore, in the investigation of H_2O_2-induced degradation of block copolymer micelles in presence of the ketone/amine catalysts, we mainly focused on the use of **A2** and **A3**.

3.2.2 Synthesis and characterization of PM16 micelles

The block copolymer p(DMA_{130}-b-$MTPA_{16}$), abbreviated as PM16, was synthesized via light-initiated RAFT polymerization as we previously described.[36] With 4-(methylthio) phenyl acrylate (MTPA) as hydrophobic monomer and N,N-dimethylacrylamide (DMA) as hydrophilic monomer, this amphiphilic polymer formed micelles in sodium phosphate buffer (1.0 mg/mL in 100 mM PB, pH = 7.4) with an average hydrodynamic diameter (D_H) of 31.6 ± 0.5 nm, measured by dynamic light scattering (DLS). A polymer concentration of 8.0 mg/mL afforded a D_H of 27.3 ± 0.3 nm. This slight decrease in PM16 micelles size for higher polymer concentration was probably due to the multi-scattering registered by DLS in presence of the higher number of micelles.[49]

3.2.3 Ketone/amine catalyzed H_2O_2 induced oxidation and hydrolysis of PM16 micelles

With the micelles and the optimized catalytic conditions in hand, the next step was to study the impact of catalysis on the H_2O_2 induced oxidation and hydrolysis of the thioether ester moieties on PM16. In neutral aqueous media, the formation of the imine catalyst is disfavored over the separate ketone and amine components.[22] Premixing $PhCOCF_3$ and the amine was fundamental to ensure catalytic activity in PM16 oxidation. The solution of **3**/amine using either **A2** or **A3** (0.2, 0.3 and 1.0 eq. compared to the estimated number of thioether functionalities) was added to PM16 (6.8 mg/mL) in PB/D_2O 9:1 (Scheme 1). After the addition of 10 mM H_2O_2, the reaction was followed at 37 °C by ^1H NMR spectroscopy over time. We analyzed process progression through the integration of the sharp aromatic peaks of **4** (Reference in Spectra section, SI), which is the degradation product obtained from the polymer hydrolysis after oxidation.[36]

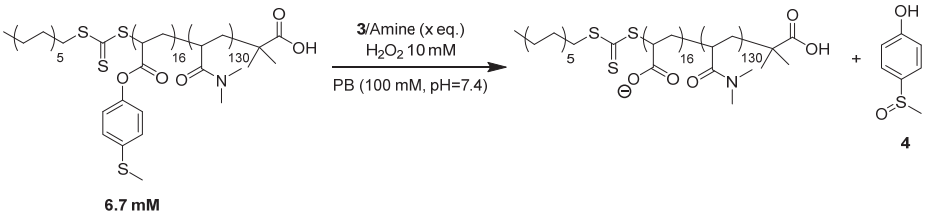

Scheme 1. Ketone/amine catalysis of PM16 block copolymer micelle (6.7 mM thioether units) oxidation by H_2O_2, followed by ester hydrolysis.

The addition of 10 mM H_2O_2 to the micelles, in the absence of a catalyst, led to the formation of 94 % of **4** in 123 h (Figure 3A). A similar conversion was obtained when 0.2 eq. of **3**/**A3** was added with H_2O_2 to the micelles, but now the conversion to **4** reached 50% ($T_{1/2}$) within 25 h against the 39 h necessary without a catalyst present (Figure 3B). Increasing the amount of **3**/**A3** catalyst to 0.3 eq. further reduced the half-life time to 19 h. Using **A2** together with **3** as catalysts in the H_2O_2-triggered oxidation of the micelles led to $T_{1/2}$ about 17 and 11 h when 0.2 and 0.3 eq. were used, respectively. Interestingly, for these catalytic conditions, we observed sigmoidal profiles of **4** formation, meaning that the degradation mechanism mainly follows the autocatalytic behavior of sulfoxidation and hydrolysis of the PM16 micelles.[36, 50, 51] The dramatic improvement in the rate of PM16 oxidation and hydrolysis with higher amount of **3**/**A2** brought us to push the system using 1.0 eq. of the catalyst mixture. In this case, 96% of **4** formed in 24 h, reaching $T_{1/2}$ in less than 7 hours (Figure 3B). Thus, with equal H_2O_2 concentrations, PM16 micelles degraded 5.5 times faster with catalysis than in catalyst-free conditions. For all experiments with 0.2-0.3 eq. catalysts, the ^{1}H NMR spectra at t=0 showed substantially diminished aromatic peaks of **3** (Figure S1 and S2), reaching an estimated integration corresponding to less than 0.1 eq. even when the conversion to **4** was close to 100% at t =120 h. This observation suggests that **3** is first partially encapsulated

in PM16 micelles and then in the residual clusters of the hydrolyzed polymer chains.[36] In contrast, the signals of the **A2** were clearly visible in all the ^{1}H NMR spectra, confirming that L-*tert*-leucine is well solubilized in the aqueous phase. These observations suggest that the ketone and amine continuously form enough imine catalyst at the interface of the core and the corona of PM16 micelles to activate the H_2O_2 that surrounds the micelles.

To further investigate the role of the different catalysts into the PM16 micelles oxidation and hydrolysis, we also studied the catalytic effect of having only **3** present (Figure 3C). After the addition of 10 mM H_2O_2 to the micellar dispersions, the $T_{1/2}$ was about 7 and 17 h for respectively 1.0 and 0.2 eq. of **3**. Surprisingly, these results were similar to those obtained when mixtures of **3** and **A2** were used as catalyst. However, roughly about t = $T_{1/2}$, the average conversion decreased compared to the combined use of **3**/**A2**, and large variance was observed for all data close to 90% conversion of **4**. Our interpretation here is that the kinetic profile would be heavily influenced by the scarce solubility of **3** when the micelles gradually disassembled. H_2O_2-activation by **3** is well known,[47, 52, 53] but in neutral conditions the formation of the corresponding dioxirane is considered unfavorable.[53-55] Possibly, $PhCOCF_3$ activates H_2O_2 by forming the corresponding perhydrate. However, this perhydrate is a metastable compound that continuously reverts to $PhCOCF_3$ and H_2O_2.[56] When at t = $T_{1/2}$ more than 0.5 eq. of H_2O_2 was consumed, the formation of the perhydrate became progressively less favored. In addition, the first part of the kinetic profile in presence of 0.2 eq. of **3** compares well with that in presence of 0.3 eq. of **3**/**A3** (Figure S3). However, after 24 h the conversion to **4** slowed down, aligning with the profile obtained with 0.2 eq. of **3**/**A3**. For **3**/**A3**, we noticed that the ^{1}H NMR signal at 0.97 ppm (the tert-butyl group of **A3**) completely disappeared after 18 h (Figure S1). This observation suggests that **A3** was not present in the system after that time point, resulting in **3** remaining as the only catalytic species. Likely,

the nucleophilic secondary amine group of **A3** substituted compound **4** on the ester moiety of the polymer, leading to a decrease of **A3** available for catalysis. This undesired effect is prevented by using **A2** because the primary amine is not nucleophilic enough to attack the carbonyl moiety of the ester in neutral conditions.[57] In fact, [**A2**] appeared to be constant over time (Figure S2) under the applied conditions. These observations explain the catalytic superiority of **A2** over **A3** and also the improved control and reproducibility compared to the exclusive use of **3**.

To confirm that **A2** does not act as a phase transfer catalyst, we synthesized *N*,*N*-dimethyl *tert*-leucine **A4**, a tertiary amine that is not able to form the imine with **3**, but may have influence on the solubility of the ketone. In the micellar degradation studies, we chose to have the amine 10 times in excess compared to the ketone to push the imine formation. We conducted these experiments with 0.2 eq. of **3** to have the conversion profile of **4** with only 0.2 eq. of the ketone as reference and, at the same time, to avoid an extreme excess of charged species (both **A2** and **A4**) that could destabilize the micellar system. In Figure 3D, we show how the use of 1:10 **3**/**A4** produced a profile in line with that one obtained in presence of only 0.2 eq. of **3**. Here, use of **A4** led to lower variance in the data. This effect confirms the assumption that once most of the micelles are disassembled, the catalytic activity of the ketone is influenced by its solubility in solution. The oxidation catalyzed by 1:10 **3**/**A2** compared to those in presence of 0.2 eq. of **3** and of 1:10 **3**/**A4** showed almost 2-fold faster formation of **4** as well as higher conversion (98% against 90-94%). Moreover, with only 0.2 eq. of **3** but a large excess of **A2**, we obtained a conversion profile similar to the one with 0.3 eq. of 1:1 **3**/**A2**. This dependency on the ratio **3**/**A2** confirms the formation of the imine. Here, despite the fact that the imine formation is disfavored in aqueous environment, an excess of the amine can promote this equilibrium and then activate H_2O_2, likely through an oxaziridine intermediate.

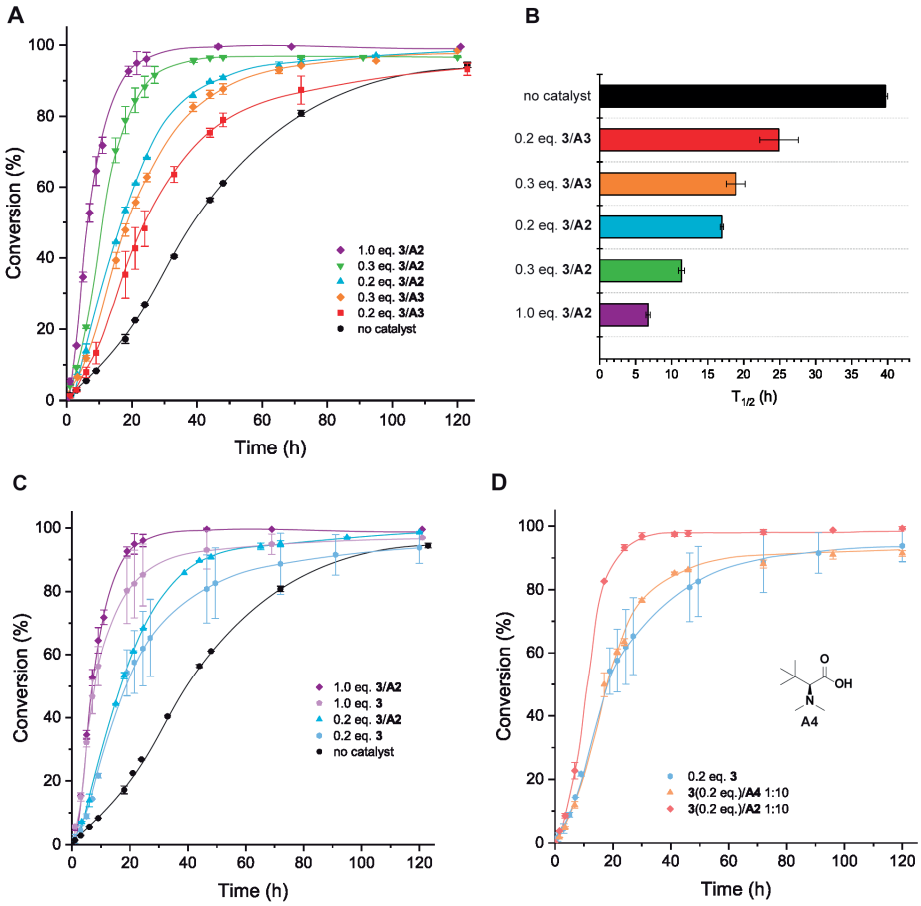

Figure 3. A) Conversion measured through ^{1}H NMR spectroscopy of **4** after addition of 10 mM H_2O_2 to PM16 micellar solutions (6.8 mg/mL) in PB (100 mM, pH = 7.4)/D_2O 9:1 at 37 °C. B) Evaluation of the use of different ketone/amino catalysts conditions based on $T_{1/2}$ of ^{1}H NMR conversion of **4**. C) Comparison of the ^{1}H NMR conversion of **4** in presence of 1.0 and 0.2 eq. of **3**/**A2** with 1.0 and 0.2 eq. of **3** in PM16 micelles degradation with 10 mM H_2O_2. D) Comparison of the ^{1}H NMR conversion of **4** between the use of 0.2 eq. of **3** with an excess of **A2** versus an excess of **A4** (10 eq. in respect to **3**) in PM16 micelles degradation with 10 mM H_2O_2. All curves are drawn as a guide for the eye.

3.2.4 Morphological study of ketone/amine catalyzed H_2O_2 induced oxidation and hydrolysis of PM16 micelles

After demonstrating that the cooperative catalysis between ketone and amine of H_2O_2 can enhance PM16 micelles oxidation and subsequent hydrolysis, we then pursued to study how this catalytic system would influence morphological change at the material level. To PM16 (6.7 mM thioether units at 6.8 mg/mL of polymer concentration) in PB, 0.2 eq. of premixed catalyst **3**/**A2** or **3**/**A3** was added. Then, similarly to ^{1}H NMR experiments, 10 mM H_2O_2 was added and the micelles were analyzed by DLS, following Z-average diameter (Figure S5A, top) and scatter count (Figure S5A, bottom) at different time points. In presence of **3**/**A2** as catalyst, the scatter count of PM16 micelles dropped from 12.0 to 1.6 Mcps in 48 h, reaching an equilibrium. The Z-average diameter of micelles remained constant during this time, but from 48 h onwards increased from 31 to 53 nm at 120 h (Figure S5A, ▲ blue line). When **3**/**A3** was employed as catalyst, the minimum scatter count was 2.9 Mcps and the Z-average diameter increased to 49 nm in 72 h, reaching 78 nm at 120 h (Figure S5A, ■ red line). These results show that the employed catalysis accelerated the H_2O_2-induced PM16 micelle disassembly compared to the control in which no catalyst was used (Figure S5A, ● black line). Interestingly, at the same concentrations of polymer and reactants in presence of **3**/**A2**, the minimum value in scatter count and the 90% conversion of **4** found in the ^{1}H NMR study were reached at the same time point (44 h) (Figure 4A, ▲ blue line). A similar outcome can be noted for the control experiments at 120 h. This effect confirms that the morphological change in the micellar structure is directly dependent on the ester cleavage into **4** and the acrylate anion. In the DLS data of the micelle degradation in presence of **3**/**A3**, the fast increase of the Z-average diameter together with the slow decrease in scatter count (Figure S5A, ■ red line) suggests the formation of new amphiphilic structures. This result is in line with ^{1}H NMR evidence and supports our previous hypothesis about the reaction of **A3** with the polymer acrylate esters. In view of

this outcome, we chose to use **A2** instead of **A3** as the amine in our catalytic system.

Subsequently, we wanted to test organocatalysis at polymer and H_2O_2 concentrations that are more relevant for drug delivery. We followed the Z-average diameter and scatter count of PM16 micelles at a polymer concentration of 0.9 mg/mL in presence of 1.3 mM H_2O_2 (1.5 eq. relative to the 0.9 mM thioether units). We observed a 40% decrease of the normalized scatter count under these conditions in 120 h, against the 40 h necessary to achieve the same result for the 8-times more concentrated sample. The Z-average diameter increased from 30 to 43 nm for PM16 micelles at a polymer concentration of 6.8 mg/mL and from 33 to 39 nm for PM16 micelles at a polymer concentration of 0.9 mg/mL at 120 h, showing a minor change in micellar size for both dilution conditions. (Figure S5B). These results demonstrate that 8-fold dilution causes a 3 times decrease in the disintegration kinetics of 1:1.5 PM16/H_2O_2, but a negligible morphological change of the micelles. Knowing this, we pursued to apply the optimized catalytic system 1.0 eq. of **3**/**A2** for the diluted conditions. Immediately after adding H_2O_2, the Z-average diameter of PM16 micelles in presence of the catalyst was 41.0 ± 1.3 against 33.4 ± 2.9 nm in the absence of catalyst (Figure 4B, top). This size increase of the micelles may be caused by the partial encapsulation of **3**, as anticipated from ^{1}H NMR data. Despite the different starting Z-average diameter, the micellar size change in time showed a similar trend for both catalyzed and non-catalyzed conditions over 140 h (Figure 4B, top). PM16 micelles showed stable values for both Z-average diameter and scatter count in absence of catalyst and oxidant (Figure 4B, ■ orange line). In presence of 1.0 eq. of **3**/**A2** and 1.3 mM H_2O_2 the normalized scatter count showed more than 40% decrease after about 72 h, while it decreased barely 20% in absence of catalyst (Figure 4B, bottom). Therefore, the dissociation of PM16 micelles after H_2O_2 addition proceed two times faster when 1.0 eq. of **3**/**A2** is

employed in diluted conditions. Here, the effect of organocatalysis on the oxidation of thioether moieties of low concentration PM16 micelles with H_2O_2 is smaller than the 5.5 times increase in rate obtained for the ^{1}H NMR experiment concentrations. Still, despite this dilution-induced effect, the data shows that organocatalysis can be applied to increase the rate of nanocarrier disassembly even at very low oxidant concentrations.

3.2.5 Cargo release studies

To study the role of the organocatalytic **3**/**A2** system for oxidation-triggered release of cargo from PM16 micelles, we loaded PM16 micelles (1.0 mg/mL) with the hydrophobic dye Nile Red as previously reported.[36] Then, similarly to the samples measured by DLS, we added 1.0 eq. of **3**/**A2** and 1.3 mM H_2O_2 to the Nile Red loaded micelles and we followed the Nile Red fluorescence over time. Figure 4C shows 80% dye release within 72 h in presence of organocatalysis against the 168 h necessary in non-catalyzed conditions. In line with the DLS data (Figure 4B), cargo release is approximately twice as fast under catalytic conditions compared to the uncatalyzed scenario.

Finally, we tested the organocatalyzed system under tumor-mimicking conditions, where sub-millimolar concentrations of oxidant are continuously produced.[30] We used syringe pumps for the addition of 0.5 mM H_2O_2 (24 µL) per day to Nile Red loaded PM16 micelles (1.0 mg/mL) with 1.0 eq. of **3**/**A2**. After only 15% release after 72 h, the release reached 90% over the subsequent 90 h (Figure 4C, ▼blue line), similar to the sample in which 1.3 mM H_2O_2 was added directly from the start. The initial delay in release may be due to the initial absence of the catalytically active species, which requires reaction between the ketone/amine precatalyst and an equivalent of hydrogen peroxide to form. On the other hand, in the absence of catalyst, the continuous addition of 0.5 mM H_2O_2 (24 µL) per day led to only 55% release at 168 h. When the same volume of PB (■ orange line) was continuously added instead of the H_2O_2 solution, the

release profile remained relatively stable over time, reaching less than 20% release after 180 h. This minor passive leakage of Nile Red from PM16 micelles was already noticed in our previous work,[36] and it may be slightly increased by the progressive dilution of the micellar dispersions. In the end, in presence of **3**/**A2**, PM16 micelles showed about two times faster response to low H_2O_2 concentrations such as 0.5 mM per day compared to the uncatalyzed case and good stability in non-oxidative conditions for more than 7 days. Overall, when sub-millimolar concentrations of H_2O_2 are used, the 2-fold decrease of degradation time for PM16 micelles coupled with the organocatalyst translate in saving several days to achieve the complete cargo release.

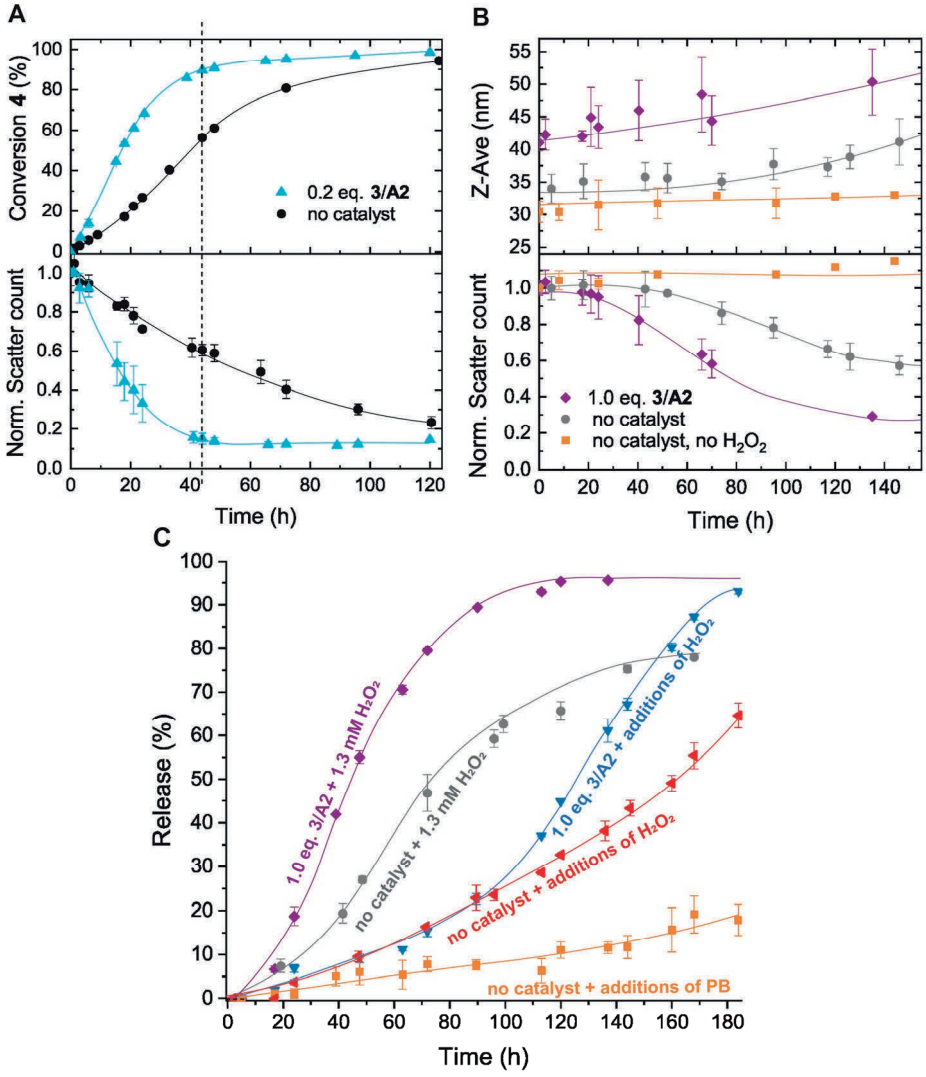

Figure 4. A) Conversion to **4** (%) measured by ^{1}H NMR (top) and normalized scatter count (bottom) measured by DLS of PM16 micelles (6.8 mg/mL) with 0.2 eq. of **3**/**A2** against the control (without any catalyst) after addition of 10 mM H_2O_2 at 37 °C. The catalyzed samples reached 90% conversion of **4** and a scatter count plateau value at 44 h (vertical dashed line). B) Z-Average diameter (top) and scatter count (bottom) of PM16 micelles (0.9 mg/mL) after addition of 1.3 mM H_2O_2 with 1.0 eq. of **3**/**A2** (♦ purple line) and without catalyst (● grey line). Z-Average diameter (top) and scatter count (bottom)

of PM16 micelles (0.9 mg/mL) measured by DLS at 37 °C (■ orange line). C) Nile Red release from PM16 micelles (0.9 mg/mL) after addition of 1.3 mM H_2O_2 with 1.0 eq. of **3**/**A2** (♦ purple line) and without catalyst (● grey line). Nile Red release from PM16 micelles (0.9 mg/mL) with 1.0 eq. of **3**/**A2** (▼ blue line) and without catalyst (◀ red line) after continuous addition of 0.5 mM H_2O_2 (24 µL) per day. Nile Red release from PM16 micelles (0.9 mg/mL) after continuous addition of 24 µL PB per day (■ orange line). The curves are drawn as a guide for the eye.

3.3 Conclusion

In this study, we present organocatalytic enhancement of oxidation-triggered disassembly and release from block-copolymer micelles, even at very low oxidant concentrations. We applied an *in situ* formed imine to catalyze the oxidation of thioether phenyl ester based polymer surfactants in presence of H_2O_2. Micelles assembled from these surfactants are able to disrupt following a logic gate response in which, after the oxidation of the thioether, the adjacent ester bond cleaves through hydrolysis. The micellar system was then doped with the ketone $PhCOCF_3$ **3** and the unnatural amino acid L-*tert*-leucine **A2**. The *in situ* formed imine is able to catalytically activate H_2O_2 in aqueous buffer at pH 7.4. The use of organocatalysis on PM16 micelles showed a 5.5-fold acceleration compared to non-catalyzed conditions, at low millimolar concentrations of H_2O_2. In 8 times diluted conditions, Nile Red loaded micelles in presence of **3**/**A2** show 80% release more than two times faster than in absence of catalyst. In addition, the same system is able to reach almost complete release over 7 days when only 0.5 mM H_2O_2 is supplied per day. At the same time, these PM16 micelles show only dilution-induced release over the same time frame in a non-oxidative environment. The concept of using organocatalysis for oxidant activation opens the possibility of using the low oxidant concentrations present in living tissues as triggers for bond breaking reactions and controlled release materials.

3.4 References

1. G.-Y. Liou and P. Storz, *Free Radic. Res.*, 2010, **44**, 479-496.
2. S. J. Forrester, D. S. Kikuchi, M. S. Hernandes, Q. Xu and K. K. Griendling, *Circ. Res.*, 2018, **122**, 877-902.
3. E. C. Cheung and K. H. Vousden, *Nat. Rev. Cancer*, 2022, **22**, 280-297.
4. B. Perillo, M. Di Donato, A. Pezone, E. Di Zazzo, P. Giovannelli, G. Galasso, G. Castoria and A. Migliaccio, *Exp. Mol. Med.*, 2020, **52**, 192-203.
5. A. I. Casas, V. T.-V. Dao, A. Daiber, G. J. Maghzal, F. Di Lisa, N. Kaludercic, S. Leach, A. Cuadrado, V. Jaquet, T. Seredenina, K. H. Krause, M. G. López, R. Stocker, P. Ghezzi and H. H. H. W. Schmidt, *Antioxid. Redox Signaling*, 2015, **23**, 1171-1185.
6. C. Zhao, J. Chen, R. Zhong, D. S. Chen, J. Shi and J. Song, *Angew. Chem. Int. Ed.*, 2021, **60**, 9804-9827.
7. C. Kang, S. Gwon, C. Song, P. M. Kang, S.-C. Park, J. Jeon, D. W. Hwang and D. Lee, *ACS Nano*, 2017, **11**, 6194-6203.
8. W. Ke, J. Li, F. Mohammed, Y. Wang, K. Tou, X. Liu, P. Wen, H. Kinoh, Y. Anraku, H. Chen, K. Kataoka and Z. Ge, *ACS Nano*, 2019, **13**, 2357-2369.
9. S. Wang, G. Yu, Z. Wang, O. Jacobson, L.-S. Lin, W. Yang, H. Deng, Z. He, Y. Liu, Z.-Y. Chen and X. Chen, *Angew. Chem. Int. Ed.*, 2019, **58**, 14758-14763.
10. A. Napoli, M. Valentini, N. Tirelli, M. Müller and J. A. Hubbell, *Nat. Mater.*, 2004, **3**, 183-189.
11. L. Xu, M. Zhao, W. Gao, Y. Yang, J. Zhang, Y. Pu and B. He, *Colloids Surf., B*, 2019, **181**, 252-260.
12. L. Yu, M. Zhang, F.-S. Du and Z.-C. Li, *Polym. Chem.*, 2018, **9**, 3762-3773.

13. F. El Mohtadi, R. d'Arcy, J. Burke, J. M. Rios De La Rosa, A. Gennari, R. Marotta, N. Francini, R. Donno and N. Tirelli, *Biomacromolecules*, 2020, **21**, 305-318.

14. M. Criado-Gonzalez and D. Mecerreyes, *J. Mater. Chem.B*, 2022, **10**, 7206-7221.

15. K. M. Poole, C. E. Nelson, R. V. Joshi, J. R. Martin, M. K. Gupta, S. C. Haws, T. E. Kavanaugh, M. C. Skala and C. L. Duvall, *Biomaterials*, 2015, **41**, 166-175.

16. M. K. Gupta, C. E. Meyer Ta Fau - Nelson, C. L. Nelson Ce Fau - Duvall and C. L. Duvall, *J. Controlled Release*, 2012, **162**, 591-598.

17. J. Herzberger, K. Fischer, D. Leibig, M. Bros, R. Thiermann and H. Frey, *J. Am. Chem. Soc.*, 2016, **138**, 9212-9223.

18. W.-X. Wu, X.-L. Yang, B.-Y. Liu, Q.-F. Deng, M.-M. Xun, N. Wang and X.-Q. Yu, *RSC Advances*, 2016, **6**, 11870-11879.

19. B. L. Allen, J. D. Johnson and J. P. Walker, *ACS Nano*, 2011, **5**, 5263-5272.

20. E. Secret and J. S. Andrew, in *Stimuli-responsive Drug Delivery Systems*, eds. A. Singh and M. M. Amiji, The Royal Society of Chemistry, London (UK), 2018, DOI: 10.1039/9781788013536-00209, pp. 209-231.

21. T. Yoshii, S. Onogi, H. Shigemitsu and I. Hamachi, *J. Am. Chem. Soc.*, 2015, **137**, 3360-3365.

22. M. P. van der Helm, B. Klemm and R. Eelkema, *Nat. Rev. Chem.*, 2019, **3**, 491-508.

23. A. Bossion, K. V. Heifferon, L. Meabe, N. Zivic, D. Taton, J. L. Hedrick, T. E. Long and H. Sardon, *Prog. Polym. Sci.*, 2019, **90**, 164-210.

24. M. K. Kiesewetter, E. J. Shin, J. L. Hedrick and R. M. Waymouth, *Macromolecules*, 2010, **43**, 2093-2107.

25. S. Kaiho, A. A. R. Hmayed, K. R. Delle Chiaie, J. C. Worch and A. P. Dove, *Macromolecules*, 2022, **55**, 10628–10639.

26. T. J. Bannin and M. K. Kiesewetter, *Macromolecules*, 2015, **48**, 5481-5486.

27. J. M. W. Chan, J. P. K. Tan, A. C. Engler, X. Ke, S. Gao, C. Yang, H. Sardon, Y. Y. Yang and J. L. Hedrick, *Macromolecules*, 2016, **49**, 2013-2021.

28. R. P. Brinkhuis, F. de Graaf, M. B. Hansen, T. R. Visser, F. P. J. T. Rutjes and J. C. M. van Hest, *Polym. Chem.*, 2013, **4**, 1345-1350.

29. C. de Gracia Lux, S. Joshi-Barr, T. Nguyen, E. Mahmoud, E. Schopf, N. Fomina and A. Almutairi, *J. Am. Chem. Soc.*, 2012, **134**, 15758-15764.

30. N. Yang, W. Xiao, X. Song, W. Wang and X. Dong, *Nano-Micro Lett.*, 2020, **12**, 15.

31. H. Iida, Y. Imada and S. I. Murahashi, *Org. Biomol. Chem.*, 2015, **13**, 7599-7613.

32. T. Sakai, T. Kumoi, T. Ishikawa, T. Nitta and H. Iida, *Org. Biomol. Chem.*, 2018, **16**, 3999-4007.

33. A. B. E. Minidis and J.-E. Bäckvall, *Chem. Eur. J.*, 2001, **7**, 297-302.

34. P. Ménová, F. Kafka, H. Dvořáková, S. Gunnoo, M. Šanda and R. Cibulka, *Adv. Synth. Catal.*, 2011, **353**, 865-870.

35. S. Zhang, G. Li, L. Li, X. Deng, G. Zhao, X. Cui and Z. Tang, *ACS Catal.*, 2020, **10**, 245-252.

36. I. Piergentili, P. R. Bouwmans, L. Reinalda, R. W. Lewis, B. Klemm, H. Liu, R. M. de Kruijff, A. G. Denkova and R. Eelkema, *Polym. Chem.*, 2022, **13**, 2383-2390.

37. K. A. Stingl and S. B. Tsogoeva, *Tetrahedron: Asymmetry*, 2010, **21**, 1055-1074.

38. K. Sato, M. Hyodo, M. Aoki, X.-Q. Zheng and R. Noyori, *Tetrahedron*, 2001, **57**, 2469-2476.

39. W. D. Emmons, *J. Am. Chem. Soc.*, 1957, **79**, 5739-5754.

40. F. A. Davis, S. G. Lal and H. D. Durst, *J. Org. Chem.*, 1988, **53**, 5004-5007.

41. K. S. Williamson, D. J. Michaelis and T. P. Yoon, *Chem. Rev.*, 2014, **114**, 8016-8036.

42. S. Schoumacker, O. Hamelin, S. Téti, J. Pécaut and M. Fontecave, *J. Org. Chem.*, 2005, **70**, 301-308.

43. D. D. DesMarteau, V. A. Petrov, V. Montanari, M. Pregnolato and G. Resnati, *J. Org. Chem.*, 1994, **59**, 2762-2765.

44. P. C. B. Page, J. P. Heer, D. Bethell, E. W. Collington and D. M. Andrews, *Tetrahedron Lett.*, 1994, **35**, 9629-9632.

45. D. Bethell, P. C. Bulman Page and H. Vahedi, *J. Org. Chem.*, 2000, **65**, 6756-6760.

46. M. Cai, K. Xu, Y. Li, Z. Nie, L. Zhang and S. Luo, *J. Am. Chem. Soc.*, 2021, **143**, 1078-1087.

47. C. Kokotos, E. Voutyritsa and I. Triandafillidi, *Synthesis*, 2016, **49**, 917-924.

48. V. Hulea and P. Moreau, *J. Mol. Catal. A: Chem.*, 1996, **113**, 499-505.

49. S. Bhattacharjee, *J. Controlled Release*, 2016, **235**, 337-351.

50. F. H. Sobotta, M. T. Kuchenbrod, F. V. Gruschwitz, G. Festag, P. Bellstedt, S. Hoeppener and J. C. Brendel, *Angew. Chem. Int. Ed.*, 2021, **60**, 24716-24723.

51. S. Fredenberg, M. Wahlgren, M. Reslow and A. Axelsson, *Int. J. Pharm.*, 2011, **415**, 34-52.

52. C. J. Pierce and M. K. Hilinski, *Org. Lett.*, 2014, **16**, 6504-6507.

53. I. Triandafillidi, D. I. Tzaras and C. G. Kokotos, *ChemCatChem*, 2018, **10**, 2521-2535.

54. C. D. Ritchie, *J. Am. Chem. Soc.*, 1984, **106**, 7187-7194.

55. S. Yacob, M. J. Caulfield and T. A. Barckholtz, *Philos. Trans. R. Soc., A*, 2018, **376**, 20170055.

56. W. Adam, C. R. Saha-Möller and P. A. Ganeshpure, *Chem. Rev.*, 2001, **101**, 3499-3548.

57. F. Brotzel, Y. C. Chu and H. Mayr, *J. Org. Chem.*, 2007, **72**, 3679-3688.

3.5 Supporting information

3.5.1 Materials

All reagents were obtained from commercial suppliers (Sigma Aldrich, TCI Chemicals or Acros Organics) and used without further purification unless otherwise specified. Reference compounds 4-(methylthio)phenol and 4-(methylsulfonyl)phenol were purchased respectively from Sigma Aldrich and TCI. SDS of these compounds reports that chemical, physical, and toxicological properties have not been thoroughly investigated. 4-(methylthio)phenol: this substance/mixture contains no components considered to be either persistent, bioaccumulative and toxic (PBT), or very persistent and very bioaccumulative (vPvB) at levels of 0.1% or higher. 2,2,2-trifluoroacetophenone, L-tert-leucine and *p*-anisidine were purchased from Sigma Aldrich. Air and moisture sensitive reagents were transferred via syringe. All air and/or moisture sensitive reactions were carried out in oven-dried glassware under a positive pressure of argon gas with commercially available anhydrous solvents. Petroleum ether refers to the fraction boiling in the range 40 – 60 °C. Reactions were monitored by analytical thin-layer chromatography (TLC) on silica gel plates (Merck $60F_{254}$) and either visualized by UV light (254 nm) or by staining with a solution of $KMnO_4/K_2CO_3$/AcOH in water followed by heating. Flash chromatography was performed on 230-400 mesh silica gel (Sigma Aldrich). ^{1}H NMR and ^{13}C NMR spectra were recorded on an Agilent-400 MR DD2 (400 MHz and 101 MHz for ^{1}H and ^{13}C, respectively) spectrometer at 298 K. Chemical shifts are reported in ppm relative to the residual solvent peak, the multiplicity is reported as follows: s = singlet, d = doublet, t = triplet, q = quartet, m = multiplet, and J-couplings (*J*) are reported in Hertz (Hz). To suppress the water peak, PRESAT configuration (suppress one highest peak) was used. NMR spectra were processed by MNova NMR software (Mestrelab Research). GC-MS samples were analyzed using an Agilent 5977 GC/MSD equipped with a Stabilwax MS column (oven

temperature: 250 °C, flow: 2.5 mL/min). ESI-MS was performed using LTQ XL spectrometer equipped with Shimadzu HPLC setup operating at 0.2 mL/min flow rate with water/MeCN mobile phase containing 0.1 vol% formic acid and Discovery C18 column. Dynamic light scattering (DLS) measurements were performed on a Malvern Zetasizer Nano-ZS equipped with a 4 mW laser operating at 633 nm. Fluorescence release was measured by Jasco J-815 CD spectrometer with an FMO-4275 emission monochromator (163 – 900 nm).

3.5.2 Synthesis and molecular model procedures

Synthesis of Catalyst A3

The catalyst **A3** was synthesized similarly to the procedure previously reported by Luo's group.[1] To a solution of N-Boc-L-tert-leucine (23.1 g, 100 mmol) in anhydrous CH_2Cl_2 (200 mL) at 0 °C , was added N,N-Diisopropylethylamine (DIPEA, 28.4 g, 220 mmol) followed by HBTU (41.7 g, 110 mmol). After stirring for 30 min at room temperature, ethylamine (4.51 g, 100 mmol) in anhydrous CH_2Cl_2 (20 mL) was added under ice bath, and the solution was stirred at room temperature for an additional 12 h. The reaction mixture was washed with HCl (0.1 M), water, saturated $NaHCO_3$ and brine, then dried with anhydrous Na_2SO_4. After removal of the solvent, the residue was purified by chromatography with petroleum ether and ethyl acetate. To the obtained product was added CH_2Cl_2, then 35 mL TFA at 0 ºC and stirred overnight. The solvent was concentrated to 100 mL, and H_2O (50 mL) was added. The aqueous phase was extracted with additional 50 mL CH_2Cl_2. The pH value of the solvent was adjusted to 12 by the addition of K_2CO_3 in an ice bath. The aqueous phase was extracted with CH_2Cl_2 (40 mL), and the organic layers were combined and dried with anhydrous Na_2SO_4. After removal of the solvent, the intermediate compound (9.15 g, 58% yield) was directly used for the next step without purification. To the above-obtained intermediate (9.15 g) in anhydrous THF (150 mL) at 0 °C was added $LiAlH_4$ (5.51 g, 145 mmol) in portions, then the solution

was stirred at room temperature for 10 minutes and heated to reflux for 6 h. After cooling to room temperature, 10 mL water was added at 0 °C, followed by 15% aqueous NaOH (10 mL), and anhydrous Na_2SO_4 after 10 minutes. The solid formed was filtered and washed with ethyl acetate several times. The solvent was removed, and pure catalyst **A3** (5.45 g, 66 % yield) was obtained as a colorless oil by distillation under reduced pressure. **^{1}H NMR** (400 MHz, $CDCl_3$) δ 2.78 (dd, J = 11.4, 2.5 Hz, 1H), 2.74 – 2.54 (m, 2H), 2.47 (dd, J = 10.5, 2.4 Hz, 1H), 2.21 (t, J = 10.9 Hz, 1H), 1.44 – 1.18 (br, 3H), 1.11 (t, J = 7.1 Hz, 3H), 0.88 (s, 9H). **^{13}C NMR** (101 MHz, $CDCl_3$) δ 56.65, 48.75, 43.69, 33.73, 25.69, 11.59. **ESI-HR** calcd for $C_8H_{21}N_2^+$: 145.1699, found 145.1699.

Synthesis of *N*,*N*-dimethyl tert-leucine (A4)

A solution of **A2** (131 mg, 1.00 mmol) in formic acid (98%, 0.45 mL, 12.0 mmol) and aqueous formaldehyde (37%, 0.53 mL, 7.20 mmol) was heated to reflux overnight. Upon cooling, the mixture was concentrated in vacuo to remove formic acid and residual formaldehyde. The aqueous solution was then neutralized with NaOH 1M to pH = 7.4 and freeze dried overnight. Precipitation in 1.0 mL of MeOH allowed the removal of salts through filtration (syringe filter 0.45 μm). After rotatory evaporation of MeOH, **A4** was obtained as a white solid (151 mg, 95% yield). **^{1}H NMR** (400 MHz, DMSO-d_6) δ = 3.91 (s, 1H), 2.87 (s, 6H), 1.15 (s, 9H). **^{13}C NMR** (101 MHz, DMSO-d_6) δ = 168.3, 74.3, 33.5, 27.6. MS (ESI+) *m*/*z*: $[M + H]^+$ calcd. for $C_8H_{17}NO_2$, 160.13, found 160.13. Spectroscopic data are in line with those reported in literature.[2, 3]

Screening of ketone/amine catalysis for the oxidation of thioether ester molecular model

An oven-dried tube equipped with stir bar was charged with thioether (**1**, 0.20 mmol, 36.4 mg) and amine **A1** (20 mol%, 4.90 mg). After dissolution in tert-butanol, trifluoroacetophenone (20 mol%) was added to the vial. Then H_2O_2 (30 wt.% in water, 0.30 mmol) was added via syringe. Upon completion of the

addition, the reaction was conducted at room temperature for 3 hours (TLC analysis). The solvent was removed under reduced pressure and the residue was purified by silica gel chromatography (ethyl acetate/hexane 1:4) to give product **2**.

Kinetic study of standard conditions of the oxidation of thioether

An oven-dried tube equipped with stir bar was charged with thioether (**1**, 0.20 mmol, 36.4 mg) and amine **A1** (20 mol%, 4.90 mg). After dissolution in tertiary butanol, trifluoroacetophenone (20 mol%) was added to the vial. For the control experiment pure tertiary butanol was added instead. The reactions were monitored by GC *in situ* after the addition of H_2O_2 (30 wt.% in water, 0.30 mmol) via syringe. The conversions were plotted vs. T measured for each reaction (Figure 2B).

3.5.3 Synthesis and characterization of p(DMA$_{130}$-b-MTPA$_{16}$) micelles

The amphiphilic block copolymer p(DMA$_{130}$-b-MTPA$_{16}$) (PM16) was synthesized and characterized as previously described.[4] 40.0 mg of p(DMA$_{130}$-b-MTPA$_{16}$) was dissolved in 0.3 mL of THF. 5.0 or 40 mL of sodium phosphate buffer (PB, 10 mL, 100 mM, pH = 7.4) was added slowly while stirring to obtain respectively 8.0 mg/mL or 1.0 mg/mL of micellar dispersion.

Table S1. Average hydrodynamic diameter (DH) and scatter count measured by DLS for PM16 micelles in the two concentrations used in this work.

PM16 concentration (mg/mL)	D_H [unloaded] (nm)	Scatter count (Mcps)
8.0 mg/mL	27.4 ± 0.6	12.6 ± 0.23
1.0 mg/mL	30.9 ± 1.3	3.13 ± 0.05

3.5.4 ^{1}HNMR study of H_2O_2-induced oxidation and hydrolysis of PM16 micelles

^{1}HNMR study of ketone/amine catalyzed H_2O_2-induced oxidation and hydrolysis of PM16 micelles

Stock solutions of trifluoroacetophenone (**3**) were prepared in ^{t}BuOH in varying concentrations (0.50, 0.75, 2.50 M). Stock solutions of amine **A3** or **A2** were prepared in phosphate buffer (PB, 100 mM, pH= 7.4) at different concentrations: 50.0, 75.0 and 250 mM. 1.6 µL of the stock solution of **3** and 16.0 µL of the amine stock solution was mixed and let stir in the vortex for 1 h.

In a NMR tube 0.5 mL of PM16 micelles dispersion (8.0 mg/mL), 58.0 µL D_2O and 17.6 µL of the premixed catalysts mixture was added. For control experiments 17.6 µL of PB/^{t}BuOH 10:1 was added instead the catalysts mixture. Then, 6.00 µL of 3.0 wt% H_2O_2 was added to yield a final 10.0 mM concentration. The micelles hydrolysis at 37 °C was tracked following the conversion to **4** by ^{1}H NMR in PRESAT mode. The experiments were performed in duplicates to obtain mean and standard deviation values.

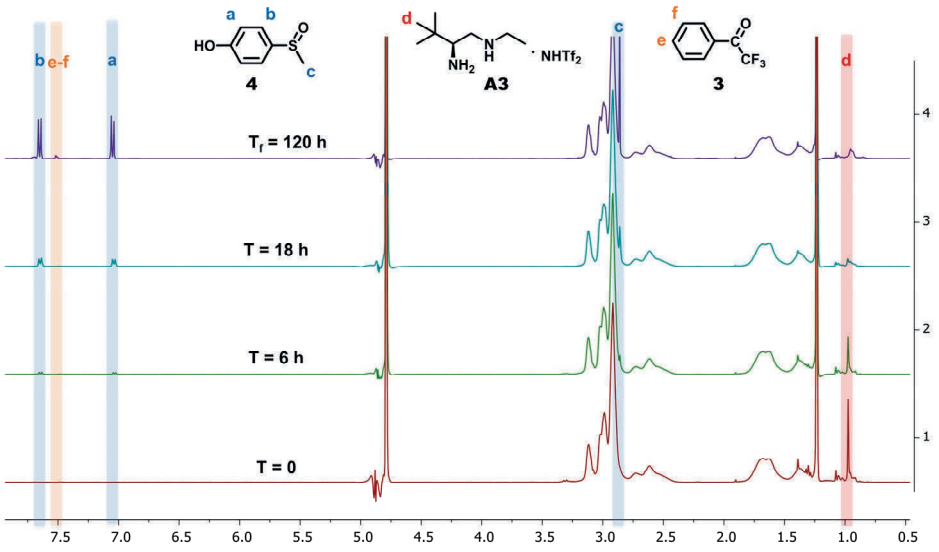

Figure S1. ^{1}H NMR spectra over time at 37 °C of PM16 micellar solutions (6.8 mg/mL) in PB (100 mM, pH = 7.4)/D_2O 9:1 upon the addition of 10.0 mM H_2O_2 in presence of 0.2 eq. of **3**/**A3**.

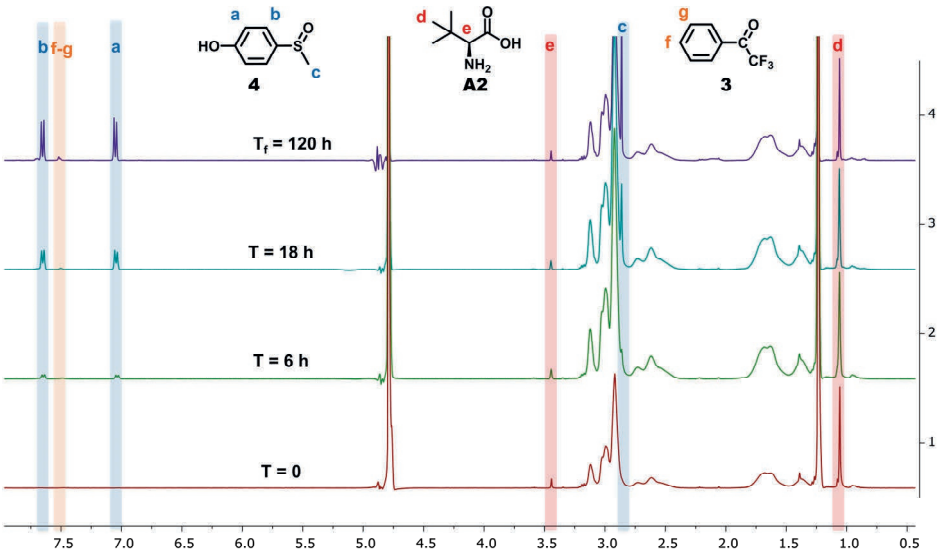

Figure S2. ^{1}H NMR spectra over time at 37 °C of PM16 micellar solutions (6.8 mg/mL) in PB (100 mM, pH = 7.4)/D_2O 9:1 upon the addition of 10.0 mM H_2O_2 in presence of 0.2 eq. of **3**/**A2**.

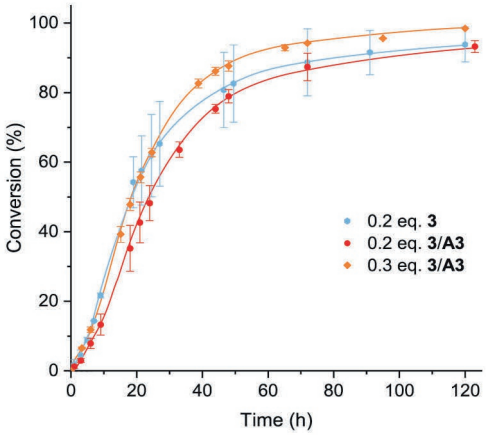

Figure S3. Comparison of the ^{1}H NMR conversion of **4** between the use of 0.2 eq. of **3**/**A3**, 0.3 eq. of **3**/**A3** and 0.2 eq. of **3** in PM16 micelles degradation with 10.0 mM H_2O_2.

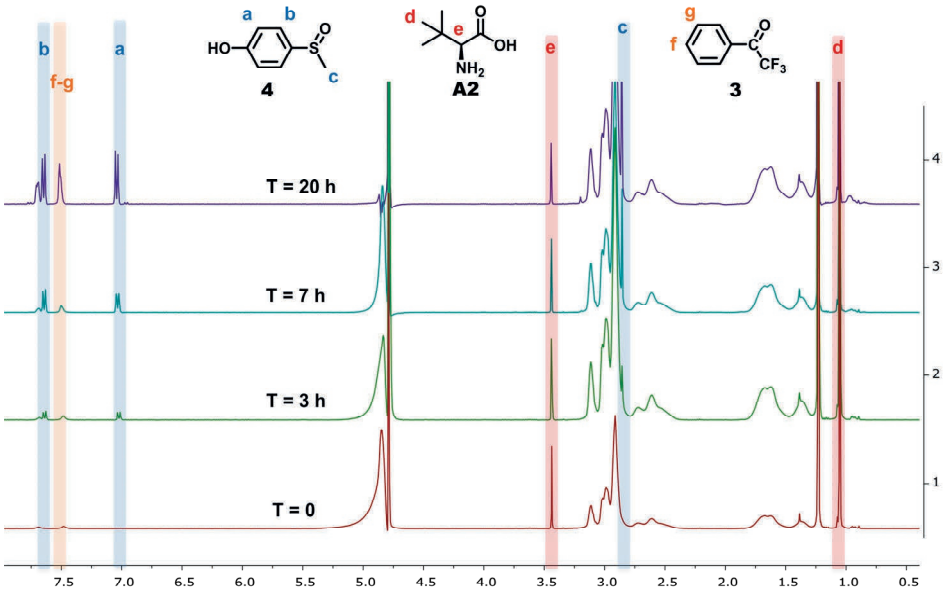

Figure S4. ^{1}H NMR spectra over time at 37 °C of PM16 micellar solutions (6.8 mg/mL) in PB (100 mM, pH = 7.4)/D_2O 9:1 upon the addition of 10.0 mM H_2O_2 in presence of 1.0 eq. of **3**/**A2**.

^{1}HNMR study of 3/A2 against 3/A4 as catalysts for H_2O_2-induced oxidation and hydrolysis of PM16 micelles

500 mM stock solution of **3** was prepared in ^{t}BuOH. 500 mM stock solutions of **A2** and **A4** were prepared in phosphate buffer (PB, 100 mM, pH= 7.4). In a 1.5 mL glass vial 1.6 µL of 500 mM stock solution of **3** and 16.0 µL of 500 mM stock solution of **A2** or **A4** was mixed and let stir in the vortex for 1 h. In a NMR tube 0.5 mL of PM16 micelles dispersion (8.0 mg/mL), 58.0 µL D_2O and 17.6 µL of premixed catalysts mixture was added. Then, 6.00 µL of 3.0 wt% H_2O_2 was added to yield a final 10.0 mM concentration. The micelles hydrolysis at 37 °C was tracked following the conversion to **4** by ^{1}H NMR in PRESAT mode. The experiments were performed in duplicates to obtain mean and standard deviation values.

3.5.5 DLS study of ketone/amine catalyzed H_2O_2-induced oxidation and hydrolysis of PM16 micelles

DLS study of ketone/amine catalyzed H_2O_2-induced oxidation and hydrolysis of PM16 micelles (6.8 mg/mL)

500 mM stock solution of **3** was prepared in ^{t}BuOH. 50.0 mM stock solution of amine **A3** or **A2** was prepared in phosphate buffer (PB, 100 mM, pH= 7.4). 1.6 µL of the stock solution of **3** and 16.0 µL of the amine stock solution was mixed and let stir in the vortex for 1 h.

In a DLS disposable cuvette 0.5 mL of PM16 micelles dispersion (8.0 mg/mL), 58.0 µL PB and 17.6 µL of the premixed catalysts mixture were added. For control experiments 17.6 µL of PB/^{t}BuOH 10:1 was added instead the catalysts mixture. Then, 6.00 µL of 3.0 wt% H_2O_2 was added to yield a final 10.0 mM concentration. The micelles hydrolysis at 37 °C was tracked following over time the Z-Average diameter and scatter count in DLS. The experiments were performed in duplicates to obtain mean and standard deviation values.

DLS study of ketone/amine catalyzed H_2O_2-induced oxidation and hydrolysis of PM16 micelles (0.9 mg/mL)

1.6 µL of 620 mM stock solution of **3** in ^{t}BuOH and 16.0 µL of 62.0 mM stock solution of amine **A2** in PB was mixed and let stir in the vortex for 1 h.

In a DLS disposable cuvette 1.0 mL of PM16 micelles dispersion (1.0 mg/mL), 17.6 µL of the premixed catalysts mixture was added. For control experiments 17.6 µL of PB/ ^{t}BuOH 10:1 was added instead the catalysts mixture. Then, 73.0 µL of H_2O_2 20.0 mM was added to yield a final 1.3 mM concentration. The micelles hydrolysis at 37 °C was tracked following over time the Z-Average diameter and scatter count in DLS. The experiments were performed in duplicates to obtain mean and standard deviation values.

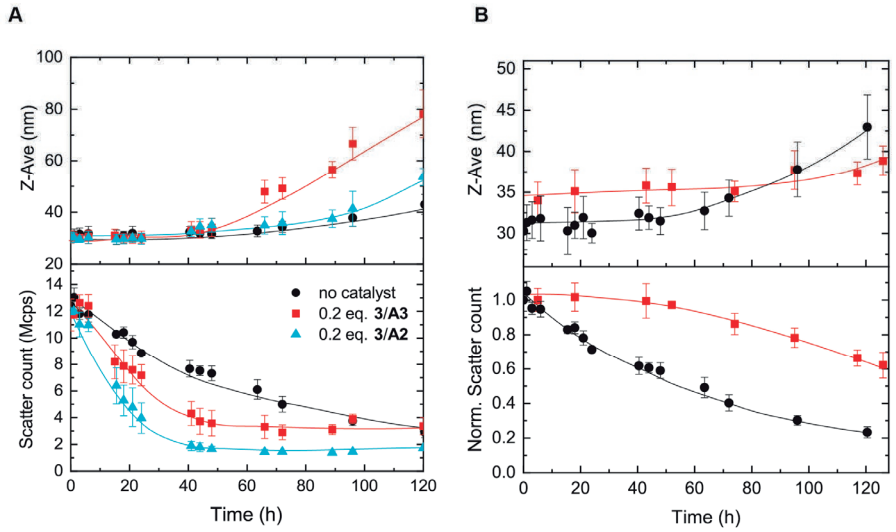

Figure S5. A) Z-Average diameter (top) and scatter count (bottom) of PM16 micelles (6.8 mg/mL) after addition of 10.0 mM H_2O_2 with 0.2 eq. of **3**/**A2** and 0.2 eq. **3**/**A3** against the control (without any catalyst) measured by DLS at 37 °C. B) Z-Average diameter (top) and normalized scatter count (bottom) of PM16 micelles (6.8 mg/mL) after addition of 10.0 mM H_2O_2 (● black data) and PM16 micelles (0.9 mg/mL) after addition of 1.3 mM H_2O_2 (■ red data).

3.5.6 Nile Red release from PM16 in presence of ketone/amine catalysis

Nile Red release from PM16 micelles after addition of 1.3 mM H_2O_2 in presence of ketone/amine catalysis

1.60 µL of 620 mM stock solution of **3** in ^{t}BuOH and 16.0 µL of 62.0 mM stock solution of amine **A2** in PB was mixed and let stir in the vortex for 1 h. To 1.0 mL of Nile Red loaded PM16 micelles (1.0 mg/mL), 17.6 µL of the premixed catalysts mixture was added. For control experiments 17.6 µL of PB/^{t}BuOH 10:1 was added instead the catalysts mixture. Then, 73.0 µL of H_2O_2 20.0 mM was added to yield a final 1.3 mM concentration. The samples were kept at 37 °C and Nile Red fluorescence was followed over time, using an excitation wavelength of 540 ± 10 nm and emission wavelength of 620 ± 20 nm. The experiments were performed in duplicates to obtain mean and standard deviation values.

Nile Red release from PM16 micelles after continuous addition of H_2O_2 in presence of ketone/amine catalysis

1.60 µL of 620 mM stock solution of **3** in ^{t}BuOH and 16.0 µL of 62.0 mM stock solution of amine **A2** in PB was mixed and let stir in the vortex for 1 h. To 1.0 mL of Nile Red loaded PM16 micelles (1.0 mg/mL), 17.6 µL of the premixed catalysts mixture was added. For control experiments 17.6 µL of PB/^{t}BuOH 10:1 was added instead the catalysts mixture. Then, syringe pumps were set to influx 1.0 µL/h of varying stock solutions of H_2O_2 to provide 0.50 mM H_2O_2 per day. The samples were kept at 37 °C and Nile Red fluorescence was followed over time, using an excitation wavelength of 540 ± 10 nm and emission wavelength of 620 ± 20 nm. The experiments were performed in duplicates to obtain mean and standard deviation values.

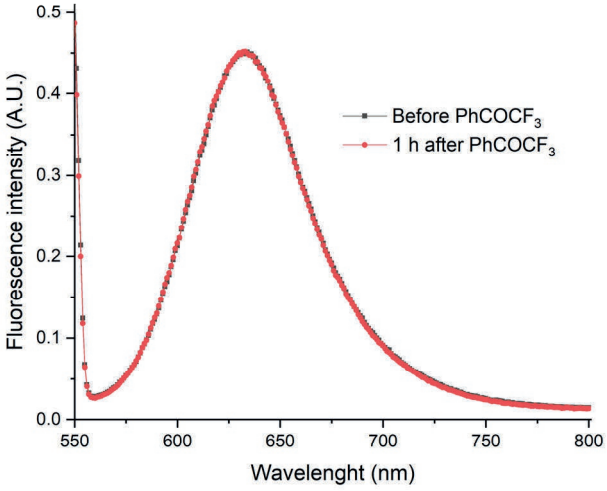

Figure S6. Fluorescence intensity of Nile Red loaded PM16 (1.0 mg/mL) before (black) and after (red) the addition of 1.0 eq. **3** (in 1.60 µL ^{t}BuOH). The fluorescence intensity remained stable demonstrating that **3** was not substituting Nile Red in the micelles core.

3.5.7 Supplementary references

1. S. Hu, L. Zhang, J. Li, S. Luo and J.-P. Cheng, *Eur. J. Org. Chem.*, 2011, 3347-3352.

2. D. R. Fandrick, J. T. Reeves, J. M. Bakonyi, P. R. Nyalapatla, Z. Tan, O. Niemeier, D. Akalay, K. R. Fandrick, W. Wohlleben, S. Ollenberger, J. J. Song, X. Sun, B. Qu, N. Haddad, S. Sanyal, S. Shen, S. Ma, D. Byrne, A. Chitroda, V. Fuchs, B. A. Narayanan, N. Grinberg, H. Lee, N. Yee, M. Brenner and C. H. Senanayake, *J. Org. Chem.*, 2013, **78**, 3592-3615.

3. A. D. Headley and S. D. Starnes, *J. Am. Chem. Soc.*, 1995, **117**, 9309-9313.

4. I. Piergentili, P. R. Bouwmans, L. Reinalda, R. W. Lewis, B. Klemm, H. Liu, R. M. de Kruijff, A. G. Denkova and R. Eelkema, *Polym. Chem.*, 2022, **13**, 2383-2390.

3.5.8 Spectra overview

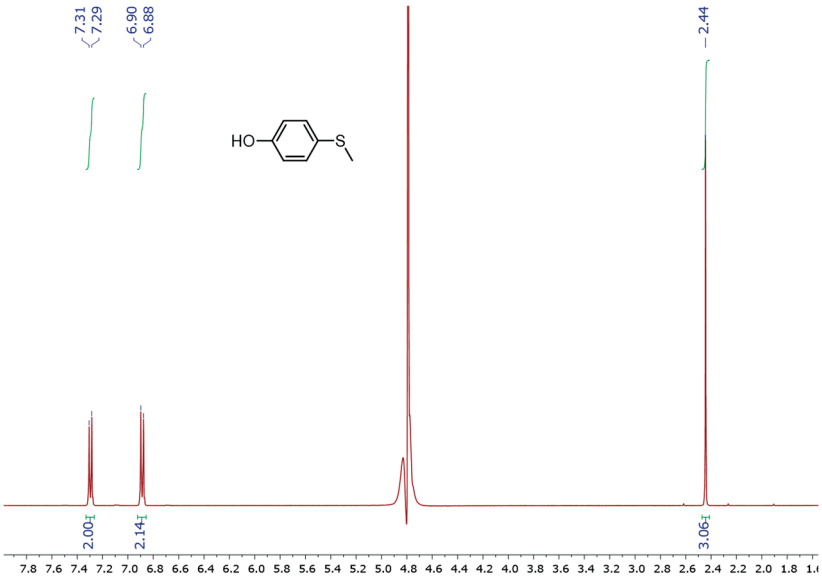

^{1}H NMR spectrum (400 MHz) of 4-(methylthio)phenol in PB (100 mM, pH=7.4)/D_2O 9:1.

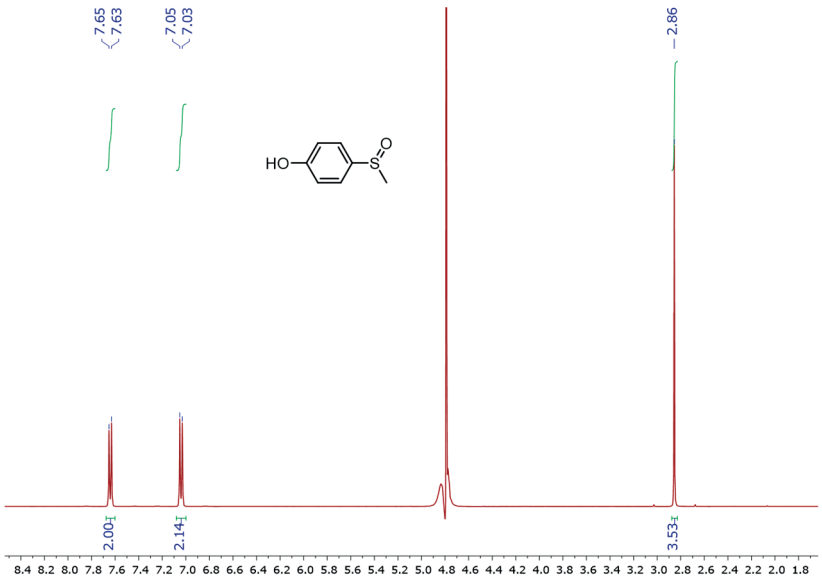

^{1}H NMR spectrum (400 MHz) of 4-(methylsulfinyl)phenol (**4**) in PB (100 mM, pH=7.4)/D_2O 9:1.

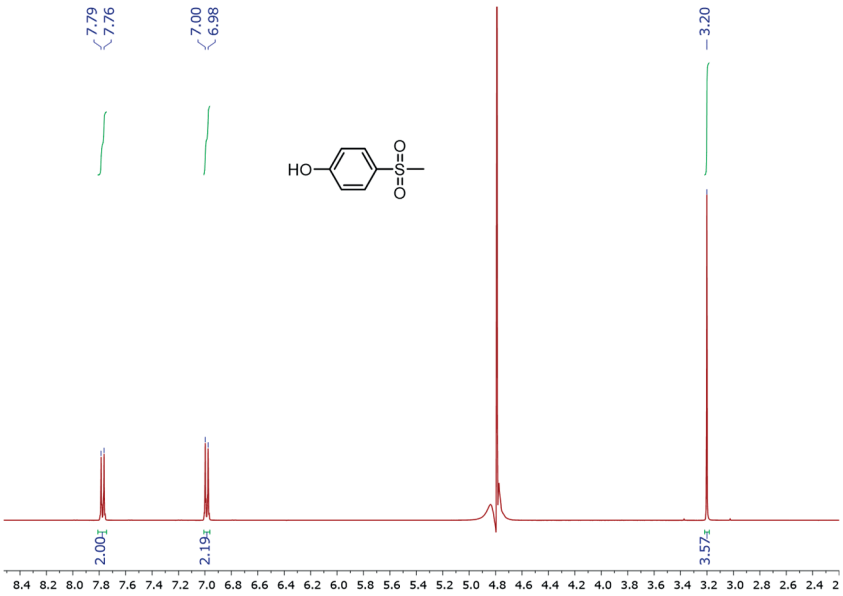

^{1}H NMR spectrum (400 MHz) of 4-(methylsulfonyl)phenol in PB (100 mM, pH=7.4)/D_2O 9:1.

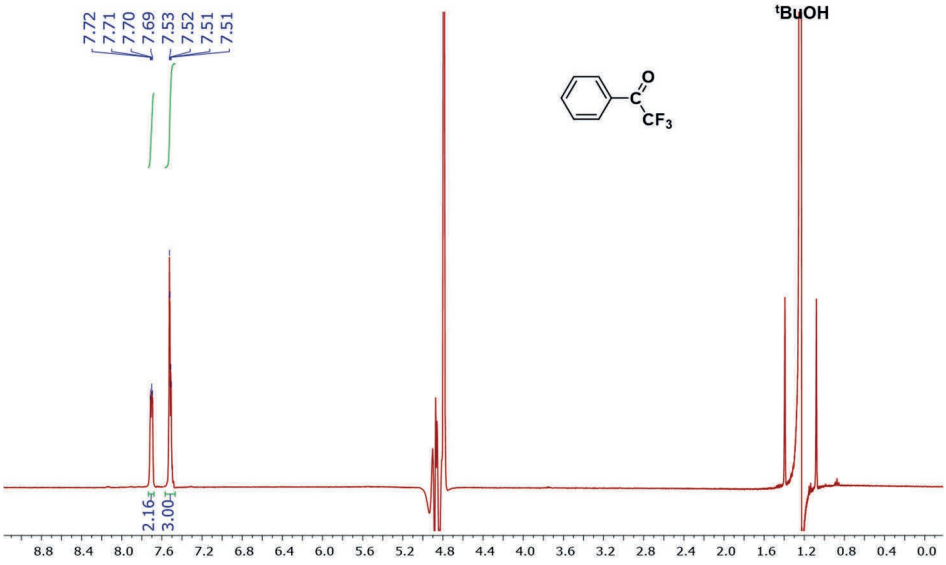

^{1}H NMR spectrum (400 MHz) of **3** in PB (100 mM, pH=7.4)/D_2O 9:1.

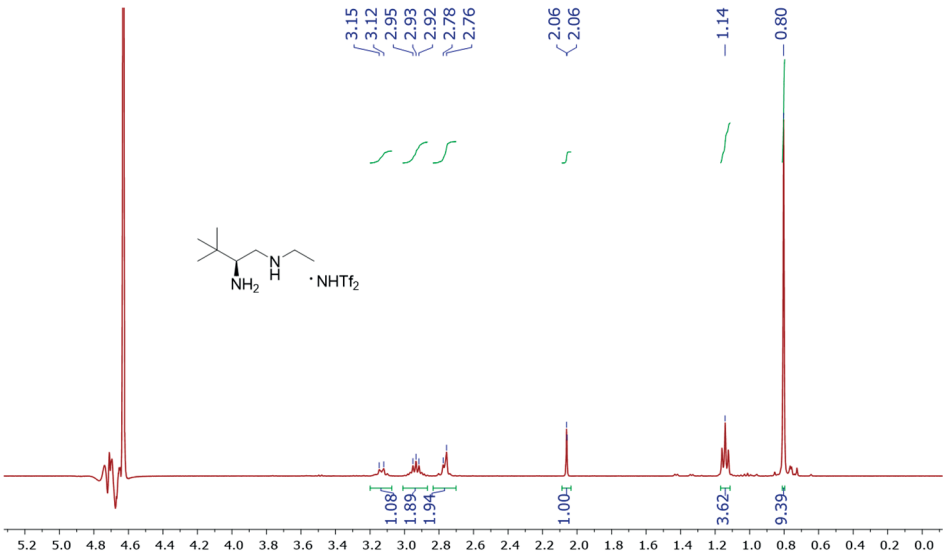

^{1}H NMR spectrum (400 MHz) of **A3** in PB (100 mM, pH=7.4)/D_2O 9:1.

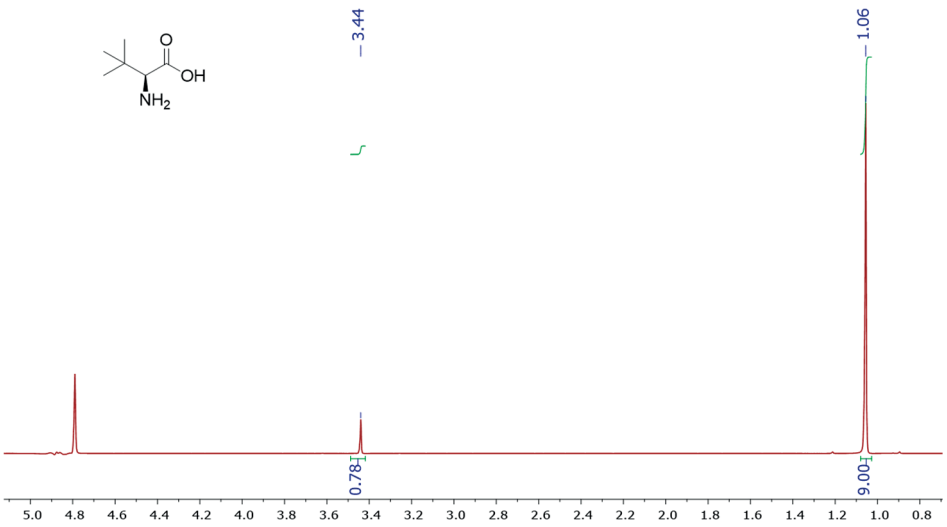

^{1}H NMR spectrum (400 MHz) of **A2** in PB (100 mM, pH=7.4)/D_2O 9:1.

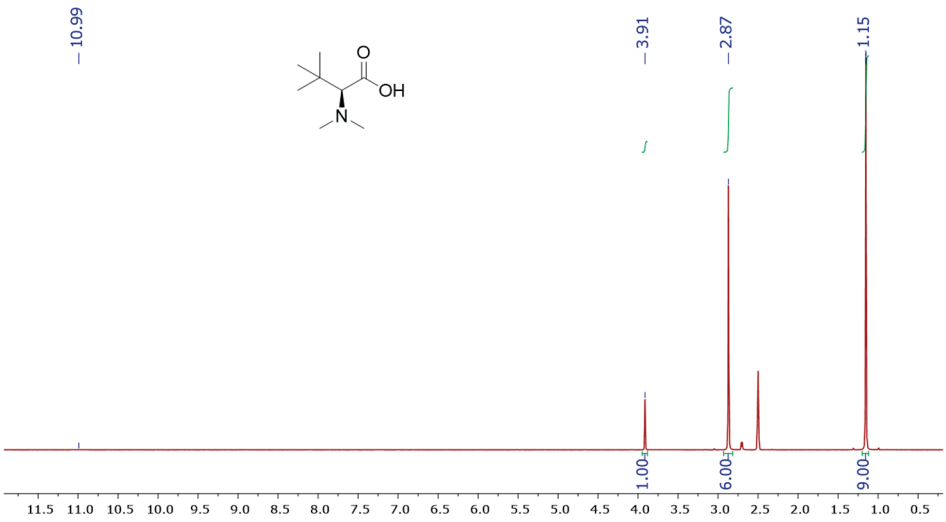

^{1}H NMR spectrum (400 MHz) of **A4** in DMSO-d_6.

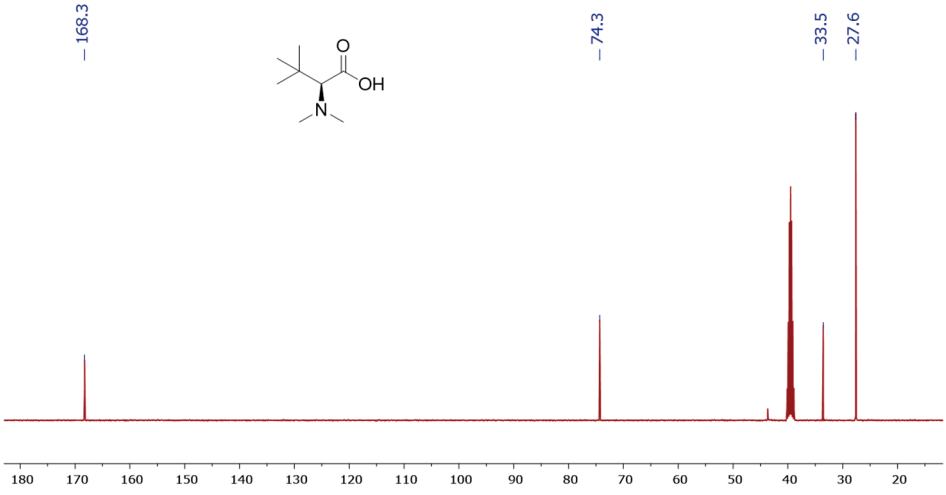

^{13}C NMR spectrum (101 MHz) of **A4** in DMSO-d_6.

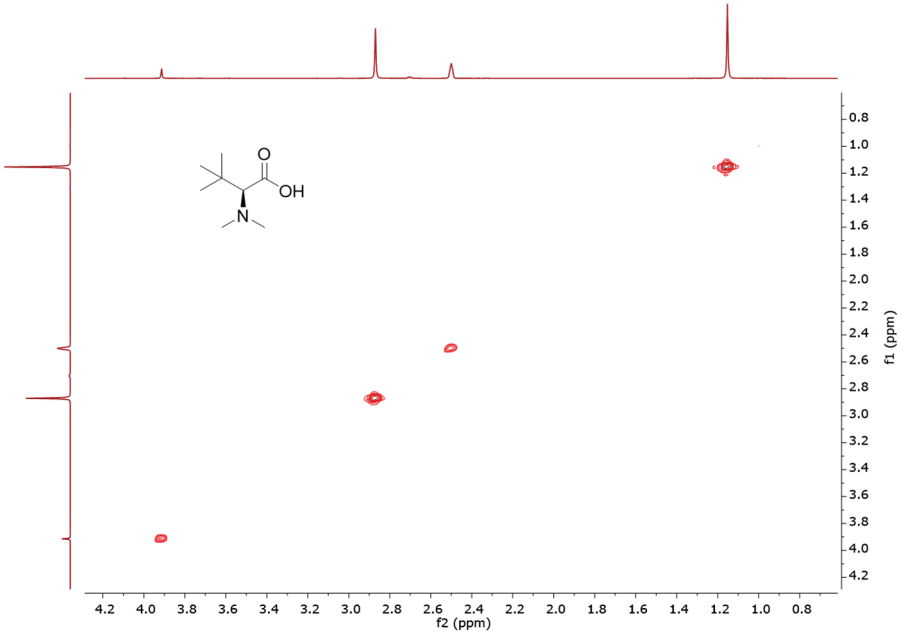

^{1}H NMR COSY spectrum of **A4** in DMSO-d_6.

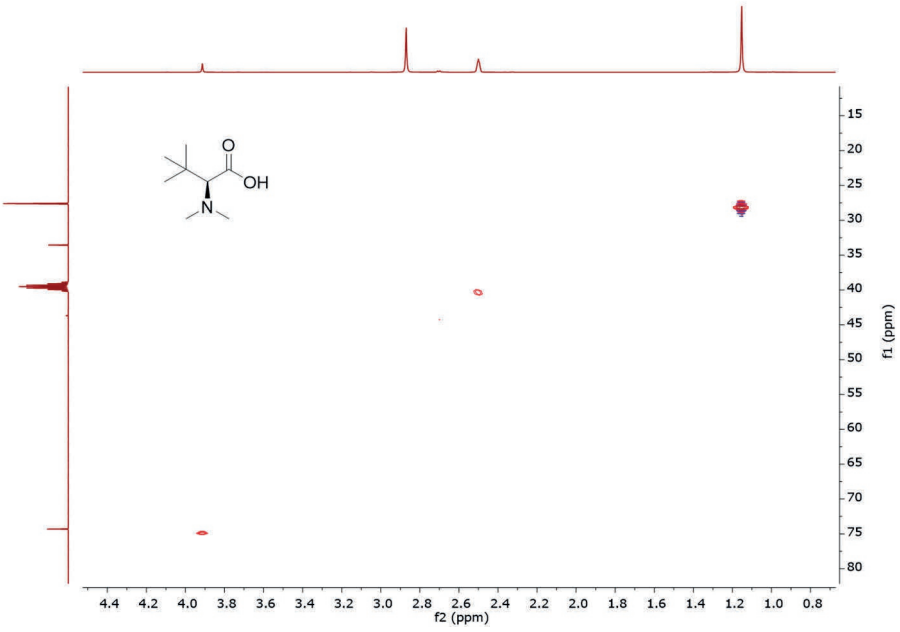

2D-HSQC NMR spectrum of **A4** in DMSO-d_6.

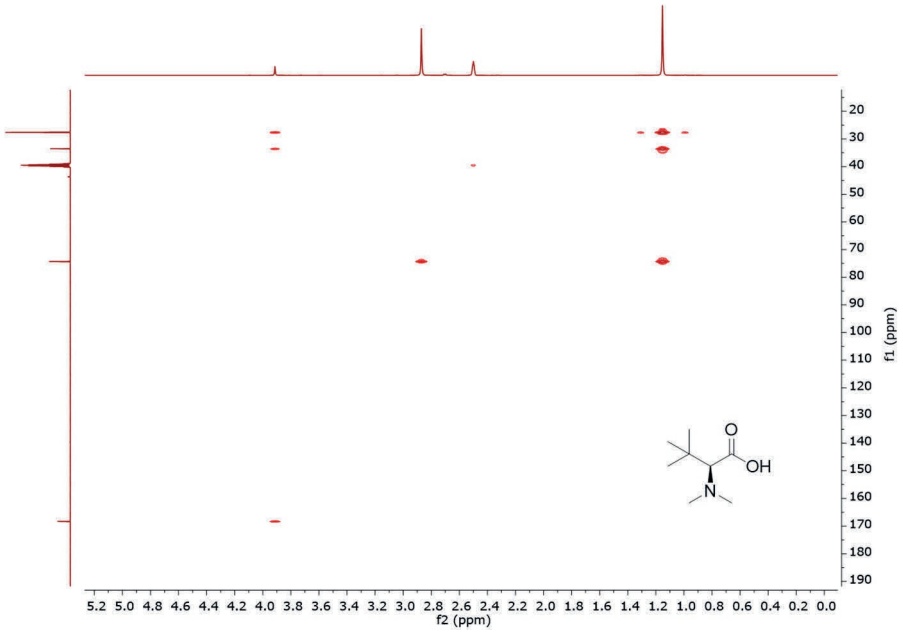

2D-HMBC NMR spectrum of **A4** in DMSO-d_6.

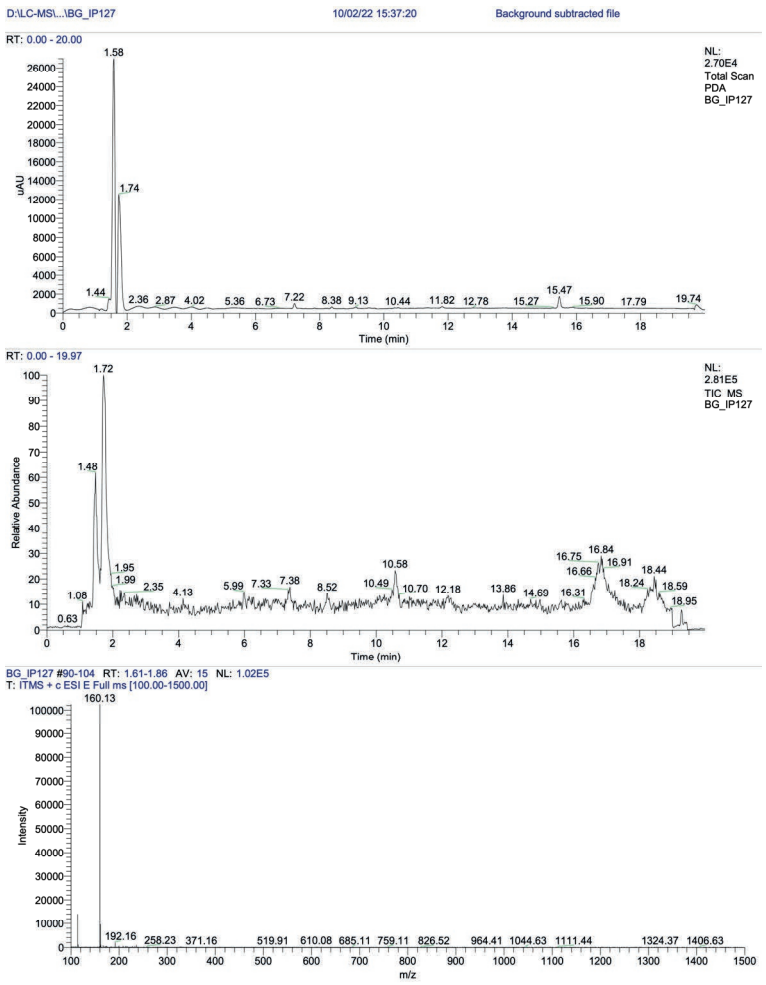

LC-MS spectra of **A4** in acetonitrile.

Chapter 4

Enhancing the ROS sensitivity of a responsive supramolecular hydrogel using peroxizyme catalysis

Hydrogels that can disintegrate upon exposure to reactive oxygen species (ROS) have potential for targeted drug delivery to tumor cells. In this study, we developed a diphenylalanine (FF) derivative with a thioether phenyl moiety attached to the N-terminus that can form supramolecular hydrogels at neutral and mildly acidic pH. The thioether can be oxidized by ROS to the corresponding sulfoxide, which makes the gelator hydrolytically labile. The resulting oxidation and hydrolysis products alter the polarity of the gelator, leading to disassembly of the gel fibers. To enhance ROS-sensitivity, we incorporated peroxidases in the gels, namely chloroperoxidase *Ci*VCPO and the unspecific peroxygenase r*Aae*UPO. Both enzymes accelerated the oxidation process, enabling the hydrogels to collapse with 10 times lower H_2O_2 concentrations than those required for enzyme-free hydrogel collapse. These ROS-responsive hydrogels have great potential as biomedical platforms for targeted drug delivery in the tumor microenvironment.

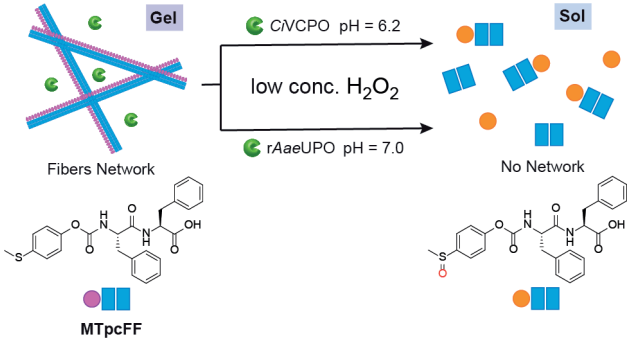

This chapter is published as:

I. Piergentili, T. Hilberath, B. Klemm, F. Hollmann, R. Eelkema, *Biomacromolecules*, 2023, **24**, 7, 3184–3192.

4.1 Introduction

Hydrogels made by self-assembly of small molecules have been drawing attention for over two decades, due to the perspective of using these soft materials for applications ranging from drug delivery to tissue engineering.[1,2] The initial fascination over serendipitously discovered gels was soon replaced by the need to understand the forces that drive gel formation in way to design *a priori* molecules that are able to gelate.[3,4] Considering the pool of self-assembled structures in biological systems,[5] nature was once again where researchers found inspiration. The first example of peptide based low-molecular-weight gelator (LMWG), reported in 1995, was used to realize a thermoreversible gel as carrier for antigen delivery and presentation.[6] Then, recognition of diphenylalanine (**FF**) as a basic structure able to form ordered nanostructures[7] led to the derivatization of this sequence to obtain a large variety of novel hydrogelators.[8-11] The biocompatibility, the possibility of bottom-up fabrication and easy chemical modification made diphenylalanine the natural choice as short peptide sequence for biomedical materials.[12-14] Subsequently, this versatile building block was functionalized with groups sensitive to various stimuli such as pH,[15,16] enzymes,[17,18] UV[19,20] and redox change[21] to realize responsive hydrogels. Reactive oxygen species (ROS) overproduction is typical in many tumor and diseased cells, causing a redox imbalance in the microenvironment. Ikeda and coworkers prepared **FF** type peptides with a boronoaryl group, which fragments in presence of hydrogen peroxide (H_2O_2), one of the most used ROS.[22]

Beside the boronates, sulfides are commonly used oxidation-sensitive groups for stimuli-triggered nanomedicine.[23,24] In aqueous medium, the oxidation of a sulfide into sulfoxide or sulfone produces a switch in solubility that can be used to destabilize self-assembled structures bearing these moieties.[25] The solubility switch from thioether to sulfoxide to trigger the gel-sol transition of hydrogels is not unprecedent,[26, 27] but to the best of our knowledge, it has not been used for

short peptide based gelators.[28,29] Recently, we developed a thioether phenyl ester based cascade mechanism in which the oxidation to sulfoxide induces the hydrolysis of the ester.[30] We functionalized diphenylalanine with the thioether phenyl moiety aiming to realize a hydrogelator able to respond to H_2O_2 through a logic gate mechanism that enables the gel to disrupt. Thus, we synthesized **MTpcFF** (Figure 1), an aromatic amphiphile able to form a self-assembled network in aqueous environment both at pH 6.2 and 7.0, which are favorable conditions for biological applications.

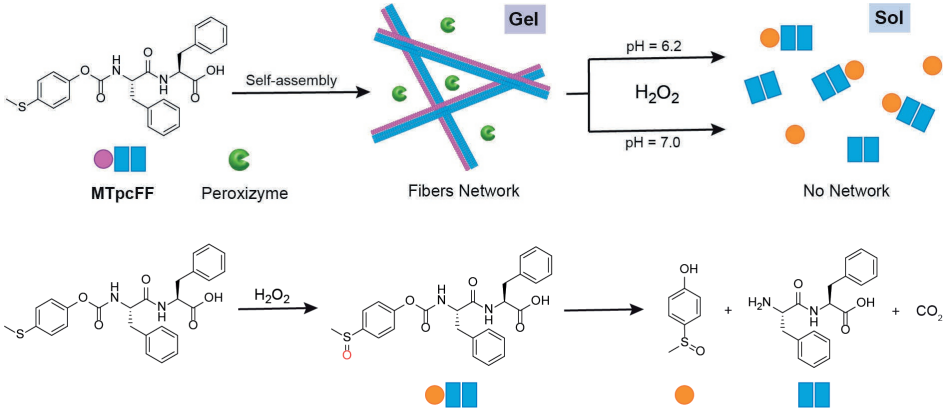

Figure 1. Schematic representation of **MTpcFF** self-assembly with peroxizymes showing the formation of a nanofiber network (gel) and H_2O_2-triggered gel-sol transition. Peroxizymes: gels with *Ci*VCPO are prepared in citrate buffer at pH = 6.2 and gels with r*Aae*UPO are prepared in phosphate buffer at pH = 7.0.

Moreover, once demonstrated the responsiveness towards H_2O_2, we included two different H_2O_2-dependent enzymes, namely the vanadium-dependent chloroperoxidase from *Curvularia inaequalis* (*Ci*VCPO) and the unspecific peroxygenase from *Agrocybe aegerita* (r*Aae*UPO, PaDaI-mutant) in the hydrogel. Chloroperoxidases are enzymes that catalyze the formation of hypohalites from H_2O_2 and halides. Despite their lower oxidation potential compared to H_2O_2 (1.78 V), hypohalites such as HOCl (1.49 V) and HOBr (1.34

V) are known to increase the rate of sulfide oxidation.[31-33] Amongst the chloroperoxidases used for oxidation of thioanisole type moieties, we chose *Ci*VCPO for its robustness and high catalytic activity.[34,35] The production of HOCl is optimal at pH below 7,[36] therefore this system is suitable for mildly acidic conditions, which are often present in tumor tissues.[37] We also incorporated r*Aae*UPO, which is known to catalyze the oxidation of aromatic sulfides with H_2O_2 at neutral pH,[38,39] in the **MTpcFF** gel.

Despite the different mechanism of the two peroxizymes, we found that their influence over the gel-sol transition of **MTpcFF** hydrogels upon addition of H_2O_2 is comparable. This establishes a versatile strategy that allows us to obtain ROS responsive hydrogels both in mildly acidic and neutral conditions.

4.2 Results and discussion

4.2.1 Oxidation and hydrolysis study on a soluble model compound

In previous work, we demonstrated the hydrolytic lability of the 4-(methylthio) phenyl ester when the thioether moiety is oxidized to the corresponding sulfoxide.[30] Here, we synthesized the taurine derivative **1** to study the oxidation process of the thioanisole moiety and whether sulfoxidation triggers carbamate hydrolysis. This model compound was also used to determine the ideal concentration of enzymes to accelerate the oxidation of the thioether unit. To avoid the inactivation of *Ci*VCPO in presence of inorganic phosphate, we performed all experiments with this chloroperoxidase in citrate buffer (CB, 50 mM, pH = 6.2, 140 mM NaCl). First, we followed product formation from 20 mM **1** in CB upon addition of 1.5 eq. H_2O_2 in absence of enzyme (Figure 2A) at 37 °C. After the first hour, the appearance of low field peaks in ^{1}H-NMR revealed the formation of sulfoxide **2** and the 4-(methylsulfinyl)phenol **3** (Figure S1). At 3 h, the conversion to **2** and **3** was 55% and 12%, respectively, and 33% of **1** was still present. Compound **1** was completely consumed after 8 h, but the amount of

2 dropped to 45% while **3** increased to 52%. Sulfoxide **2** is an intermediate that hydrolyzes over time to form **3** and free taurine, demonstrating the hydrolysis of the carbamate moiety in these conditions. It took 16 h to reach more than 80% conversion to phenol **3**, indicating that the hydrolysis rate from **2** to **3** is lower than the rate of oxidation of **1** to **2**. Considering the difficulties in enhancing the rate of hydrolysis, we focused on catalysis of the oxidation step. Therefore, we tested *Ci*VCPO in concentrations of 0.1 and 1.0 μM to seek for the optimal oxidation conditions of **1**. In the presence of 0.1 μM *Ci*VCPO, compound **1** converted into 80% of **2** in 2 h after the addition of H_2O_2 (Figure 2B, yellow line). With 1.0 μM *Ci*VCPO 85% of **2** was produced in 10 min (Figure 2B, purple line). This result demonstrates that the chloroperoxidase accelerates the oxidation of **1** more than two times for 0.1 μM and about 30 times for 1.0 μM enzyme. In addition, at 3 h the conversion of **3** was 19% for 0.1 μM *Ci*VCPO and 26% for 1.0 μM *Ci*VCPO against 12% for the enzyme-free sample (Figure 2C). However, for the samples with the chloroperoxidases, the formation of **3** was about 80% after 12 h. This indicates that the hydrolysis rate is influenced by the concentration of **2**, but this effect fades with the consumption of the sulfoxide and the oxidant, translating into a minor difference in the kinetic profile towards the end of the reaction.

Aiming to investigate the reaction in neutral conditions, we decided to follow the oxidation and hydrolysis of **1** with 1.5 equivalents of H_2O_2 in phosphate buffer (PB, 50 mM) at pH = 7.0. In Figure 2D, we show the conversion of **1** and its products in PB, in absence of enzyme. At 3 h, the production of **2** and **3** was respectively 39% and 28%, with 33% of **1** remaining. At the same time point, **1** was consumed equally whether in phosphate or in citrate buffer, but the higher concentration of **3** in PB indicates that the hydrolysis is indeed faster than in CB. Due to the incompatibility of *Ci*VCPO and phosphate buffer, we employed r*Aae*UPO as peroxizyme to catalyze the oxidation of **1** for these conditions. Similar to *Ci*VCPO, we used 0.1 and 1.0 μM r*Aae*UPO to accelerate the

oxidation of **1** with H_2O_2. Compound **2** reached 90% in only 10 min with 1.0 μM r*Aae*UPO and 48% in 2 h with 0.1 μM r*Aae*UPO (Figure 2E). The hydrolysis profile of **2** to **3** (Figure 2F) was similar in all cases, reaching about 90% in 12 h. The use of 0.1 μM r*Aae*UPO barely accelerated the oxidation of **1** compared to the uncatalyzed case. In presence of 1.0 μM r*Aae*UPO we have an almost immediate full conversion to **2**, similar to the use of the same concentration of *Ci*VCPO. Finally, at 12 h the hydrolysis rate reached 90% in PB against 80% in CB. Additionally, after 12 h in absence of oxidant, 14% 4-(methylthio)phenol had formed in PB (orange line, Figure 2F) against about 5% in CB (orange line, Figure 2C), confirming the former condition as more advantageous for hydrolytic degradation. Considering the comparable efficiency of both *Ci*VCPO and r*Aae*UPO at a concentration of 1.0 μM in the H_2O_2-driven oxidation of the thioether moiety and the balance between responsiveness and stability of the non-oxidized substrate, we chose to explore these conditions at the material level in both PB and CB with the corresponding 1.0 μM enzyme.

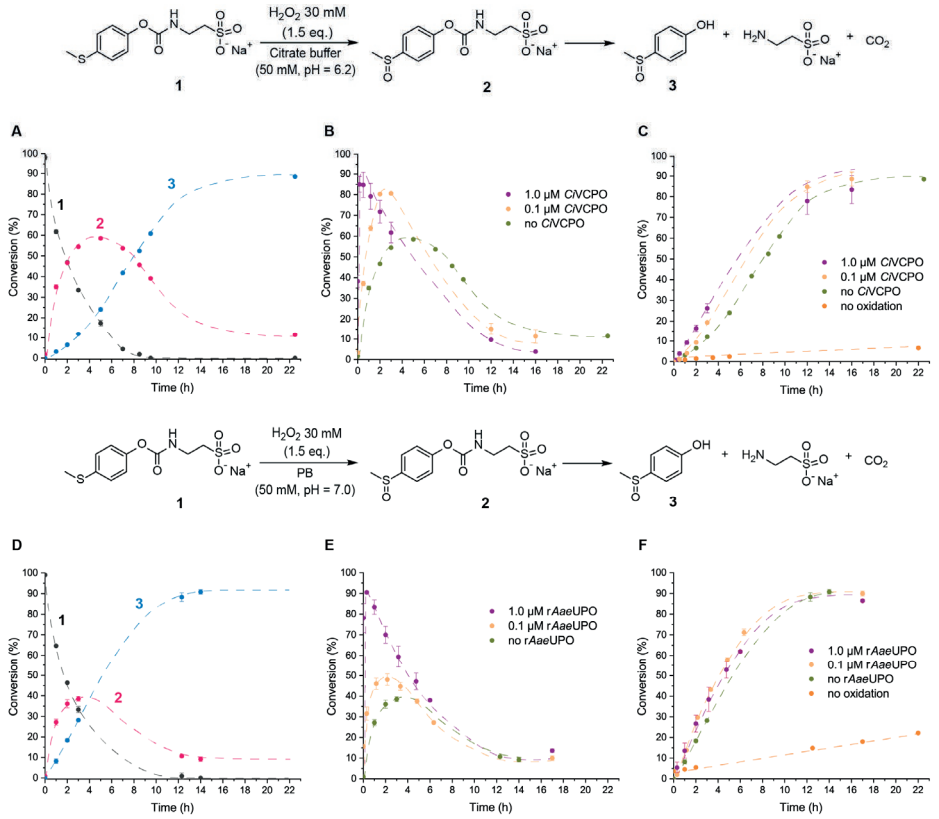

Figure 2. Scheme illustrating the species formed from compound **1** after the addition of H_2O_2 at 37 °C. A) Conversion profile without enzyme in citrate buffer. B) Conversion profile of **2** after addition of H_2O_2 in presence of 0.0, 0.1, 1.0 μM *Ci*VCPO. C) Conversion profile of **3** without H_2O_2 in citrate buffer (orange line, the conversion refers to 4-(methylthio)phenol) and after addition of H_2O_2 in presence of 0.0, 0.1, 1.0 μM *Ci*VCPO. D) Conversion profile without enzyme in phosphate buffer. E) Conversion profile of **2** after addition of H_2O_2 in presence of 0.0, 0.1, 1.0 μM r*Aae*UPO. F) Conversion profile of **3** in absence of H_2O_2 in phosphate buffer (orange line, the conversion refers to 4-(methylthio)phenol) and after addition of H_2O_2 in presence of 0.0, 0.1, 1.0 μM r*Aae*UPO. The dashed lines are drawn as a guide for the eye.

4.2.2 Properties of MTpcFF hydrogels

Short peptide based amphiphiles have great potential to form gels encapsulating large amounts of water.[40,41] Considering its promising gelation properties,[42] we

chose **FF** as peptide building block and functionalized its N-terminus with the 4-(methylthio)phenyl moiety to obtain **MTpcFF**. Using the tube-inversion method, we found that this dipeptide derivative has a critical gel concentration (CGC) of 0.70 wt% in CB and 0.95 wt% in PB.

Knowing that tripeptide based hydrogelators have generally lower CGC, we also synthesized **MTpcFFF**. However, in the tube-inversion tests the gelation of this derived tripeptide was often difficult to achieve and to replicate. We indeed noticed poor solubility in aqueous solution even at a concentration of 0.1 wt%, and without the possibility of heating to avoid the premature hydrolysis of the carbamate motif, we decided to continue our studies exclusively on **MTpcFF**.

First, we investigated the rheological properties of **MTpcFF** at 0.75 wt% in CB and at 1.0 wt% in PB. Interestingly, despite the higher concentration of the hydrogelator in PB, the storage modulus (G') is 2.5 kPa and the loss modulus (G") is 0.2 kPa for **MTpcFF** in PB against 6.4 (G') and 0.8 (G") kPa for **MTpcFF** in CB (Figure 3). This result is not surprising if we consider the influence that pH and Hofmeister effect have over the gelation of other phenylalanine based LMWG.[43-48] Lower pH leads to a higher degree of protonation of the terminal carboxylic acid of the dipeptide amphiphile, making the functionalized **FF** more hydrophobic and therefore favoring the gelation in aqueous solution. Nevertheless, obtaining G' values always higher than the G" means that both conditions produced gels with viscoelastic properties typical of fiber networks.[49] Observation of the hydrogels with optical microscopy (Figure S3) and Cryo-EM images (Figure 3C, Figure S4) confirmed the presence of nanofibers that can aggregate in bundles with microscopic diameters. Analysis of Cryo-EM images showed average fiber diameters of 7.9 ± 2.0 (citrate buffer, Figure S4C) and 4.0 ± 0.7 nm (phosphate buffer, Figure S4F) for the **MTpcFF** hydrogels.

Additives and impurities can affect the gelation of LMWG. Thus, to exclude that the encapsulation of *Ci*VCPO and r*Aae*UPO influences the mechanical properties of **MTpcFF** gels, we performed additional rheological analysis on the

enzyme loaded hydrogels. The resulting data confirmed that adding 1.0 µM *Ci*VCPO to 0.75 wt% **MTpcFF** in CB and 1.0 µM r*Aae*UPO to 1.0 wt% **MTpcFF** in PB produced G' and G" values that are only slightly lower than the corresponding gels without peroxizymes (Figure 3F). We also performed strain amplitude measurements within the linear viscoelastic region for all four different conditions. **MTpcFF** gels in CB both with and without *Ci*VCPO showed a slight drop in G' and G" values at 3% strain. In contrast, despite their lower storage and loss moduli, **MTpcFF** gels in PB demonstrated a good stability even at 5% strain. Knowing these minor differences in the mechanical properties of **MTpcFF** hydrogel in different conditions, we pursued to investigate their response to H_2O_2.

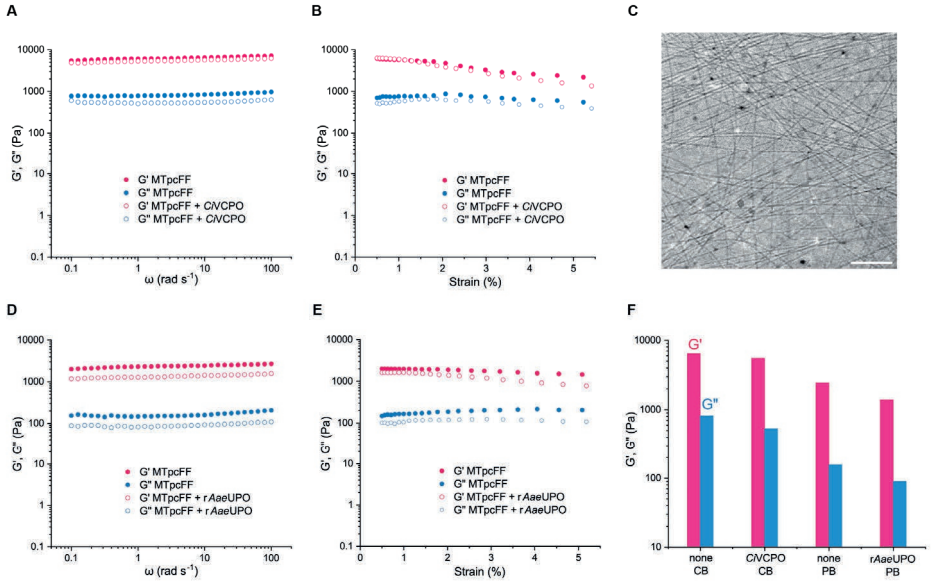

Figure 3. Properties of **MTpcFF** gels. A) Frequency sweep and B) strain sweep of **MTpcFF** with (○) and without (●) *Ci*VCPO in citrate buffer. C) Cryo-EM image of **MTpcFF** (1.0 wt%) hydrogel in PB (Scale bar = 200 nm). D) Frequency sweep and E) strain sweep of **MTpcFF** with (○) and without (●) r*Aae*UPO in phosphate buffer. F) Rheological properties of **MTpcFF** gels at an angular frequency of 1.0 Hz.

4.2.3 H_2O_2-responsive gel-sol transition of MTpcFF hydrogels

To test the sensitivity of **MTpcFF** gels towards oxidation, we followed the gel-sol transition in time after the addition of H_2O_2 via the tube-inversion method. **MTpcFF** hydrogels (0.75 wt%, 16 mM) were prepared in CB with and without *Ci*VCPO (1.0 μM) and visually followed after the addition of varying equivalents of H_2O_2 (Figure 4A). The peroxizymes-free gels turned into solution 5 h after the addition of 1.0 equivalent of H_2O_2, while *Ci*VCPO loaded **MTpcFF** hydrogels became solutions within 30 min in presence of an equimolar amount of hydrogen peroxide (Figure 4A). The hydrogels with *Ci*VCPO fully disrupted in 1 h and 3 h with 0.5 eq. and 0.25 eq. H_2O_2, respectively. Meanwhile, the *Ci*VCPO loaded control gels, where the oxidant was not added, remained intact for over 8 h.

To investigate the molecular mechanism behind the material change, we analyzed **MTpcFF** hydrogels as soon as they had disintegrated after the addition of 1.0 eq. of H_2O_2 with the HPLC. In the chromatogram, we found that after this time the peak of **MTpcFF** has decreased, while an unidentified peak appeared at t_R = 18.7 min. LC-MS analysis revealed that we obtained the corresponding sulfoxide of the gelator (Figure S6). Despite the presence in the HPLC analysis of about 15% **FF** 5 h after the addition of H_2O_2, we concluded that the main cause of the disassembly of the hydrogel is the oxidation of **MTpcFF** into the more hydrophilic sulfoxide. This result comes unexpected since the sulfoxidation-related change in hydrophilicity was previously considered to be too small to lead to disassembly of block copolymers based on this motif.[30] On the other hand, the observed gel disruption at the oxidation step accelerates the material response and removes the slow hydrolysis as the rate determining step. In addition, the slow hydrolysis rate explains the considerable stability of the hydrogels in absence of the oxidant.

The 10-fold acceleration of gel-sol transition encouraged us to explore [H_2O_2]/[**MTpcFF**] ratios as low as 0.1. Interestingly, **MTpcFF** hydrogels were responsive to such low concentrations of H_2O_2, even if the gel solubilization was

not complete at 8 h (Figure 4A, bottom left). The HPLC analysis was performed on the solutions obtained after 5 h for the hydrogels exposed to high oxidant concentration, while the partially disrupted gels exposed to 0.1 eq. H_2O_2 and the control experiments were analysed after 8 h. The HPLC data in Figure 4B show that the presence of 0.1 eq. H_2O_2 caused the consumption of about 10% gelator. Considering the corresponding gel picture, we can conclude that this variation in **MTpcFF** concentration is not sufficient to completely degrade the gel. In contrast, upon addition of 0.25 eq. H_2O_2 we obtained full collapse of the gels in 3 h, with about 75% of the remaining gelator according to HPLC analysis. This suggests that the threshold for fully solubilization of a **MTpcFF** gel (0.75 wt%) in CB is in the range 0.1-0.2 eq. H_2O_2. All these experiments were carried either with hydrogen peroxide and either NaCl or KBr, needed for the production of hypohalites by *Ci*VCPO. The chloroperoxidase is able to convert H_2O_2 and NaCl into HOCl, while in presence of KBr, HOBr is formed. In principle, HOCl has higher oxidation potential than HOBr, while the latter is more electrophilic and can react faster with the thioether.[50] In the tube-inversion tests, the use of NaCl together with H_2O_2 led to solutions that appeared slightly less viscous than when KBr was used. In the correlating HPLC analysis, for additions of 1.0 and 0.5 eq. H_2O_2, about 6% less **MTpcFF** was measured when NaCl was added instead of KBr. However, the difference is not significant, making it difficult to assess what species has more impact on the system. On a second note, considering the abundant presence of chlorine in cellular environment and the tendency of HOBr to react with a broad range of substrates other than the thioether,[51, 52] the conditions with NaCl should be favored for biological applications.

Subsequently, we proceeded to test the gel disruption upon addition of H_2O_2 between 0.1 and 1.0 eq. on 1.0 wt% **MTpcFF** hydrogels (20 mM) in PB with and without r*Aae*UPO (1.0 μM). The photographs of these inverted vial tests are shown in Figure 4C. r*Aae*UPO-free hydrogels take 5 h to turn into a viscous solution in presence of 1.0 equivalent of the oxidant, while when r*Aae*UPO was

encapsulated in the gel formulation, this time reduced to 30 min. The time to gel degradation was 1 and 3 h when respectively 0.5 and 0.25 eq. H_2O_2 were added. We found that 0.1 eq. of hydrogen peroxide is enough to achieve the gel-sol transition, even if the time scale is extended to 8 h in this case. The corresponding HPLC results (Figure 4D) showed that for 0.1 eq. H_2O_2, the expected 90% of **MTpcFF** was detected, which appeared to be below the CGC of the gels when comparing with the tube-inversion tests. Such low threshold is in line with the need of increasing the gelator concentration when performing gelation in PB compared to that achieved in CB. Despite the different concentrations and conditions of **MTpcFF** hydrogels with r*Aae*UPO and with *Ci*VCPO, the response times in gel collapse upon addition of H_2O_2 were remarkably similar. The close catalytic effect of 1.0 μM of r*Aae*UPO and of 1.0 μM *Ci*VCPO (in presence of halides) to oxidize the thioether with H_2O_2 was already anticipated from the ^{1}HNMR study on **1** (Figure 2). The translation of this effect to the hydrogels with different formulations enables these materials to have comparable sensitivity towards H_2O_2 (~ 2.0 mM), in both mildly acidic and neutral settings.

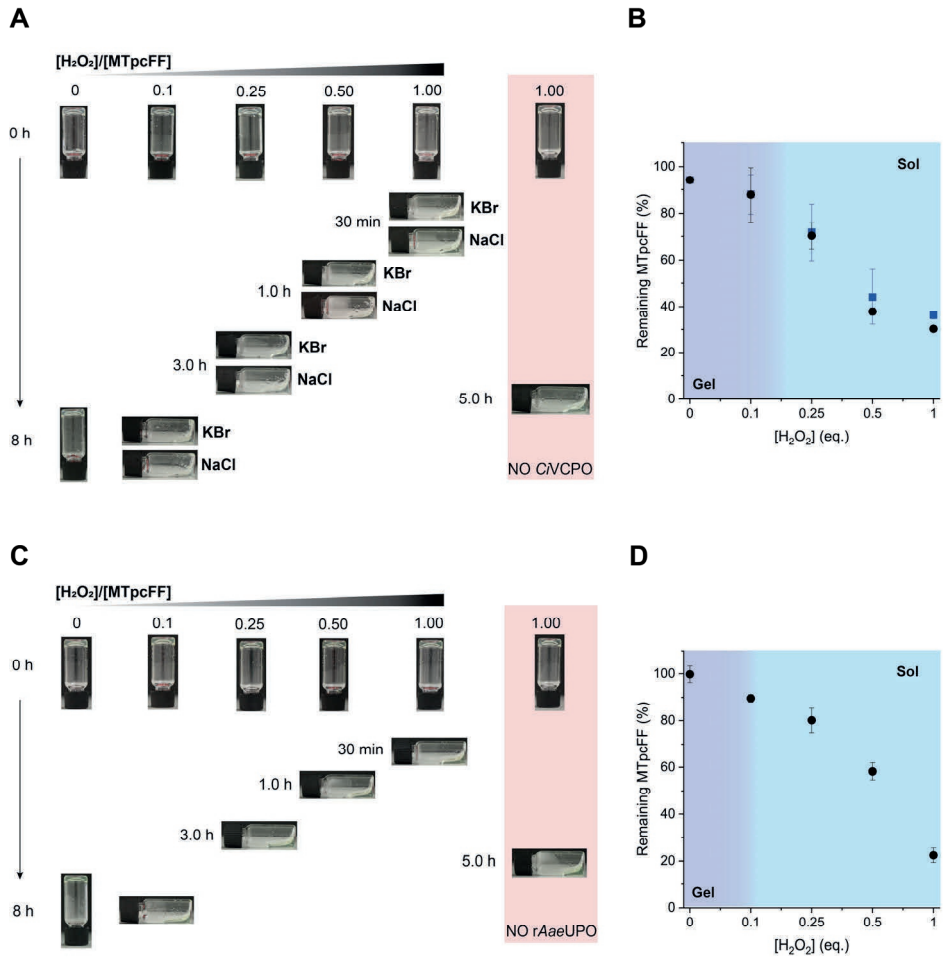

Figure 4. A) Photographs of *Ci*VCPO (1.0 μM) loaded **MTpcFF** hydrogels in CB after the addition of various amounts of H_2O_2. B) HPLC analysis of remaining **MTpcFF** after the addition of various amount of H_2O_2 in presence of *Ci*VCPO (1.0 μM) in CB with NaCl (●) or KBr (■). The experiments were performed in duplicate to obtain mean and standard deviation values (shown as error bars). C) Photographs of r*Aae*UPO (1.0 μM) loaded **MTpcFF** hydrogels in PB after the addition of various amounts of H_2O_2. D) HPLC analysis of remaining **MTpcFF** after the addition of various amount of H_2O_2 in presence of r*Aae*UPO (1.0 μM) in PB. The experiments were performed in duplicate to obtain mean and standard deviation values (shown as error bars).

4.3 Conclusion

In summary, we report here a thioether carbamate based dipeptide capable of forming hydrogels in the 6.0 – 7.0 pH range. The carbamate is stable in these conditions, assuring that these gels remain intact for more than 8 h. Contrary, the addition of H_2O_2 causes oxidation of the thioether to the corresponding sulfoxide, triggering the disruption of the gel via a solubility switch. We encapsulated two different peroxizymes in the hydrogel: the vanadium-dependent chloroperoxidase *Ci*VCPO in citrate buffer at pH 6.2 and the heme-dependent peroxidase r*Aae*UPO in phosphate buffer at pH 7.0. The presence of the two enzymes showed comparable impact, with the gel collapsing 10 times faster than the peroxizyme-free samples. The encapsulation of peroxizymes in the gel matrix proved essential to achieve a gel-sol transition at hydrogen peroxide concentrations below 2.0 mM. Moreover, we believe that the similar responsiveness of the hydrogel in the two different conditions is a key feature for application of this system in neutral and mildly acidic environments with elevated ROS concentrations.

In perspective, this simple dipeptide based gelator can be the starting point to realize a library of thioanisole carbamate based LMWG with different mechanical properties and response thresholds. This holds promise for devices sensitive to redox imbalance in biological settings. Additionally, even if it was not essential in this study, the hydrolytic instability of the carbamate after the oxidation would make the thioether phenyl group a promising ROS-labile protecting group of the amine in pharmaceutically active compounds.

4.4 References

1. M. Ni and S. Zhuo, *RSC Adv.*, 2019, **9**, 844-852.
2. N. Yadav, M. K. Chauhan and V. S. Chauhan, *Biomater. Sci.*, 2020, **8**, 84-100.
3. R. G. Weiss, *J. Am. Chem. Soc.*, 2014, **136**, 7519-7530.
4. J. K. Gupta, D. J. Adams and N. G. Berry, *Chem. Sci.*, 2016, **7**, 4713-4719.
5. A. C. Mendes, E. T. Baran, R. L. Reis and H. S. Azevedo, *Wiley Interdiscip. Rev.: Nanomed. Nanobiotechnol.*, 2013, **5**, 582-612.
6. R. Vegners, I. Shestakova, I. Kalvinsh, R. M. Ezzell and P. A. Janmey, *J. Pept. Sci.*, 1995, **1**, 371-378.
7. M. Reches and E. Gazit, *Science*, 2003, **300**, 625-627.
8. R. Roytman, L. Adler-Abramovich, K. S. A. Kumar, T.-C. Kuan, C.-C. Lin, E. Gazit and A. Brik, *Org. Biomol. Chem.*, 2011, **9**, 5755-5761.
9. M. J. Krysmann, V. Castelletto, A. Kelarakis, I. W. Hamley, R. A. Hule and D. J. Pochan, *Biochemistry*, 2008, **47**, 4597-4605.
10. J. Kim, T. H. Han, Y.-I. Kim, J. S. Park, J. Choi, D. G. Churchill, S. O. Kim and H. Ihee, *Adv. Mater.*, 2010, **22**, 583-587.
11. C. H. Görbitz, *Chem. Commun.*, 2006, 2332-2334.
12. Y. Kuang, X. Du, J. Zhou and B. Xu, *Adv. Healthcare Mater.*, 2014, **3**, 1217-1221.
13. R. Ischakov, L. Adler-Abramovich, L. Buzhansky, T. Shekhter and E. Gazit, *Biorg. Med. Chem.*, 2013, **21**, 3517-3522.
14. C. Diaferia, G. Morelli and A. Accardo, *J. Mater. Chem.B*, 2019, **7**, 5142-5155.
15. A. Z. Cardoso, A. E. Alvarez Alvarez, B. N. Cattoz, P. C. Griffiths, S. M. King, W. J. Frith and D. J. Adams, *Faraday Discuss.*, 2013, **166**, 101-116.

16. C. Tang, R. V. Ulijn and A. Saiani, *Langmuir*, 2011, **27**, 14438-14449.

17. Z. Yang, G. Liang, L. Wang and B. Xu, *J. Am. Chem. Soc.*, 2006, **128**, 3038-3043.

18. M. Yi, J. Guo, H. He, W. Tan, N. Harmon, K. Ghebreyessus and B. Xu, *Soft Matter*, 2021, **17**, 8590-8594.

19. Y. Huang, Z. Qiu, Y. Xu, J. Shi, H. Lin and Y. Zhang, *Org. Biomol. Chem.*, 2011, **9**, 2149-2155.

20. J. K. Sahoo, S. K. M. Nalluri, N. Javid, H. Webb and R. V. Ulijn, *Chem. Commun.*, 2014, **50**, 5462-5464.

21. M. Ikeda, T. Tanida, T. Yoshii and I. Hamachi, *Adv. Mater.*, 2011, **23**, 2819-2822.

22. M. Ikeda, T. Tanida, T. Yoshii, K. Kurotani, S. Onogi, K. Urayama and I. Hamachi, *Nat. Chem.*, 2014, **6**, 511-518.

23. A. Napoli, M. Valentini, N. Tirelli, M. Müller and J. A. Hubbell, *Nat. Mater.*, 2004, **3**, 183-189.

24. F. El Mohtadi, R. d'Arcy, J. Burke, J. M. Rios De La Rosa, A. Gennari, R. Marotta, N. Francini, R. Donno and N. Tirelli, *Biomacromolecules*, 2020, **21**, 305-318.

25. M. Geven, R. d'Arcy, Z. Y. Turhan, F. El-Mohtadi, A. Alshamsan and N. Tirelli, *Eur. Polym. J.*, 2021, **149**, 110387.

26. S. Yu, C. Wang, J. Yu, J. Wang, Y. Lu, Y. Zhang, X. Zhang, Q. Hu, W. Sun, C. He, X. Chen and Z. Gu, *Adv. Mater.*, 2018, **30**, 1801527.

27. Q. Xu, C. He, K. Ren, C. Xiao and X. Chen, *Adv. Healthcare Mater.*, 2016, **5**, 1979-1990.

28. X. Miao, W. Cao, W. Zheng, J. Wang, X. Zhang, J. Gao, C. Yang, D. Kong, H. Xu, L. Wang and Z. Yang, *Angew. Chem. Int. Ed.*, 2013, **52**, 7781-7785.

29. M. Criado-Gonzalez and D. Mecerreyes, *J. Mater. Chem.B*, 2022, **10**, 7206-7221.

30. I. Piergentili, P. R. Bouwmans, L. Reinalda, R. W. Lewis, B. Klemm, H.

Liu, R. M. de Kruijff, A. G. Denkova and R. Eelkema, *Polym. Chem.*, 2022, **13**, 2383-2390.

31. B. L. Allen, J. D. Johnson and J. P. Walker, *ACS Nano*, 2011, **5**, 5263-5272.

32. Z. Tóth and I. Fábián, *Inorg. Chem.*, 2004, **43**, 2717-2723.

33. Y. Hu, G. Xie and D. M. Stanbury, *Inorg. Chem.*, 2017, **56**, 4047-4056.

34. G. T. Höfler, A. But and F. Hollmann, *Org. Biomol. Chem.*, 2019, **17**, 9267-9274.

35. E. Fernández-Fueyo, M. van Wingerden, R. Renirie, R. Wever, Y. Ni, D. Holtmann and F. Hollmann, *ChemCatChem*, 2015, **7**, 4035-4038.

36. R. Wever, R. Renirie and F. Hollmann, in *Vanadium Catalysis*, eds. M. Sutradhar, A. J. L. Pombeiro and J. A. L. da Silva, The Royal Society of Chemistry, 2021, DOI: 10.1039/9781839160882-00548, pp. 548-563.

37. B. Lin, H. Chen, D. Liang, W. Lin, X. Qi, H. Liu and X. Deng, *ACS Appl. Mater. Interfaces*, 2019, **11**, 11157-11166.

38. S.-i. Ozaki, H.-J. Yang, T. Matsui, Y. Goto and Y. Watanabe, *Tetrahedron: Asymmetry*, 1999, **10**, 183-192.

39. E. Baciocchi, M. F. Gerini, P. J. Harvey, O. Lanzalunga and S. Mancinelli, *Eur. J. Biochem.*, 2000, **267**, 2705-2710.

40. M. de Loos, B. L. Feringa and J. H. van Esch, *Eur. J. Org. Chem.*, 2005, **2005**, 3615-3631.

41. L. A. Estroff and A. D. Hamilton, *Chem. Rev.*, 2004, **104**, 1201-1218.

42. L. Adler-Abramovich, L. Vaks, O. Carny, D. Trudler, A. Magno, A. Caflisch, D. Frenkel and E. Gazit, *Nat. Chem. Biol.*, 2012, **8**, 701-706.

43. J. Raeburn, G. Pont, L. Chen, Y. Cesbron, R. Lévy and D. J. Adams, *Soft Matter*, 2012, **8**, 1168-1174.

44. S. Fleming and R. V. Ulijn, *Chem. Soc. Rev.*, 2014, **43**, 8150-8177.

45. F. Hofmeister, *Archiv für experimentelle Pathologie und Pharmakologie*, 1888, **24**, 247-260.

46. S. Roy, N. Javid, P. W. J. M. Frederix, D. A. Lamprou, A. J. Urquhart, N. T. Hunt, P. J. Halling and R. V. Ulijn, *Chem. Eur. J.*, 2012, **18**, 11723-11731.

47. K. P. Gregory, G. R. Elliott, H. Robertson, A. Kumar, E. J. Wanless, G. B. Webber, V. S. J. Craig, G. G. Andersson and A. J. Page, *PCCP*, 2022, **24**, 12682-12718.

48. B. L. Abraham, P. Agredo, S. G. Mensah and B. L. Nilsson, *Langmuir*, 2022, **38**, 15494-15505.

49. A. Aggeli, M. Bell, N. Boden, J. N. Keen, P. F. Knowles, T. C. B. McLeish, M. Pitkeathly and S. E. Radford, *Nature*, 1997, **386**, 259-262.

50. V. F. Ximenes, N. H. Morgon and A. R. de Souza, *J. Inorg. Biochem.*, 2015, **146**, 61-68.

51. C. L. Hawkins and M. J. Davies, *Free Radical Biol. Med.*, 2021, **172**, 633-651.

52. M. J. Davies, *J. Clin. Biochem. Nutr.*, 2011, **48** (1), 8–19.

4.5 Supporting information

4.5.1 Materials

All commercial reagents were used without further purification unless otherwise specified. Diphenyl alanine (FF) and triphenyl alanine (FFF) were purchased from Sigma Aldrich. The chloroperoxidase *Ci*VCPO from *Curvularia inaequalis* and the unspecific peroxygenase r*Aae*UPO from *Agrocybe aegerita* were provided by Hollmann's lab following reported procedures.[1, 2] ^{1}H NMR and ^{13}C NMR spectra were recorded on Agilent-400 MR DD2 (400 MHz and 100.5 MHz for ^{1}H and ^{13}C, respectively) spectrometer at 298 K. Chemical shifts are reported in ppm relative to the residual solvent peak, the multiplicity is reported as follows: s = singlet, d = doublet, t = triplet, q = quartet, m = multiplet, and J-couplings (*J*) are reported in Hertz (Hz). ESI-MS was performed using LTQ XL spectrometer equipped with Shimadzu HPLC setup operating at 0.2 mL/min flow rate with water/acetonitrile mobile phase containing 0.1 vol% formic acid and Discovery C18 column. Reactions were monitored by analytical thin-layer chromatography (TLC) on silica gel plates (Merck 60 F_{254}) using UV light (254 nm) as the visualizing agent. Flash chromatography was performed on 230-400 mesh silica gel (Sigma Aldrich). Reverse phase HPLC (RP-HPLC) for compound purification was performed with a Shimadzu LC-20 system with a Shimadzu mSPD-20A Photo Diode Array detector. RP-HPLC of the collapsed gels was conducted with a Waters Acquity UPLC instrument. Photographs of the hydrogels were taken on a Canon EOS 600D single reflex camera with a Canon Macro Lens EF 100 mm 1:2.8 USM. Optical microscopy images were obtained via an inverted microscope (Zeiss Axio Observer) equipped with a 20x objective (N-Achroplan 20x/0.45 M27) and a CCD camera (Axiocam 705 color). Cryo-EM images were aquired on a Jeol JEM1400 plus Transmission Electron Microscope with an operating voltage of 120 kV and TVIPS F416 camera.

4.5.2 Synthesis

Synthesis of 4-(methylthio)phenyl 4-nitrophenyl carbonate (4)

4-Nitrophenyl chloroformate (0.97 g, 4.80 mmol) and 4-(methylthio)phenol (0.56 g, 4.00 mmol) were dissolved in 30 mL dichloromethane and the solution cooled to 0 °C in an ice bath. Triethylamine (0.67 ml, 4.80 mmol) was added dropwise, the mixture was allowed to warm to room temperature and stirred for 4 h. TLC analysis (silica; eluant: dichloromethane) indicated that no 4-(methylthio)phenol remained. The reaction mixture was washed with water (2x25 mL) and brine (25 mL). The organic layer was dried over Na_2SO_4, filtered, and the solvent was removed by rotatory evaporation. Recrystallization from toluene (160 mL) gave the pure product (0.92 g, yield 77%) as a yellow solid. ^{1}H NMR (400 MHz, $CDCl_3$) δ = 8.32 (d, J=9.2 Hz, 2H), 7.48 (d, J=9.2 Hz, 2H), 7.31 (d, J=8.8 Hz, 2H), 7.21 (d, J=8.8 Hz, 2H), 2.50 (s, 3H). ^{13}C NMR (101 MHz, $CDCl_3$) δ = 155.39, 151.18, 148.42, 145.78, 137.24, 127.98, 125.56, 121.86, 121.32, 16.38. Spectroscopic data aligned with those reported in literature.[3]

Synthesis of 2-(((4-(methylthio)phenoxy)carbonyl)amino)ethane-1-sulfonic acid (1)

To a solution of 4-(methylthio)phenyl 4-nitrophenyl carbonate (0.15 g, 0.50 mmol) in THF (2.0 mL) was added dropwise taurine (0.09 g, 0.75 mmol) and DIPEA (0.13 mL, 0.75 mmol) in distilled water (2.0 mL) at 0 °C. The reaction mixture was allowed to warm at room temperature and stirred overnight.[4,5] After removal of THF by rotatory evaporation, the mixture was extracted with ethyl acetate to remove the excess of p-nitrophenol. The aqueous layer was freeze dried overnight. The crude was dissolved in acetonitrile, allowing the precipitation of the free taurine as white solid. After filtration thought syringe filters (45 µm), the acetonitrile was evaporated in vacuo. The mixture was dissolved in BuOH and further purified by flash chromatography over silica gel (CH_3COOH/H_2O/BuOH 5:5:90) to remove the excess of DIPEA. Compound **1**

was obtained (0.07 g, yield 48%) as a slightly yellow solid. ^{1}H NMR (400 MHz, CD_3OD) δ = 7.29 (d, J=8.6 Hz, 2H), 7.07 (d, J=8.6 Hz, 2H), 3.62 (t, J=6.9 Hz, 2H), 3.06 (t, J=6.9 Hz, 2H), 2.48 (s, 3H). ^{13}C NMR (101 MHz, CD_3OD) δ = 156.8, 150.4, 136.6, 129.0, 123.4, 51.7, 38.3, 16.5. LCMS (ESI) calcd for $C_{10}H_{12}NO_5S^-$ $[M-H]^-$: 290.02, found: 290.04.

Synthesis of MTpcFF

To a solution of 4-(methylthio)phenyl 4-nitrophenyl carbonate (0.26 g, 0.85 mmol) in THF (16.0 mL) was added dropwise FF (0.40 g, 1.28 mmol) and DIPEA (0.22 mL, 1.28 mmol) in distilled water (4.0 mL) at 0 °C. The reaction mixture was allowed to warm at room temperature and stirred overnight.[4,6] TLC analysis confirmed that no 4-(methylthio) 4-nitrophenyl carbonate remained. After removal of THF through rotatory evaporation, the aqueous mixture was acidified (pH = 2-3) with 5% citric acid solution. The reaction mixture was extracted with ethyl acetate (3x40 mL) and the combined organic layer was washed with water. The organic layer was dried over Na_2SO_4 and filtered. The filtrate was concentrated and precipitated in hexane twice to provide **MTpcFF** (0.34 g, yield 84%) as a slightly yellow solid. ^{1}H NMR (400 MHz, CD_3CN) δ = 7.32 – 7.22 (m, 12H), 7.01 (d, *J*=7.8 Hz, 1H), 6.89 (d, *J*=8.5 Hz, 2H), 6.20 (d, *J*=8.4 Hz, 1H), 4.70 – 4.60 (m, 1H), 4.38 – 4.29 (m, 1H), 3.23 – 3.10 (m, 2H), 3.06 – 2.95 (m, 1H), 2.89 – 2.77 (m, 1H), 2.46 (s, 3H). ^{13}C NMR (101 MHz, CD_3CN) δ = 172.7, 171.8, 155.2, 149.7, 138.2, 137.8, 130.3, 129.4, 129.3, 128.3, 127.8, 127.7, 123.2, 57.2, 54.4, 38.5, 37.8, 16.3. LCMS (ESI) calcd for $C_{26}H_{26}N_2O_5S$ $[M+H]^+$: 479.16, found 479.13.

Synthesis of MTpcFFF

To a solution of 4-(methylthio)phenyl 4-nitrophenyl carbonate (0.18 g, 0.60 mmol) in THF (16.0 mL) was added dropwise FFF (0.33 g, 0.72 mmol) and DIPEA (0.12 mL, 0.72 mmol) in distilled water (4.0 mL) at 0 °C. The reaction mixture was allowed to warm at room temperature and stirred overnight.[4,6] TLC

analysis confirmed that no 4-(methylthio)phenyl 4-nitrophenyl carbonate 4-nitrophenyl carbonate remained. After removal of THF through rotatory evaporation, the aqueous mixture was acidified (pH = 2-3) with 5% citric acid solution. The reaction mixture was extracted with ethyl acetate (3x40 mL) and the combined organic layer was washed with water. The organic layer was dried over Na_2SO_4 and filtered. The residue was obtained after rotatory evaporation to remove ethyl acetate and it was further purified by RP-HPLC (column: CAPCELL PAK C8 (150 mm × 20 mm I.D.), eluent: acetonitrile/H2O (0.1% TFA) = 40:60 to 60:40 (linear gradient over 40 min), flow 5.0 mL/min. **MTpcFFF** was obtained as a white powder. ^{1}H NMR (600 MHz, CD_3CN) δ = 7.30 – 7.19 (m, 18H), 7.05 (s, 1H), 6.90 (d, J=8.0 Hz, 2H), 6.28 (s, 1H), 4.60 – 4.51 (m, 2H), 4.32 – 4.24 (m, 1H), 3.14 – 3.07 (m, 2H), 3.06 – 3.02 (m, 1H), 2.98 – 2.90 (m, 1H), 2.90 – 2.84 (m, 1H), 2.80 – 2.74 (m, 1H), 2.43 (s, 3H). ^{13}C NMR (151 MHz, CD_3CN) δ = 172.9, 171.7, 155.4, 149.6, 138.2, 136.2, 130.3, 129.3, 128.3, 127.6, 123.2, 57.6, 55.3, 54.8, 38.4, 37.8, 30.3, 16.2. LCMS (ESI) calcd for $C_{35}H_{35}N_3O_6S$ $[M+H]^+$: 626.23, found 626.17.

4.5.3 ^{1}H NMR study of oxidation and hydrolysis of 1

^{1}H NMR study of oxidation and hydrolysis of 1 with and without *Ci*VCPO

In a NMR tube, 2.90 mg of **1** was dissolved in citrate buffer (CB, 50 mM, pH= 6.2, 165 mM NaCl)/D_2O 9:1. Sodium trimethylsilylpropanesulfonate (DSS) was added in stoichiometric amount to **1** and used as NMR standard. To this solution, 0.0, 0.7 or 7.7 µL of the 65.0 µM *Ci*VCPO stock solution in Tris/H_2SO_4 buffer (50 mM, pH 8.2) was added to reach respectively of 0.0, 0.1 and 1.0 µM of *Ci*VCPO. The total volume of each experiment was 500 µL. Then, 15.0 µL of 3.0 wt% H_2O_2 was added to the tube and the reaction was followed by ^{1}H NMR in PRESAT mode over time. All the experiments were performed in duplicates to obtain mean and standard deviation values.

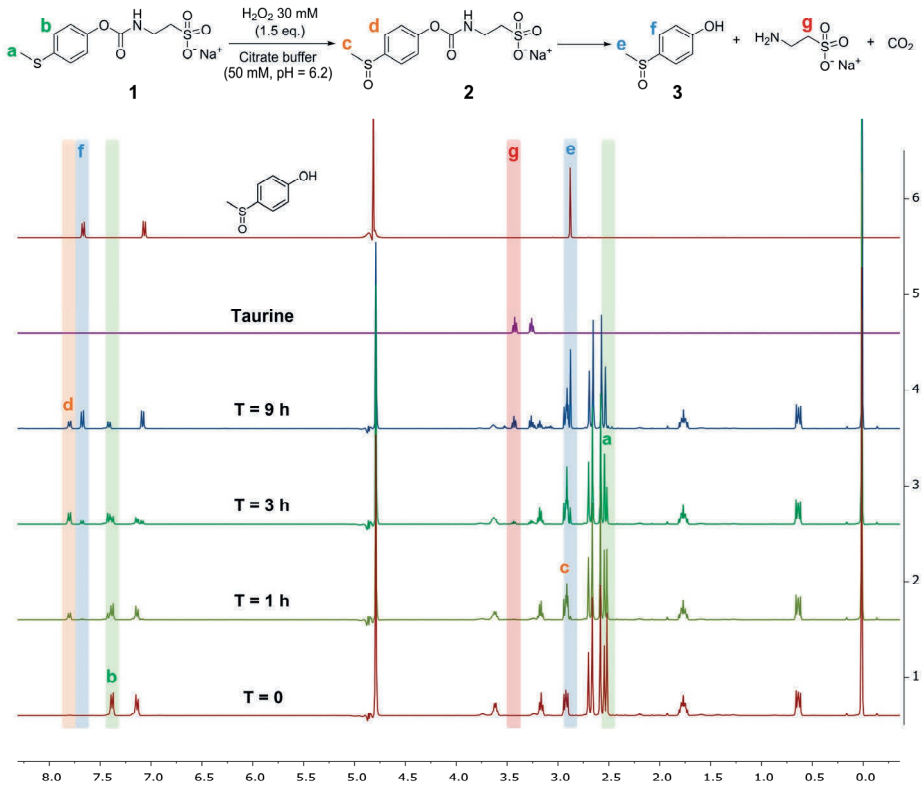

Figure S1. ^{1}H NMR spectra over time at 37 °C of **1** in CB/D_2O 9:1 upon the addition of 30 mM H_2O_2

^{1}H NMR study of oxidation and hydrolysis of 1 with and without r*Aae*UPO

In a NMR tube, 2.90 mg of **1** was dissolved in phosphate buffer (PB, 50 mM, pH = 7.0)/D_2O 9:1. Sodium trimethylsilylpropanesulfonate (DSS) was added in stoichiometric amount to **1** and used as NMR standard. To this solution, 0.0, 0.6 or 6.0 µL of the 83.9 µM r*Aae*UPO stock solution in potassium phosphate buffer (20 mM, pH 7.0) was added to reach respectively of 0.0, 0.1 and 1.0 µM of r*Aae*UPO. The total volume of each experiment was 500 µL Then, 15.0 µL of 3.0 wt% H_2O_2 was added to the tube and the reaction at 37 °C was followed by ^{1}H NMR in PRESAT mode over time. All the experiments were performed in duplicates to obtain mean and standard deviation values.

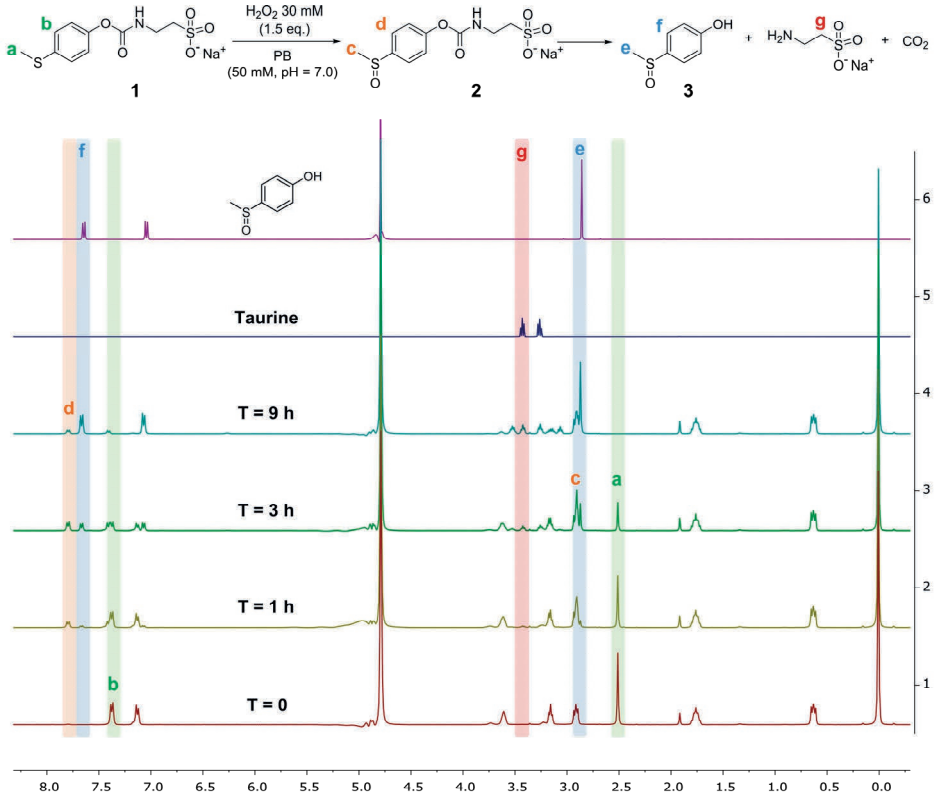

Figure S2. ^{1}H NMR spectra over time at 37 °C of **1** in PB/D_2O 9:1 upon the addition of 30 mM H_2O_2.

4.5.4 Characterization of MTpcFF hydrogels

Rheology of MTpcFF hydrogels

Oscillatory experiments were performed using a rheometer AR G2 from TA Instruments in a strain-controlled mode. The rheometer was equipped with a steel plate-and plate geometry of diameter 25 mm and a water trap. The temperature of the plates was controlled at 25 ± 0.2 °C. The total volume for each gelation experiment was 0.1 mL. The *Ci*VCPO/**MTpcFF** gels were prepared dissolving 0.75 mg **MTpcFF** in 5.0 µL of DMSO, then adding 93.5 µL of citrate buffer (CB, 50 mM, pH = 6.2) and 1.5 µL of the 65.0 µM *Ci*VCPO stock solution in Tris/H_2SO_4 buffer (50 mM, pH = 8.2). For enzyme-free gels 1.5 µL of citrate buffer was added instead of the enzyme stock solution. The r*Aae*UPO/**MTpcFF** gels were prepared dissolving 1.00 mg **MTpcFF** in 5.0 µL of DMSO, then adding 93.8 µL of phosphate buffer (PB, 50 mM, pH = 7.0) and 1.2 µL of the 83.9 µM r*Aae*UPO stock solution in potassium phosphate buffer (20 mM, pH 7.0). For enzyme-free gels 1.2 µL of phosphate buffer was added instead of the enzyme stock solution. After stirring the vial by vortexing for 3 s, the gel was pipetted on the bottom plate of the rheometer and the upper plate was slowly rotated to equally spread the gel. The storage and loss moduli G' and G" were followed over time with the rheometer during the formation of the gel, setting up the instrument with a frequency of 1.0 Hz and under 1.0% strain. The measurements were stopped when no further increase of G' was observed. A frequency sweep was measured in the range 0.01-100 rad/s, confirming that the moduli are constant in the frequency range chosen and the strain sweep revealed that the applied strain percentage is in the linear strain regime. G' was greater than G'' and both G' and G'' were frequency independent, which indicated the typical viscoelastic property of hydrogel consisting of fiber networks The rheological properties of **MTpcFF** gels were not significantly influenced by the presence of the enzymes *Ci*VCPO and r*Aae*UPO.

Optical microscopy of MTpc-FF hydrogels

MTpcFF hydrogels were prepared dissolving 1.00 mg **MTpcFF** in 5.0 μL of DMSO, then adding 95.0 μL of phosphate buffer (PB, 50 mM, pH = 7.0). **MTpcFF** gels in citrate buffer (CB, 50 mM, pH = 6.2) were prepared dissolving 0.75 mg **MTpcFF** in 5.0 μL of DMSO, then adding 95.0 μL of the buffer on top. After formation of stable gels, a portion of **MTpcFF** hydrogels was placed in the center of a glass slide, then a glass cover slip was positioned on top of the sample and observed in the microscope. Optical images were processed using ImageJ.

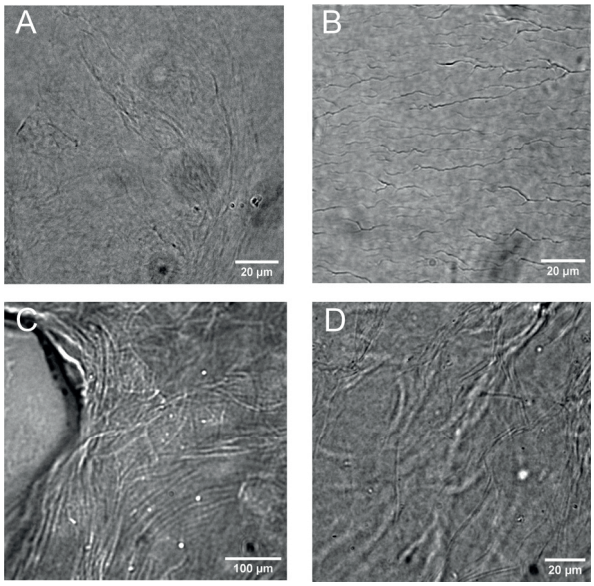

Figure S3. Optical images of **MTpcFF** hydrogels. Optical images of **MTpcFF** (0.75 wt%) hydrogel in CB (Scale bar = 20 μm) at 63X magnification show fibers of about 1.0 μm diameter, which A) intersect when surrounded by water and B) assume a parallel orientation after the evaporation of water from the sample. **MTpcFF** (1.0 wt%) hydrogel in PB at C) 20X magnification (Scale bar = 100 μm) and D) 63X magnification (Scale bar = 20 μm) present bundles of fibers with diameter up to 3.0 μm.

S4.1 Cryo-EM of MTpcFF hydrogels

MTpcFF hydrogels were prepared dissolving 1.00 mg **MTpcFF** in 5.0 μL of DMSO, then adding 95.0 μL of phosphate buffer (PB, 50 mM, pH = 7.0). **MTpcFF** gels in citrate buffer (CB, 50 mM, pH = 6.2) were prepared dissolving 0.75 mg **MTpcFF** in 5.00 μL of DMSO, then adding 95.0 μL of the buffer on top. Cryo-TEM images were obtained by placing 4.0 μL of the sample onto Quantifoil 300 mesh Cu R1.2/1.3 grids. The drop was blotted to obtain a thin layer on the grid, and vitrified by rapid immersion in liquid ethane (Leica EM GP version 16222032) with a Vitrobot plunger. The grid was finally inserted into a cryo-holder (Gatan model 626) and then transferred to the Jeol JEM 1400 TEM. Cryo-EM images were processed using ImageJ.

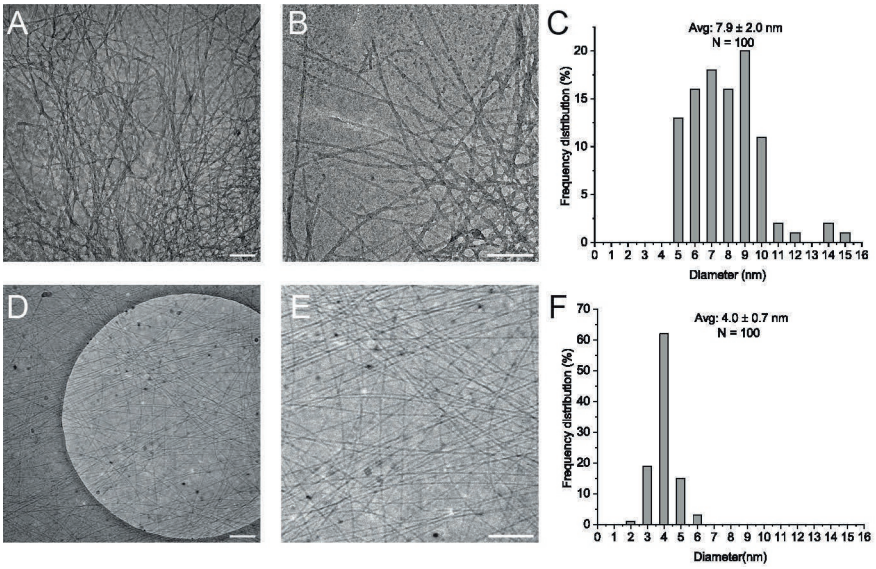

Figure S4. A, B) Cryo-EM images of **MTpcFF** (0.75 wt%) hydrogel in CB (scale bar = 200 nm) show dense fibrous network. C) Frequency distribution based on Cryo-EM images analysis of **MTpcFF** (0.75 wt%) hydrogel in CB results in an average fiber diameter of 7.9 ± 2.0 nm. D,E) Cryo-EM images of **MTpcFF** (1.00 wt%) hydrogel in PB (scale bar = 200 nm) show ordered fibers. F) Frequency distribution based on Cryo-EM images analysis of **MTpcFF** (1.00 wt%) hydrogel in PB results in an average fiber diameter of 4.0 ± 0.7 nm.

4.5.5 MTpcFF hydrogels preparation

MTpcFF hydrogels preparation with and without *Ci*VCPO (tube inversion)

In a 1.5 mL screwed vial, 0.75 mg of **MTpcFF** was dissolved in 5.0 µL of DMSO. Then, 93.5 µL of citrate buffer (50 mM, pH = 6.2) and 1.5 µL of the 65.0 µM *Ci*VCPO stock solution in Tris/H_2SO_4 buffer (50 mM, pH = 8.2) were slowly added. For enzyme-free gels 1.5 µL of citrate buffer was added instead of the enzyme stock solution. Each vial was stirred by vortexing for 3 seconds, capped, placed on a stable surface and left undisturbed overnight. The gelation was

evaluated turning the vial upside down. The gelation experiments were performed in duplicates.

MTpcFF hydrogels preparation with and without *rAae*UPO (tube inversion)

In a 1.5 mL screwed vial, 1.00 mg of **MTpcFF** was dissolved in 5.0 µL of DMSO. Then, 93.8 µL of phosphate buffer (50 mM, pH = 7.0) and 1.2 µL of the 83.9 µM r*Aae*UPO stock solution in potassium phosphate buffer (20 mM, pH = 7.0) were slowly added. For enzyme-free gels 1.2 µL of phosphate buffer was added instead of the enzyme stock solution. Each vial was stirred by vortexing for 3 seconds, capped, placed on a stable surface and left undisturbed overnight. The gelation was evaluated turning the vial upside down. The gelation experiments were performed in duplicates.

4.5.6 H_2O_2 response of MTpcFF hydrogels

H_2O_2 response of MTpcFF hydrogels with and without *Ci*VCPO (tube inversion)

To the **MTpcFF** gels prepared in CB as described above, 5.0 µL of NaCl 3.00 M was placed on top of the gels. Then, 5.0 µL of 312, 156, 78.0 or 31.0 mM H_2O_2 stock solution was added to provide respectively 1.0, 0.5, 0.25 or 0.1 equivalents of H_2O_2 to the gels. Control experiments were performed adding 10.0 µL of citrate buffer instead H_2O_2 stock solution. All the experiments were performed at 37 °C. The gel-sol transition was then visually evaluated according to the tube inversion method over time. Photographs were acquired at the different stages of the gel-sol transition. The hydrogels resulted stable in absence of H_2O_2 over 24 h, but suffered water loss due to the prolonged time at 37 °C. To maintain constant the concentrations of the gels, control experiments were stopped at 8 h.

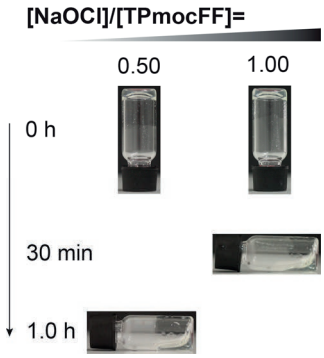

Figure S5. Photographs of **MTpcFF** hydrogels (0.75 wt%) in CB (50 mM, pH = 6.2) after the addition of 1.0 and 0.5 eq. NaOCl. The results are in line with those obtained after the addition of 140 mM NaCl and either 1.0 or 0.5 eq. H_2O_2 in presence of 1.0 μM *Ci*VCPO.

H_2O_2 response of MTpcFF hydrogels with and without *rAae*UPO (tube inversion)

To the **MTpcFF** gels prepared in PB as described above, 10.0 μL of 200, 100, 50.0 or 20.0 mM H_2O_2 stock solution was added on top of the gels to provide respectively 1.0, 0.5, 0.25 or 0.1 equivalents of H_2O_2. Control experiments were performed adding 10.0 μL of phosphate buffer instead H_2O_2 stock solution. All the experiments were performed at 37 °C. The gel-sol transition was then visually evaluated according to the tube inversion method over time. Photographs were acquired at the different stages of the gel-sol transition. The hydrogels resulted stable in absence of H_2O_2 over 24 h, but suffered water loss due by the prolonged time at 37 °C. To maintain constant the concentrations of the gels, control experiments were stopped at 8 h.

HPLC analysis of MTpcFF hydrogels upon addition of H_2O_2

To the solution or partially destructed **MTpcFF** hydrogel obtained as explained above was added 900 µL of acetonitrile 5 h after the addition of 1.0, 0.5 and 0.25 equivalents of H_2O_2 and 8 h after the addition of 0.1 and 0.0 equivalents of H_2O_2. This solution was diluted two times and an aliquot (10.0 µL) was analysed by RP-HPLC (Column: Lichrospher RP18-5 (150 × 4.6 mm, 5.0 µm). Eluent: A:B = 20:80 to 80:20 (A: Acetonitrile/0.1%TFA, B: H_2O/0.1%TFA), linear gradient over 40 min, flow rate = 0.5 mL min^{-1}) at a detection wavelength of 220 nm.

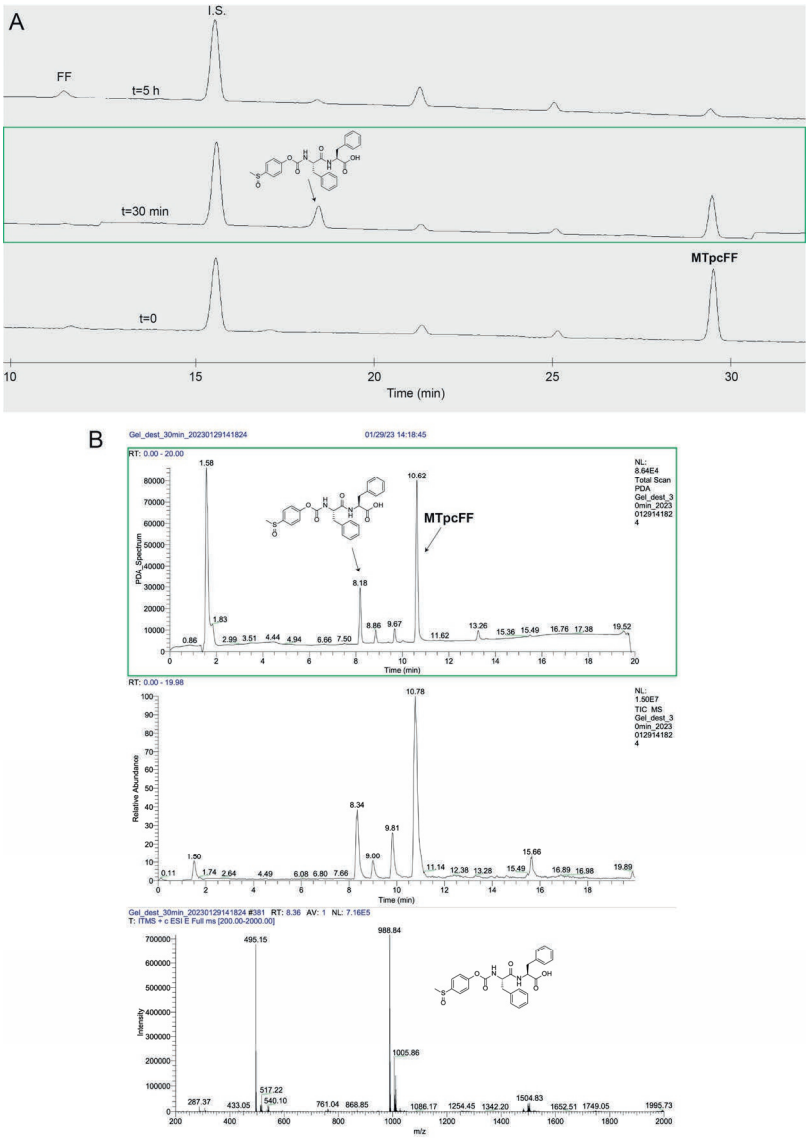

Figure S6. A) HPLC analysis of **MTpcFF** hydrogel before oxidation (bottom) and 30 min (middle) and 5 h (top) after the addition of H_2O_2 ([H_2O_2]/[**MTpcFF**] = 1.00) in presence of 1.0 μM *Ci*VCPO in CB. (Internal standard (I.S.): N-Methyl-p-toluenesulfonamide). B) LC-MS analysis of **MTpcFF** hydrogel 30 min after the addition of H_2O_2 ([H_2O_2]/[**MTpcFF**] = 1.00) in presence of 1.0 μM *Ci*VCPO in water.

4.5.7 Supplementary references

1. C. Zippilli, M. J. Bartolome, T. Hilberath, L. Botta, F. Hollmann and R. Saladino, *ChemBioChem*, 2022, **23**, e202200367.

2. T. Hilberath, A. van Troost, M. Alcalde and F. Hollmann, *Front. Catal.*, 2022, **2**, DOI: 10.3389/fctls.2022.882992.

3. R. Freer and A. McKillop, *Synth. Commun.*, 1996, **26**, 331-349.

4. S. Dadhwal, J. M. Fairhall, S. K. Goswami, S. Hook and A. B. Gamble, *Chem. Asian J.*, 2019, **14**, 1143-1150.

5. D. K. Tanwar, A. Ratan and M. S. Gill, *Org. Biomol. Chem.*, 2017, **15**, 4992-4999.

6. M. Ikeda, T. Tanida, T. Yoshii, K. Kurotani, S. Onogi, K. Urayama and I. Hamachi, *Nat. Chem.*, 2014, **6**, 511-518.

4.5.8 Spectra overview

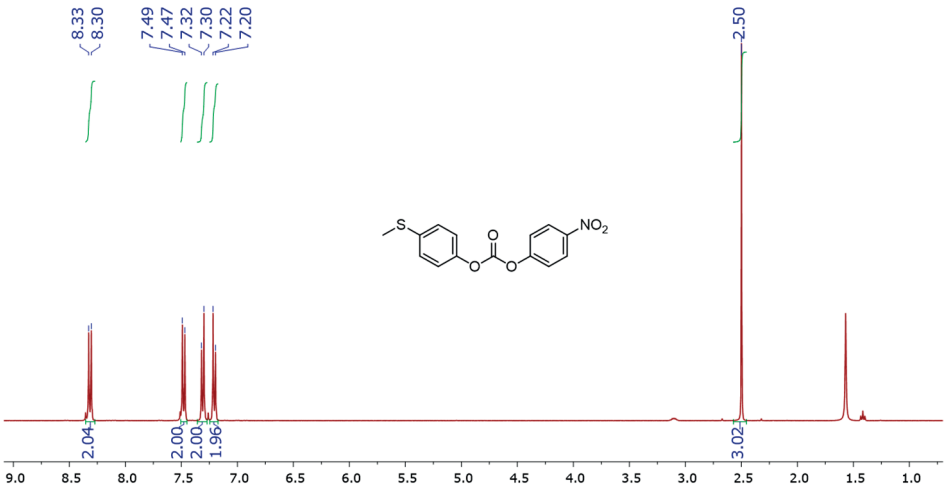

^{1}H NMR spectrum (400 MHz) of compound **4** in $CDCl_3$.

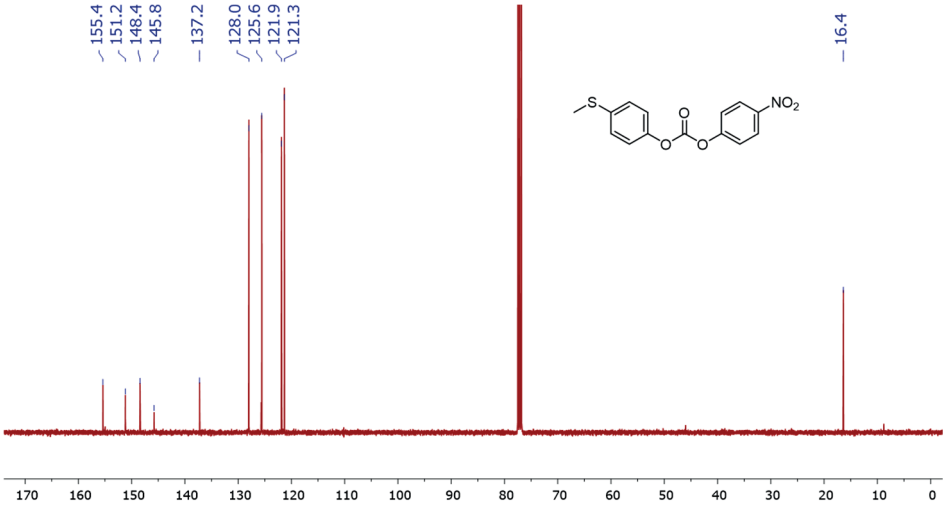

^{13}C NMR spectrum (101 MHz) of compound **4** in $CDCl_3$.

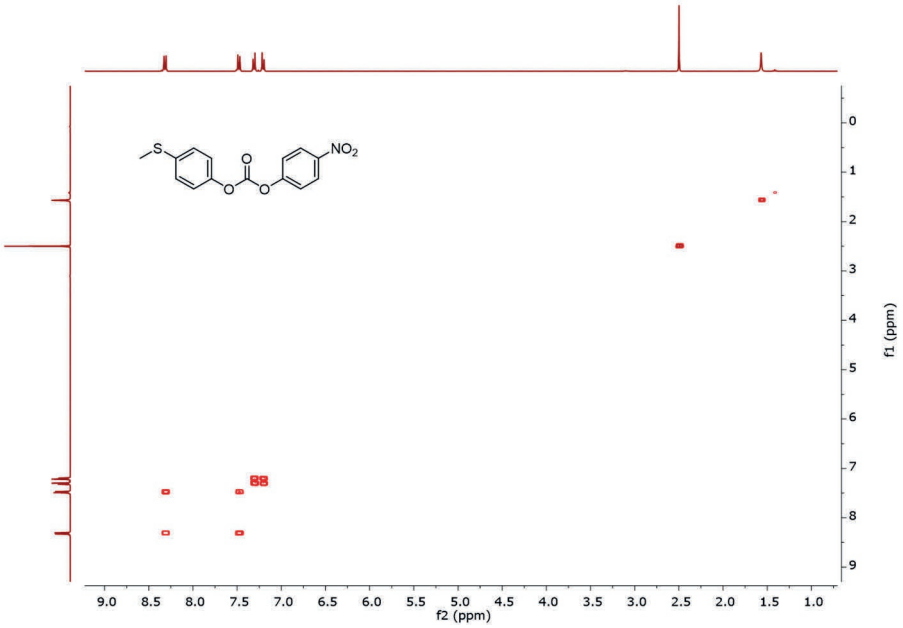

^{1}H-^{1}H-COSY spectrum of compound **4** in $CDCl_3$.

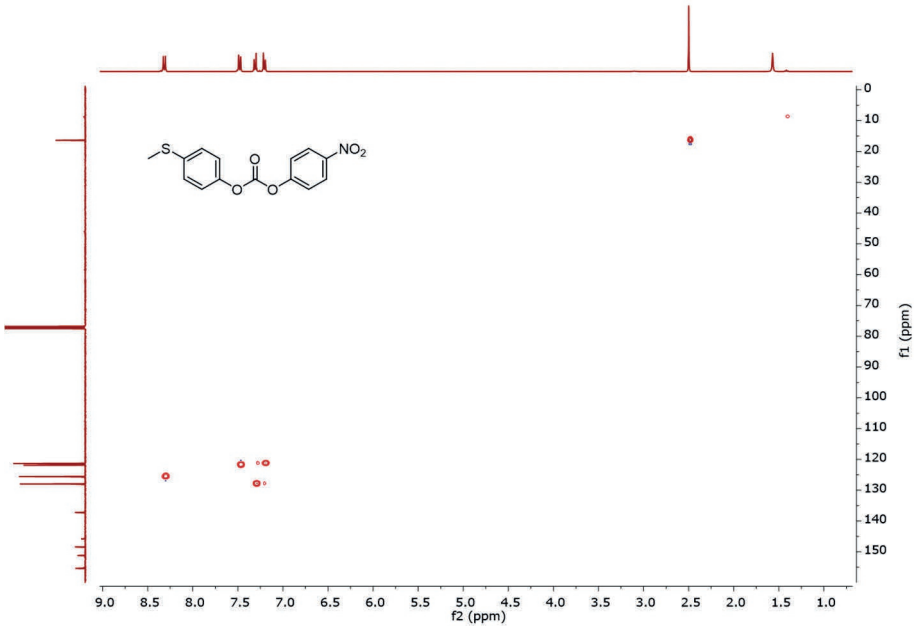

HSQC spectrum of compound **4** in $CDCl_3$.

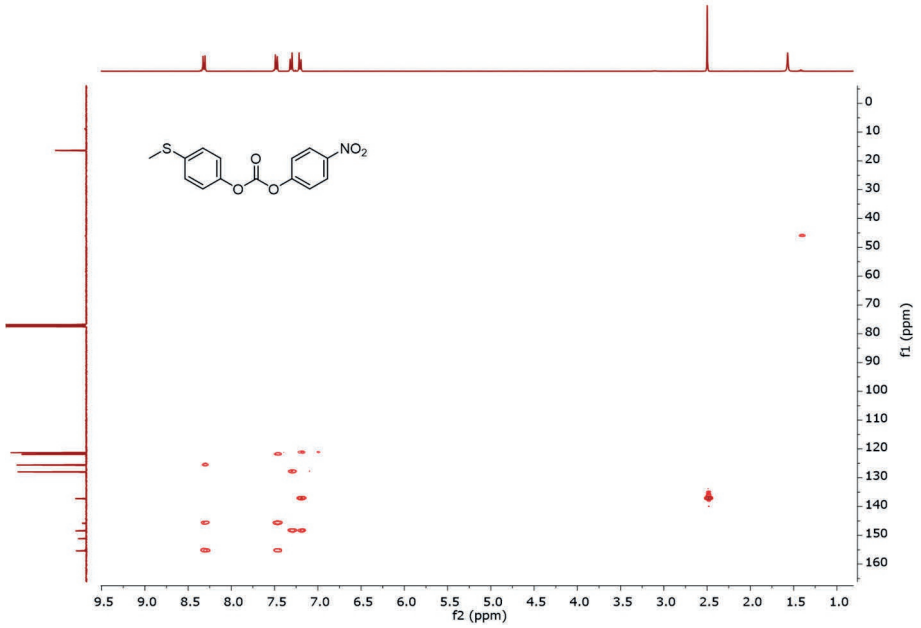

HMBC spectrum of compound **4** in $CDCl_3$.

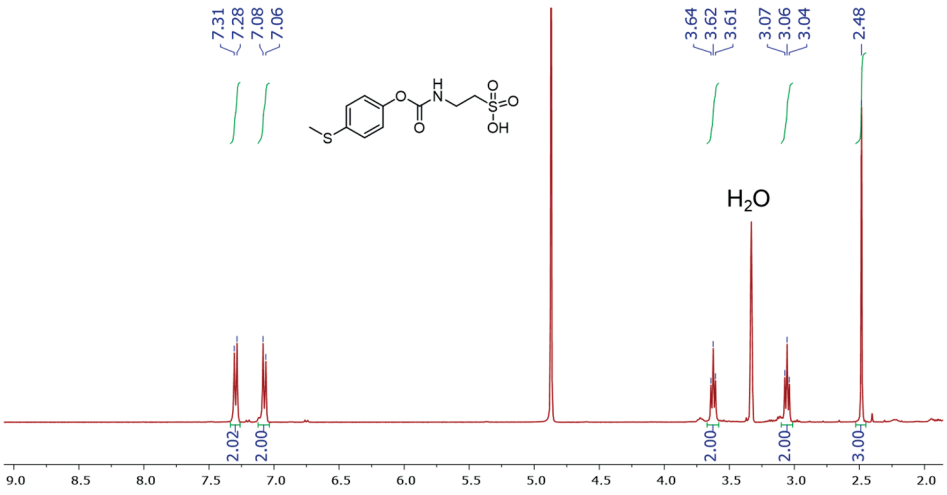

^{1}H NMR spectrum (400 MHz) of compound **1** in CD_3OD.

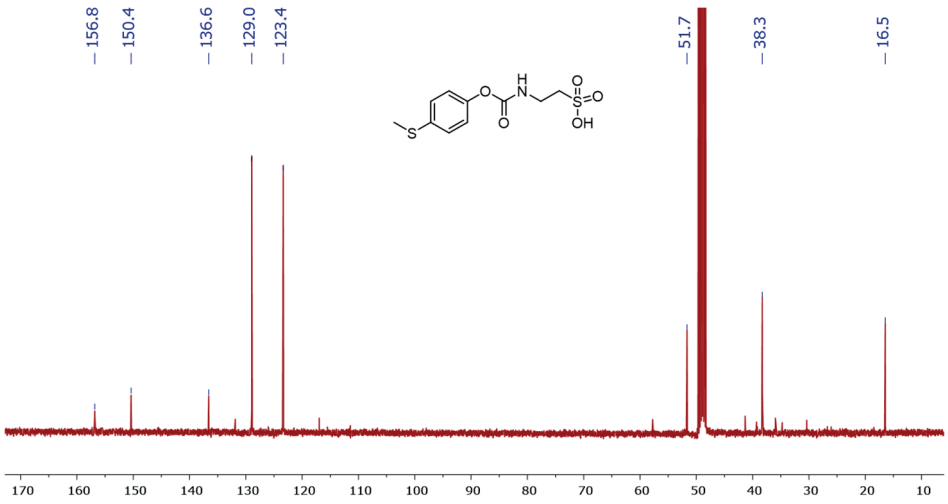

^{13}C NMR spectrum (101 MHz) of compound **1** in CD_3OD.

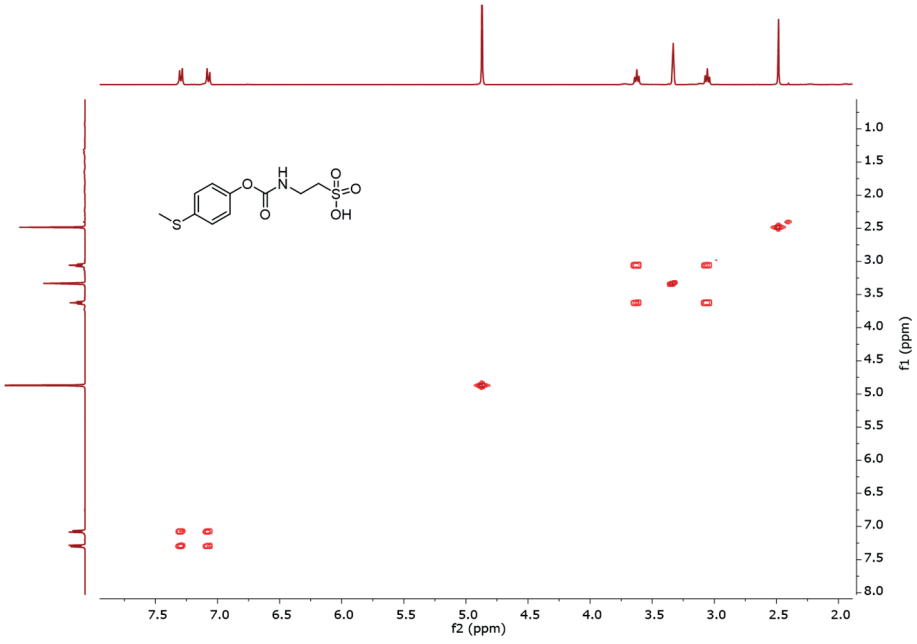

^{1}H-^{1}H-COSY spectrum of compound **1** in CD_3OD.

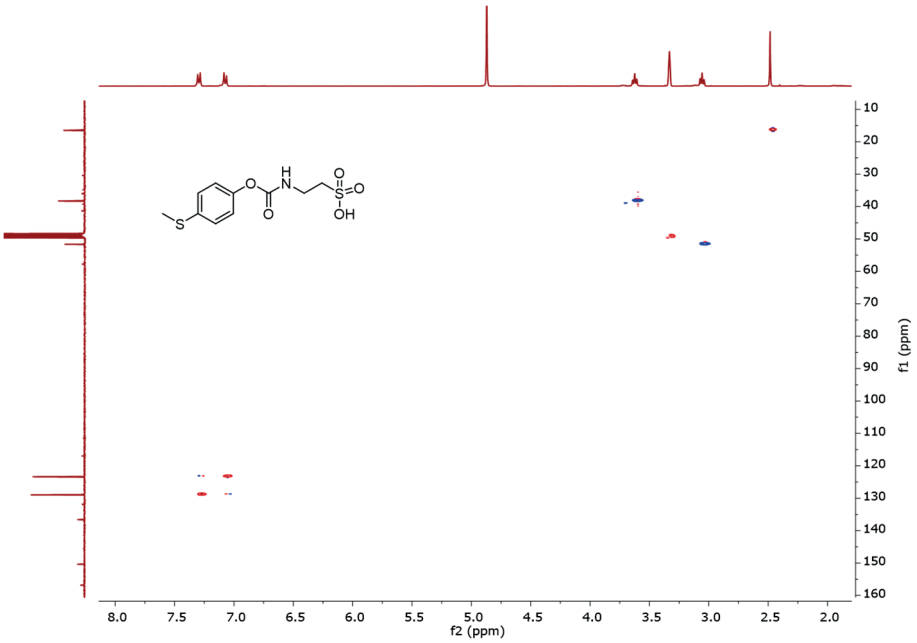

HSQC spectrum of compound **1** in CD_3OD.

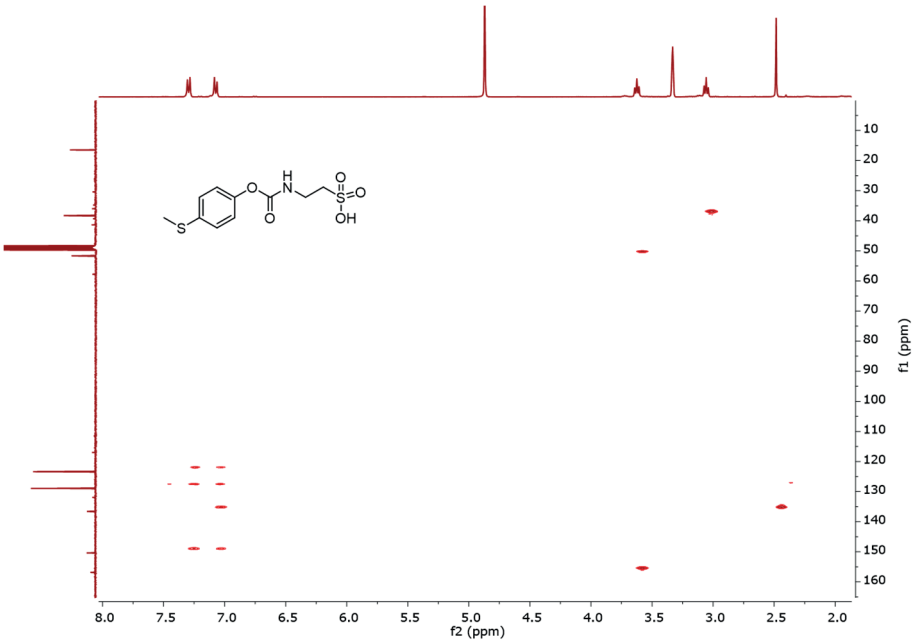

HMBC spectrum of compound **1** in CD_3OD.

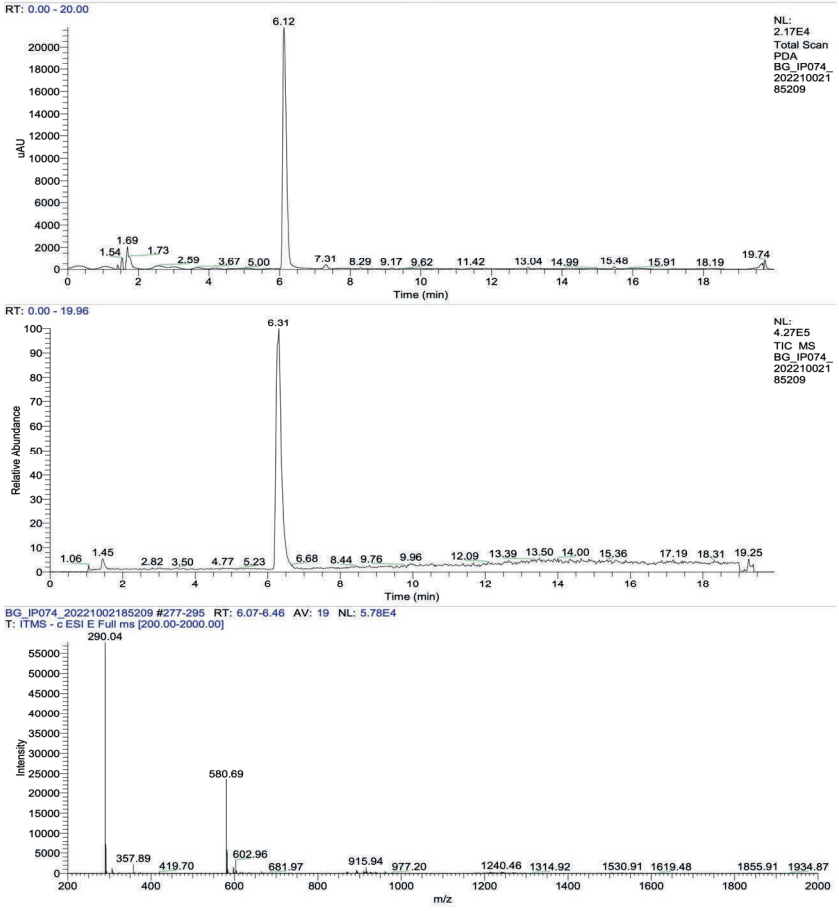

LC-MS of compound **1**

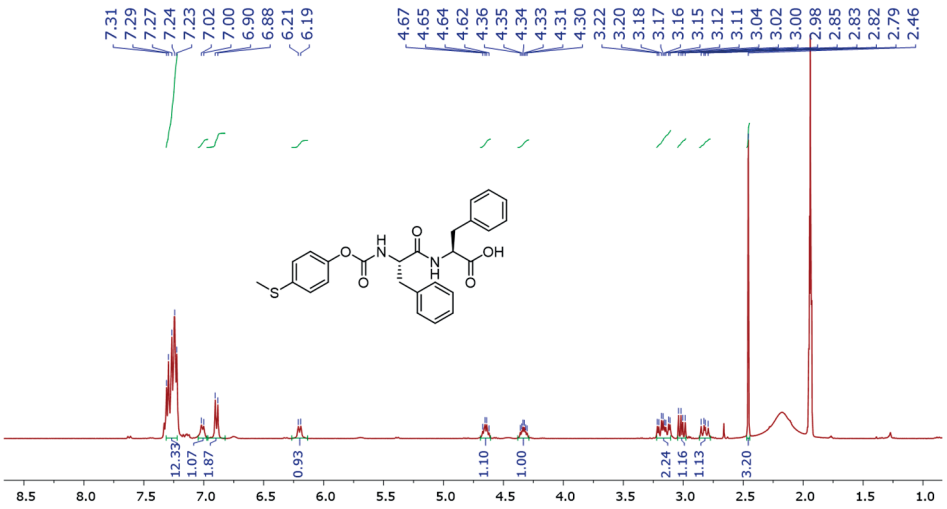

^{1}H NMR spectrum (400 MHz) of **MTpcFF** in CD_3CN.

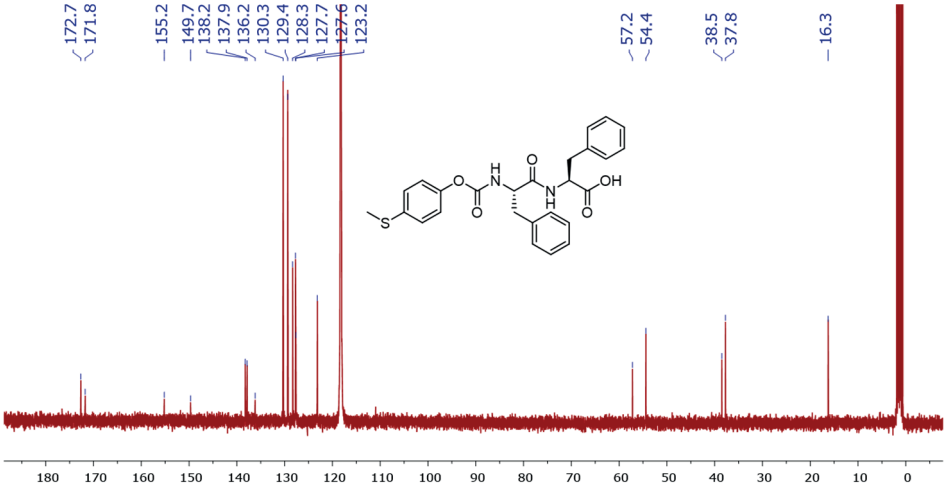

^{13}C NMR spectrum (101 MHz) of **MTpcFF** in CD_3CN.

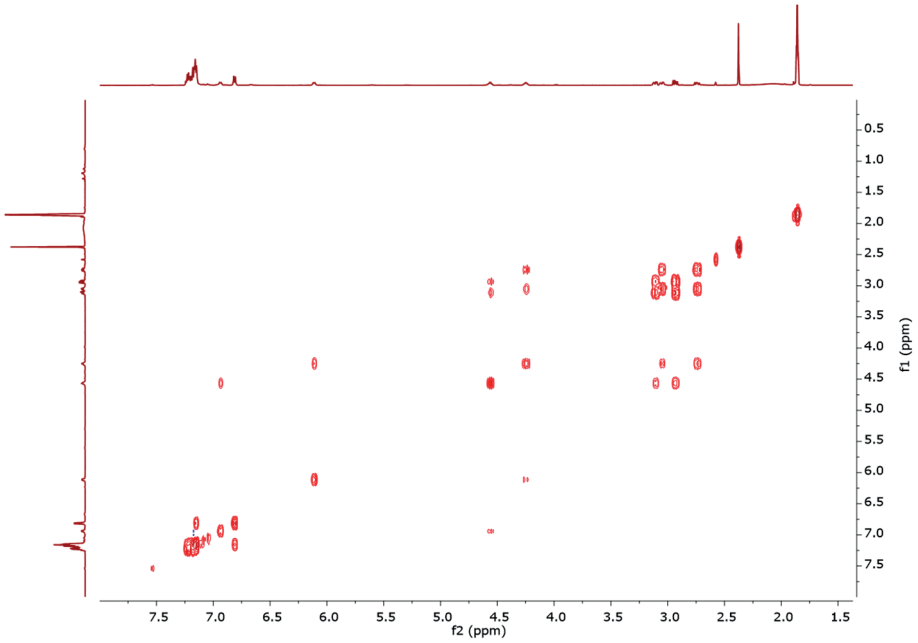

^{1}H-^{1}H-COSY spectrum of **MTpcFF** in CD_3CN.

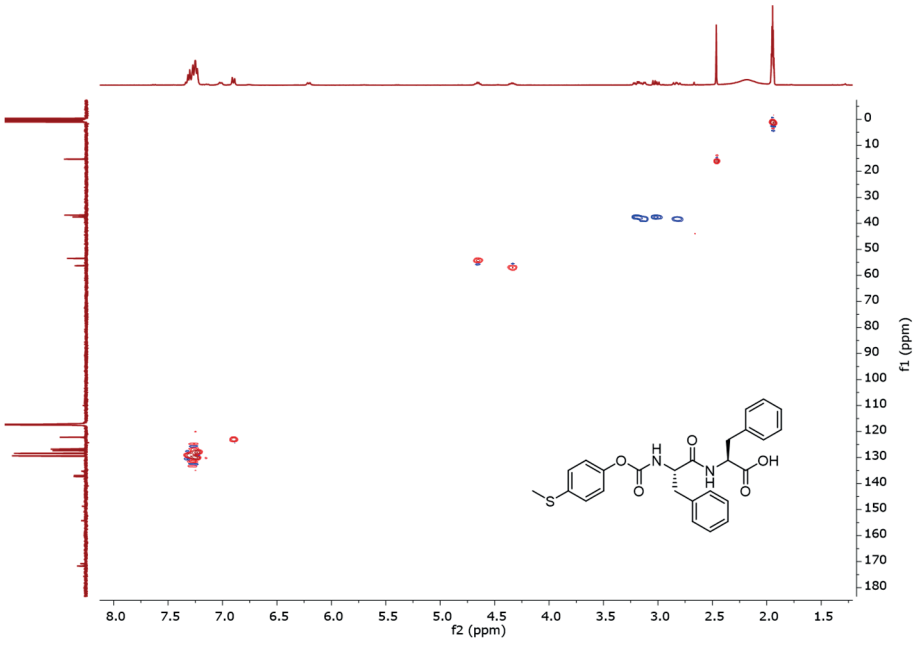

HSQC spectrum of **MTpcFF** in CD_3CN.

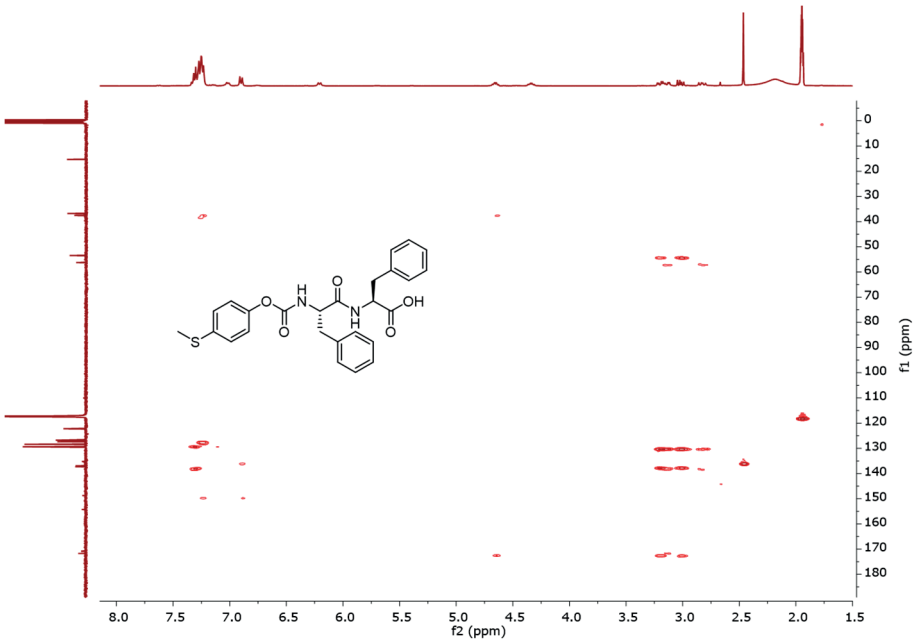

HMBC spectrum of **MTpcFF** in CD_3CN.

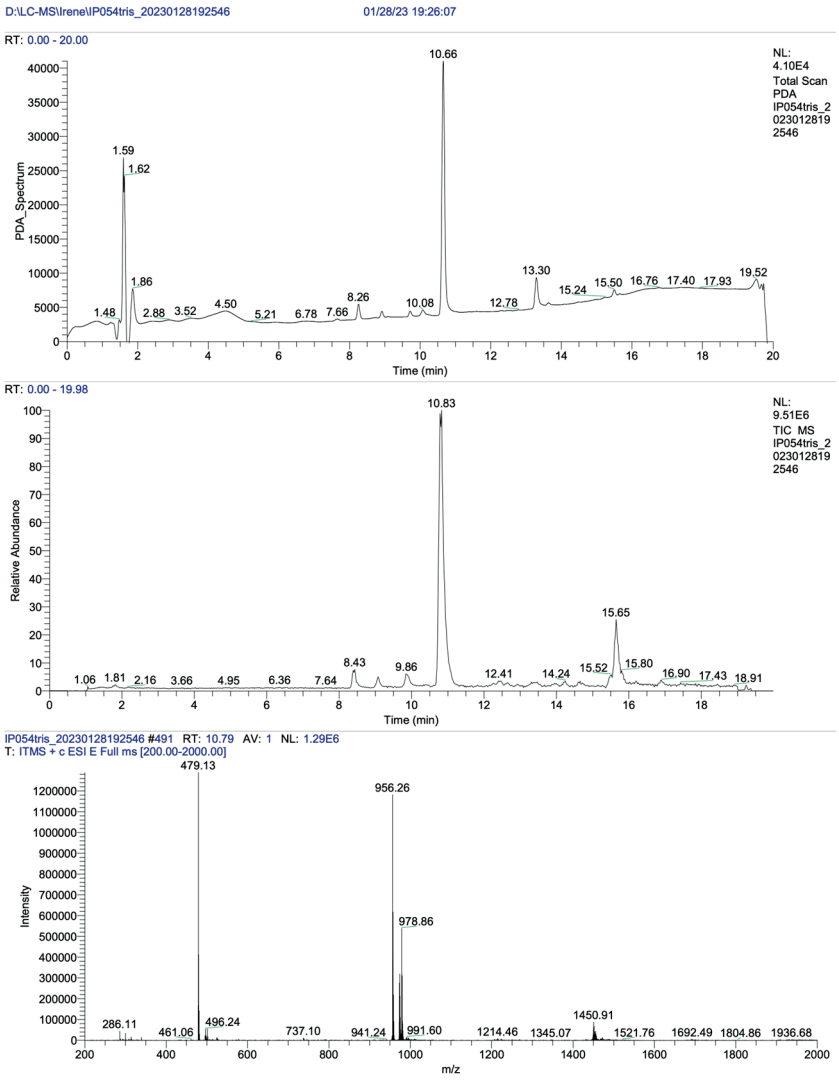

LC-MS spectra of **MTpcFF** in acetonitrile

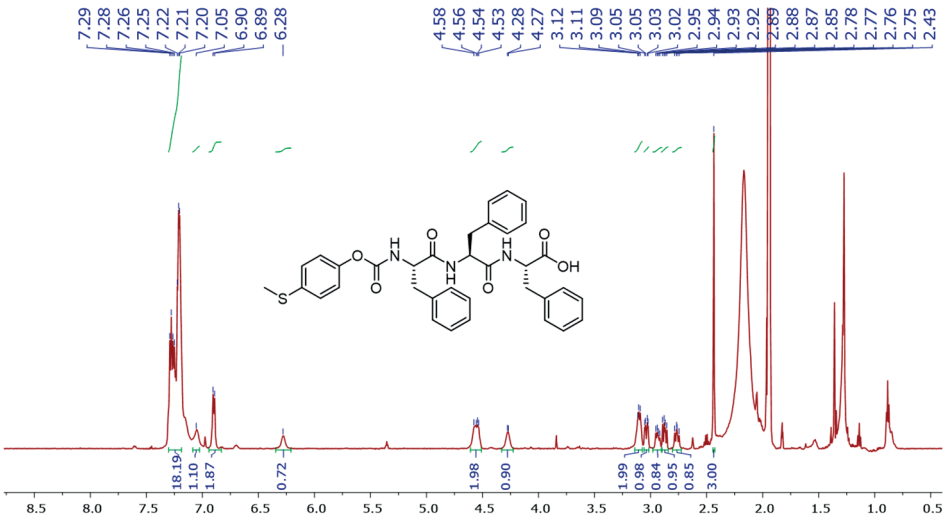

^{1}H NMR spectrum (600 MHz) of **MTpcFFF** in CD_3CN.

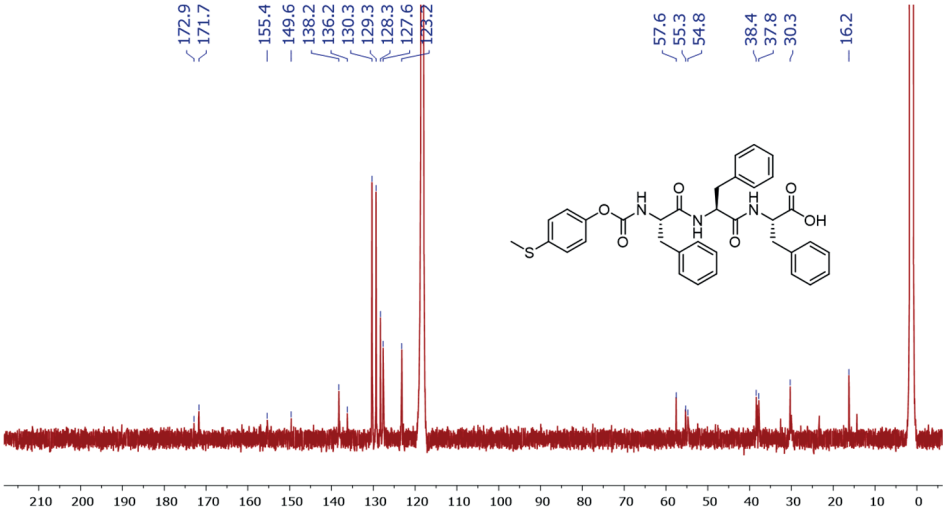

^{13}C NMR spectrum (151 MHz) of **MTpcFFF** in CD_3CN.

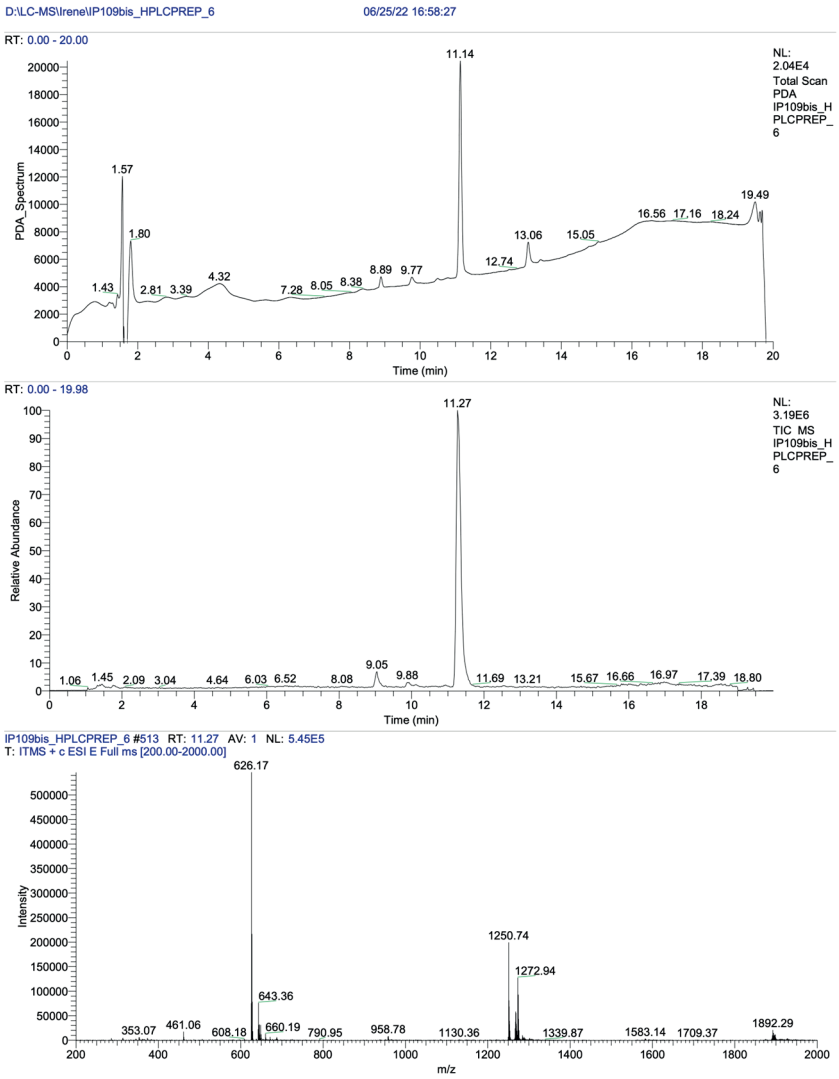

LC-MS spectra of **MTpcFFF** in acetonitrile.

Chapter 5

Indoline catalyzed gelation of sulfonate functionalized trishydrazone

Acylhydrazone formation is one of the most common click reactions used for bioconjugation and synthesis of soft materials. Our group has previously reported how the formation of a low molecular weight (LMW) hydrazone by mixing water-soluble aldehyde and hydrazine leads to supramolecular gelation. However, these processes can be very slow in neutral conditions. Here, indoline derivatives have been used to catalyze the hydrazone reaction via an iminium intermediate, and therefore to accelerate hydrogel formation at neutral pH. Then, we applied these conditions to obtain hydrazone based hydrogels functionalized with alkylsulfonate groups, which have shown potential antiviral properties. Indoline catalysis can accelerate material formation under neutral aqueous conditions, enabling a method for the preparation of biomedical platforms.

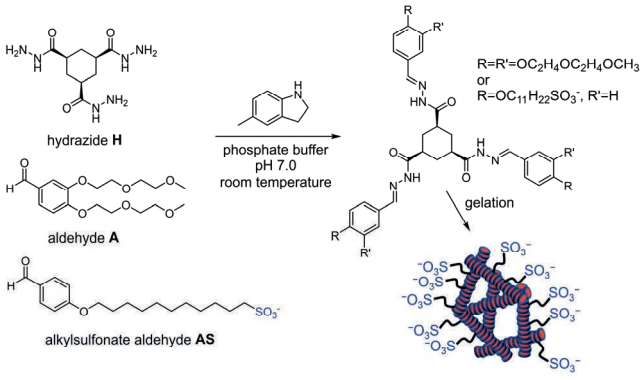

This chapter is adapted from:

Y. Zhou, I. Piergentili, J. Hong, M. P. van der Helm, M. Macchione, Y. Li, R. Eelkema, S. Luo, *Org. Lett.*, 2020, ***22*** (15), 6035-6040.

5.1 Introduction

Hydrazone formation is a condensation reaction extensively used in bioconjugation,[1,2] biomolecular labeling,[3] polymer chemistry,[4,5] and dynamic covalent chemistry,[6,7] which can be exploited to realize responsive systems and soft materials.[8-11]

Most of these works have benefited of the discovery of aniline as nucleophilic catalyst made by Cordes and Jencks in 1962.[12] Previously, the slow reaction rate of hydrazone formation in neutral conditions was a major drawback for its applicability in biological settings. Aniline forms a Schiff base with aldehydes and ketones, which is the rate limiting step in the hydrazone formation. Then, the attack of hydrazide allows the formation of hydrazone and the elimination of aniline, facilitated by its aromatic ring which delocalizes the lone pair electrons of the amine.[13] Despite the high concentration of catalyst needed,[14] the aniline catalyzed hydrazone formation is a beautiful example of how organocatalysis can avoid the use of harsh acidic conditions.[13,15-17] However, the toxicity of aniline and its derivatives in high concentration can pose a problem for biological applications.[18]

Secondary amine catalysts, such as the widely used L-proline, showed negligible activity in hydrazone formation at neutral pH.[16] However, Luo and coworkers recently found that some indoline derivatives catalysts showed up to 15 times rate enhancement over aniline. Secondary aromatic amines would condense to form an iminium ion intermediate, which would be positively charged also at neutral pH (Scheme 1). This intermediate has enhanced electrophilicity over the typical imine formed with aniline, facilitating the subsequent attack of the hydrazide through the elimination of the recovered indoline. In addition, the transition from a positively charged intermediate to a neutral and stable leaving

group, such as the indoline, would further drive the reaction towards the hydrazone product, accelerating the overall rate of the reaction.

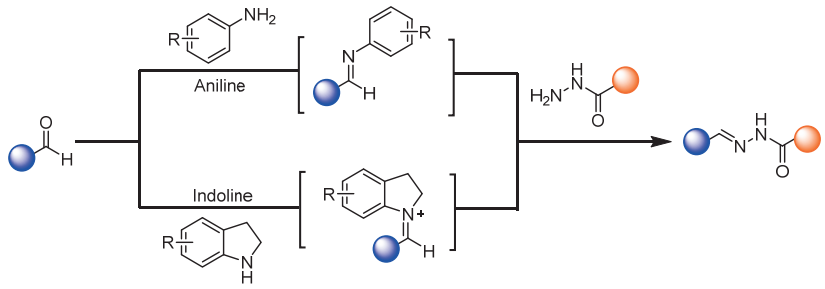

Scheme 1. Acylhydrazone formation pathways via aniline and via indoline catalysis under neutral conditions.

In collaboration with Luo's group, we wanted to apply indoline catalysis in the trishydrazone gel formation emerged previously in our lab.[19] We reported how the formation of low molecular weight (LMW) hydrazone hydrogelators obtained from aldehyde **A** and hydrazide **H** (Figure 1) can be controlled directly by catalytic action.[20-22] In those systems, control over the rate of hydrazone formation is crucial to achieve local gel formation, and to tune gel object dimensions and mechanical properties.

Moreover, we sought in the work of Stellacci, Lembo, and Jones the possibility of expanding these hydrogels as broad spectrum antiviral materials.[23,24] Virustatic drugs have low toxicity and target cell-virus interaction mechanisms that are typical to many different viruses. However, these drugs proved to be medically ineffective because of their reversible binding to the virus.[24] Virucidal drugs cause irreversible viral deactivation, but the technologies used to date have intrinsic cytotoxicity.[25,26] Combining the non-toxicity of virustatic drugs with the irreversibility of the virucidal ones would lead to the ideal antiviral drug. Virustatic substances usually have short sulfonate linkers, the rigidity of which limits the number of sites available for drug-virus binding, causing weak and

reversible effect of the drug.[27,28] For this reason, Stellacci, Lembo and Jones decided to functionalize nanoparticles with long sulfonate chains, successfully producing a virucidal drug effective against multiple virus types.[23]

In our case study, the incorporation of aldehydes with alkylsulfonate groups with a structure similar to aldehyde **A** in the gelation process would produce a sulfonate decorated supramolecular gel. For this purpose, our group designed aldehyde **AS** taking in account the need of both successful gelation and efficient functionalization of the gel fibers with long alkylsulfonated chains. Amongst the indoline derivatives studied by Luo and coworkers, 5-methylindoline and 5-methoxyindoline showed respectively 11 and 15-fold enhancement over the catalytic activity of aniline. However, because the tendency of 5-methoxyindoline to oxidize, we focused our attention on 5-methylindoline to study the gel formation under catalytic control. Hereby, we report that indoline derivatives accelerate the trishydrazone gel formation at neutral pH. Implementing alkylsulfonate groups in the formulation leads to gel fibers with multivalent functionalities that can bind to the virus, representing a potential biomedical device for virus inhibition.

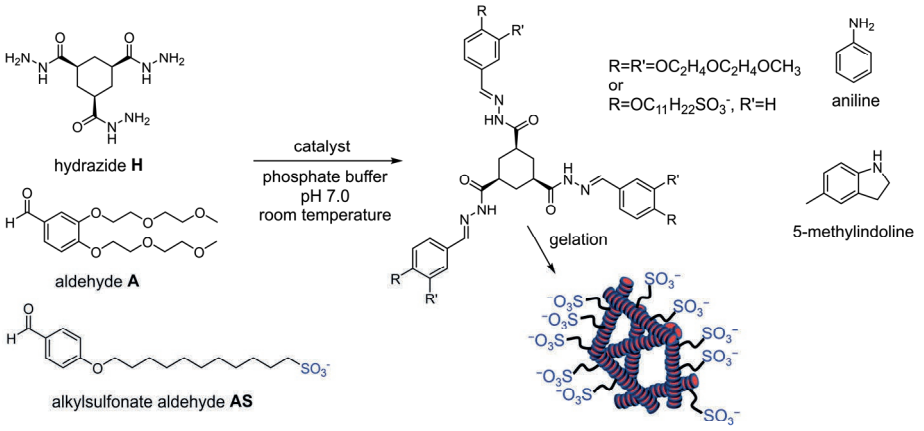

Figure 1. Scheme of catalyzed formation of sulfonate functionalized trishydrazone hydrogelator.

5.2 Results and discussion

Having discovered the superiority of indoline derivatives over aniline as catalysts for hydrazone formation in neutral conditions, we pursued in testing their efficacy in the trishydrazone gel formation. Following the general procedure,[19] hydrazide **H** and aldehyde **A** are mixed together in 1:6 ratio, corresponding to two aldehyde groups per hydrazide. Through inverted tube tests, we found the critical gel concentration (CGC) with [**H**] = 8 mM in 0.1 M phosphate buffer at pH 7.0. Then, we determined the kinetics of gelation *via* inverted tube tests and rheology both with aniline and 5-methylindoline (Figure 2). The gelation time, as determined by the inverted vial method, was within 2 h when 10 mM 5-methylindoline was used as catalyst against the 4 h required with the same concentration of aniline (Gelation 4.1 in Table S1). In contrast, the uncatalyzed sample remained a liquid suspension even after 7 h. Rheological measurements showed that 5-methylindoline catalyzed gelation gives a constant G' of 6 kPa, 50 min after starting the reaction. Aniline catalysis leads to a gel with similar stiffness (G'= 5 kPa), but reaching the G' plateau value after 110

min. These results demonstrate more than 2-fold acceleration of the gelation time and slightly more stable gels for 5-methylindoline catalysis compared to aniline catalysis.

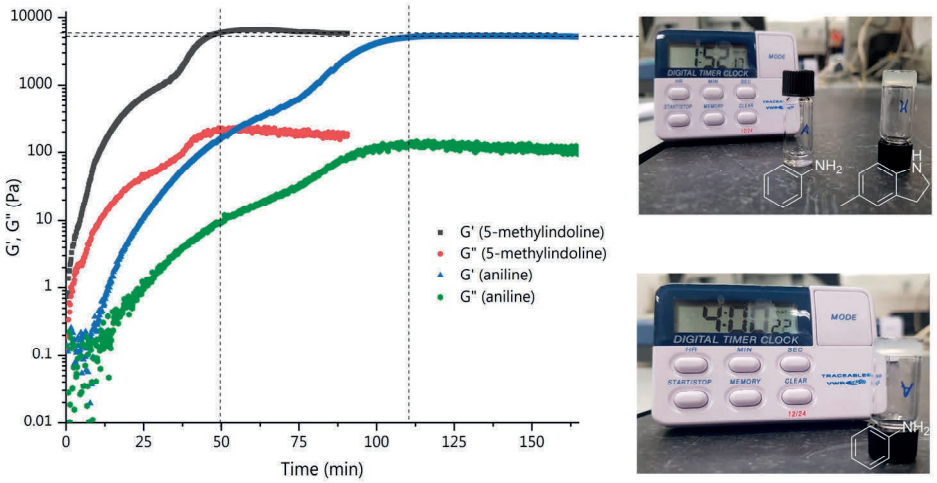

Figure 2. Left: Time-dependent rheology gel formation over time. G' and G'' for aniline-catalyzed gel (blue and green line, respectively) and for 5-methylindoline-catalyzed gel (black and red line, respectively) are plotted. The gelation time (vertical dashed lines) was considered as the moment the G' value measures 95% of the plateau value (horizontal dashed lines). Top-right: Inverted tube test of aniline (left vial) and 5-methylindoline (right vial) catalyzed gel formation in less than 2 h. Bottom- right: Inverted tube test of aniline catalyzed gel formation in 4 h.

Increasing [**H**] to 20 mM and [**A**] to 120 mM, but keeping the catalyst concentration at 10 mM, the gelation time obtained with the vial method was confirmed at 2 h for 5-methylindoline catalysis (Gelation 4.2 in Table S1). Note that in these conditions we used 0.5 eq. of catalyst compared to [**H**], instead of an excess of catalyst as reported in the previous procedure (Gelation 4.1, Table S1). Once we proved the beneficial effect of 5-methylindoline catalysis for the trishydrazone gel formation, we integrated the sulfonated aldehyde **AS** in the gel

composition (Figure 1). The choice of increasing the gel concentration should favor high density of alkylsulfonate chains in the gel fibers. Considering that the maximum concentration of **AS** that allowed reproducible gel formation was below 40 mol% (of the total [**A** + **AS**]), we decided to set 30 mol% of **AS** for our formulation in the indoline catalyzed gel formation. When we used 10 mM 5-methylindoline as catalyst, the mixture of **A** and **AS** with **H** gelled in 1.5 h against the 6 h needed in absence of catalyst (Figure 3, Gelation 4.3 in Table S1). These results show reduced gelation times compared to those obtained in absence of **AS** (Table S1). The influence of **AS** over the kinetic of gel formation could be due to the reduced electron donating effect of the alkyl chain of **AS** compared to the two oligoethylene arms of **A**. In the end, we obtained stable and stiff sulfonated gels using 5-methylindoline catalysis. The slight yellow color of these materials is likely caused by partial oxidation of the indoline catalyst.

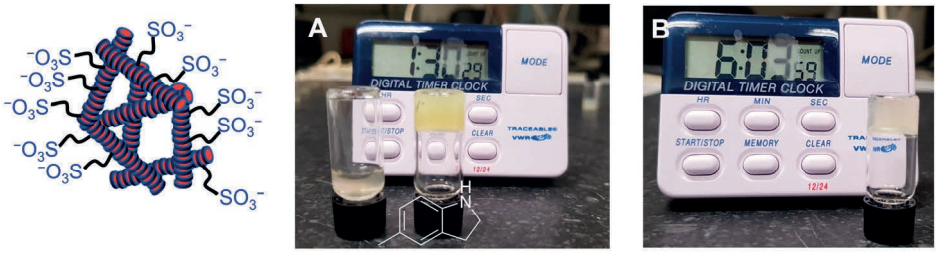

Figure 3. A) Inverted tube test after 1.5 h of uncatalyzed gelation (on the left) and 5-methylindoline catalyzed gelation (on the right); B) Inverted tube test after 6.0 h of uncatalyzed gelation. Conditions: 20 mM acylhydrazide **H**, 120 mM aldehyde **A**, sulfonate aldehyde **AS** (30 mol %), 10 mM 5-methylindoline catalyst in phosphate buffer (100 mM pH=7.0).

5.3 Conclusion

In summary, we have shown that indoline catalysis accelerates trishydrazone hydrogel formation in aqueous neutral environment. The 2-fold decrease in gelation time compared to aniline catalysis represents a step forward to control the formation of these materials. To achieve medical relevance of these hydrogels, we successfully functionalized them with sulfonate groups using 4-hydroxybenzaldehyde bearing a single alkylsulfonate (C11) chain. The gels, obtained in only 1.5 h in presence of 10 mM indoline, were stiff and stable, establishing a potential antiviral platform.

5.4 References

1. T. P. King, S. W. Zhao and T. Lam, *Biochemistry*, 1986, **25**, 5774-5779.
2. E. M. Sletten and C. R. Bertozzi, *Angew. Chem. Int. Ed.*, 2009, **48**, 6974-6998.
3. A. Dirksen and P. E. Dawson, *Bioconjugate Chem.*, 2008, **19**, 2543-2548.
4. J. F. Folmer-Andersen and J.-M. Lehn, *J. Am. Chem. Soc.*, 2011, **133**, 10966-10973.
5. S. Mukherjee, A. P. Bapat, M. R. Hill and B. S. Sumerlin, *Polym. Chem.*, 2014, **5**, 6923-6931.
6. A. Dirksen, S. Dirksen, T. M. Hackeng and P. E. Dawson, *J. Am. Chem. Soc.*, 2006, **128**, 15602-15603.
7. V. T. Bhat, A. M. Caniard, T. Luksch, R. Brenk, D. J. Campopiano and M. F. Greaney, *Nat. Chem.*, 2010, **2**, 490-497.
8. T. Ono, S. Fujii, T. Nobori and J.-M. Lehn, *Chem. Commun.*, 2007, 4360-4362.
9. A. Ryabchun, Q. Li, F. Lancia, I. Aprahamian and N. Katsonis, *J. Am. Chem. Soc.*, 2019, **141**, 1196-1200.
10. J. Boekhoven, J. M. Poolman, C. Maity, F. Li, L. van der Mee, C. B. Minkenberg, E. Mendes, J. H. van Esch and R. Eelkema, *Nat. Chem.*, 2013, **5**, 433-437.
11. S. Ulrich, *Acc. Chem. Res.*, 2019, **52**, 510-519.
12. E. H. Cordes and W. P. Jencks, *J. Am. Chem. Soc.*, 1962, **84**, 826-831.
13. D. K. Kölmel and E. T. Kool, *Chem. Rev.*, 2017, **117**, 10358-10376.
14. C. Godoy-Alcántar, A. K. Yatsimirsky and J. M. Lehn, *J. Phys. Org. Chem.*, 2005, **18**, 979-985.
15. P. Crisalli and E. T. Kool, *J. Org. Chem.*, 2013, **78**, 1184-1189.

16. D. Larsen, M. Pittelkow, S. Karmakar and E. T. Kool, *Org. Lett.*, 2015, **17**, 274-277.

17. W. P. Jencks, *J. Am. Chem. Soc.*, 1959, **81**, 475-481.

18. L. H. Yuen, N. S. Saxena, H. S. Park, K. Weinberg and E. T. Kool, *ACS Chem. Biol.*, 2016, **11**, 2312-2319.

19. J. M. Poolman, J. Boekhoven, A. Besselink, A. G. L. Olive, J. H. van Esch and R. Eelkema, *Nat. Protoc.*, 2014, **9**, 977-988.

20. M. Lovrak, W. E. Hendriksen, M. T. Kreutzer, V. van Steijn, R. Eelkema and J. H. van Esch, *Soft Matter*, 2019, **15**, 4276-4283.

21. C. Maity, W. E. Hendriksen, J. H. van Esch and R. Eelkema, *Angew. Chem. Int. Ed.*, 2015, **54**, 998-1001.

22. F. Trausel, F. Versluis, C. Maity, J. M. Poolman, M. Lovrak, J. H. van Esch and R. Eelkema, *Acc. Chem. Res.*, 2016, **49**, 1440-1447.

23. V. Cagno, P. Andreozzi, M. D'Alicarnasso, P. Jacob Silva, M. Mueller, M. Galloux, R. Le Goffic, S. T. Jones, M. Vallino, J. Hodek, J. Weber, S. Sen, E.-R. Janeček, A. Bekdemir, B. Sanavio, C. Martinelli, M. Donalisio, M.-A. Rameix Welti, J.-F. Eleouet, Y. Han, L. Kaiser, L. Vukovic, C. Tapparel, P. Král, S. Krol, D. Lembo and F. Stellacci, *Nat. Mater.*, 2018, **17**, 195-203.

24. S. T. Jones, V. Cagno, M. Janeček, D. Ortiz, N. Gasilova, J. Piret, M. Gasbarri, D. A. Constant, Y. Han, L. Vuković, P. Král, L. Kaiser, S. Huang, S. Constant, K. Kirkegaard, G. Boivin, F. Stellacci and C. Tapparel, *Sci. Adv.*, **6**, eaax9318.

25. A. R. Bastian, Kantharaju, K. McFadden, C. Duffy, S. Rajagopal, M. R. Contarino, E. Papazoglou and I. Chaiken, *ChemMedChem*, 2011, **6**, 1335-1339.

26. J. J. Broglie, B. Alston, C. Yang, L. Ma, A. F. Adcock, W. Chen and L. Yang, *PLoS One*, 2015, **10**, e0141050.

27. R. Lipowsky and H. G. Döbereiner, *EPL*, 1998, **43**, 219-225.

28. A. Chaudhuri, G. Battaglia and R. Golestanian, *Phys. Biol.*, 2011, **8**, 046002.

5.5 Supporting Information

5.5.1 Materials

All Commercial reagents were used without further purification unless otherwise specified. ^{1}H NMR and ^{13}C NMR spectra were recorded on Bruker NMR instrument or an Agilent-400 MR DD2 (400 MHz and 100.5 MHz for ^{1}H and ^{13}C, respectively) spectrometer at 298 K. Chemical shifts are reported in ppm relative to the residual solvent peak, the multiplicity is reported as follows: s = singlet, d = doublet, t = triplet, q = quartet, m = multiplet, and J-couplings (*J*) are reported in Hertz (Hz). HPLC-MS analysis was performed on a Shimadzu Liquid Chromatography Mass Spectrometer LCMS-2010, LC-8A pump with a diode array detector SPD-M20. High-resolution mass spectral data was performed on the Thermo Scientific Q Exactive hybrid quadrupole-Orbitrap mass spectrometer. Reactions were monitored by analytical thin-layer chromatography (TLC) on silica gel plates (Merck 60F_{254}) using UV light (254 nm) as the visualizing agent. Flash chromatography was performed on 230-400 mesh silica gel (Sigma Aldrich).

5.5.2 Synthesis

Synthesis of trishydrazide H

Trishydrazide **H** was prepared according to reported literature.[1]

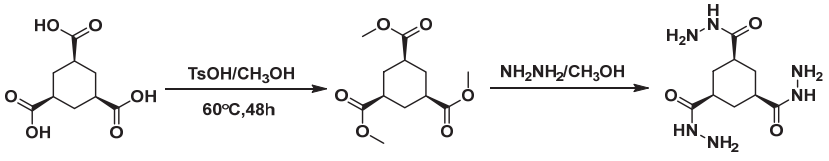

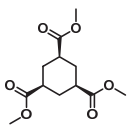

White powder, 88% yield, ^{1}H NMR (400 MHz, $CDCl_3$) δ 3.69 (s, 9H), 2.39 (t, *J* = 12.6 Hz, 3H), 2.28 (d, *J* = 12.5 Hz, 3H), 1.53 (dd, *J* = 24.1, 11.1 Hz, 3H). ^{13}C NMR (101 MHz, $CDCl_3$) δ 174.4, 51.9, 41.74, 30.4.

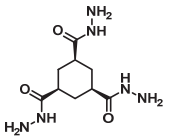

White powder, 99% yield. ^{1}H NMR (400 MHz, DMSO-d_6) δ 8.96 (s, 3H), 4.16 (s, 6H), 2.15 – 2.09 (m, 3H), 1.60 – 1.57 (m, 3H), 1.52 – 1.43 (m, 3H). ^{13}C NMR (101 MHz, DMSO-d_6) δ 173.5, 40.7, 31.3. HRMS (ESI) calcd for $C_9H_{18}N_6O_3Na^+$: 281.13326, found: 281.13266.

Synthesis of aldehyde A

Aldehyde **A** was prepared according to our previous reported literature.[2]

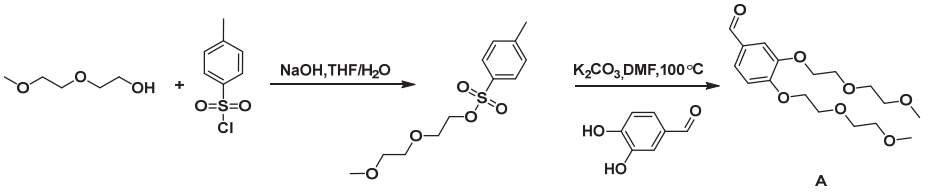

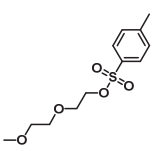

Colourless oil, 88% yield. ^{1}H NMR (400 MHz, $CDCl_3$) δ 7.82 (d, J = 8.3 Hz, 2H), 7.36 (d, J = 8.0 Hz, 2H), 4.20 – 4.18 (m, 2H), 3.72 – 3.70 (m, 2H), 3.61 – 3.59 (m, 2H), 3.51 – 3.49(m, 2H), 3.37 (s, 3H), 2.47(s, 3H). ^{13}C NMR (101 MHz, $CDCl_3$) δ 144.8, 133.0, 129.8, 128.0, 71.8, 70.7, 69.2, 68.7, 59.1, 21.6

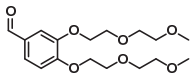

Colourless oil, 97% yield. ^{1}H NMR (400 MHz, $CDCl_3$) δ 9.86 (s, 1H), 7.47 – 7.45 (m, 2H), 7.01 (d, J = 7.9 Hz, 1H), 4.29 – 4.24 (m, 4H), 3.95 – 3.91 (m, 4H), 3.78 – 3.75 (m, 4H), 3.60 – 3.58 (m, 4H), 3.41 (s, 6H). ^{13}C NMR (101 MHz, $CDCl_3$) δ 190.8, 154.3, 149.2, 130.4, 126.7, 112.5, 112.0, 99.9, 72.01, 72.0, 70.9, 70.8, 69.6, 69.4, 68.8, 68.7, 59.1. HRMS (ESI) calcd for $C_{17}H_{26}O_7Na^+$: 365.15707, found: 365.15659.

Synthesis of 4-(11-bromoundecyloxy)benzaldehyde

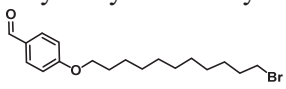

4-hydroxybenzaldehyde (2.00 g, 16.4 mmol) was dissolved in 9.0 mL of dry THF. The solution was cooled at 0°C under stirring and 4.12 g (16.4 mmol) of 11-bromoundecanol was added. The system was placed under nitrogen atmosphere by applying vacuum and filling with nitrogen three times. Triphenylphosphine (4.73 g, 18.0 mmol) was added to the solution under nitrogen atmosphere, and DIAD (3.72 g, 18.4 mmol) was added dropwise. The reaction was stirred at 0° C for the first hour and then slowly allowed to heat to room temperature. The reaction was monitored by TLC and, after four hours, the mixture was concentrated under reduced pressure. The resulting residue was dissolved in ethyl acetate, washed first with a saturated solution of $NaHCO_3$ and successively with brine. The combined organic layers were dried over Na_2SO_4 and the solvent was removed through rotatory evaporation. The crude product was further purified by flash chromatography over silica gel (petroleum ether/ethyl acetate 8:2) to yield 45% of the final product (2.66 g, 7.49 mmol) as a yellow crystalline solid. ^{1}H-NMR, ^{13}C-NMR and MS data aligns with those reported in literature.[3]

Synthesis of 11-(4-formylphenoxy)undecane-1-sulfonate (AS)

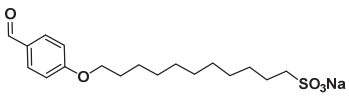

To a three-neck 50 mL round-bottom flask 4-(11-bromoundecyloxy)benzaldehyde (500 mg, 1.41 mmol), sodium sulfite (355 mg, 2.82 mmol), benzyltriethyl-ammonium bromide (19.3 mg, 0.07 mmol), methanol (4.00 mL) and water (5.10 mL) were added under stirring.[4] The reaction was refluxed overnight. The resulting mixture was extracted with Et_2O and water (2 times) and, the aqueous layer was collected. Once the aqueous solution was cooled at 0°C, white crystals were obtained. The remaining water was freeze dried. The product was recrystallized by re-dissolving the dry crystals in Milli-

Q water under heating and sonification and letting the solution slowly cool down at room temperature, leading to crystallization. The mixture was centrifuged for 45 minutes and the supernatant was carefully removed. The obtained crystals were dried again with the freeze dryer to obtain 158 mg (32%) of the pure product. ^{1}H NMR (400 MHz, DMSO-d_6) δ 9.85 (s, 1H), 7.84 (d, J = 8.22 Hz, 2H), 7.10 (d, J = 8.26 Hz, 2H), 4.06 (t, J = 6.54 Hz, 2H), 2.45 – 2.35 (m, 2H), 1.65 – 1.79 (m, 2H), 1.61 – 1.49 (m, 2H), 1.46 – 1.19 (m, 14H). ^{13}C NMR (101 MHz, DMSO-d_6) δ 191.3, 163.7, 131.8, 129.5, 114.9, 68.0, 51.5, 29.0, 29.0, 28.9, 28.7, 28.5, 28.4, 25.5, 25.4, 25.1. LRMS (ESI) calcd 355.16 [M-H$^+$], found: 355.25. HRMS (ESI) calcd 355.1585 [M-H$^+$], found: 355.1510.

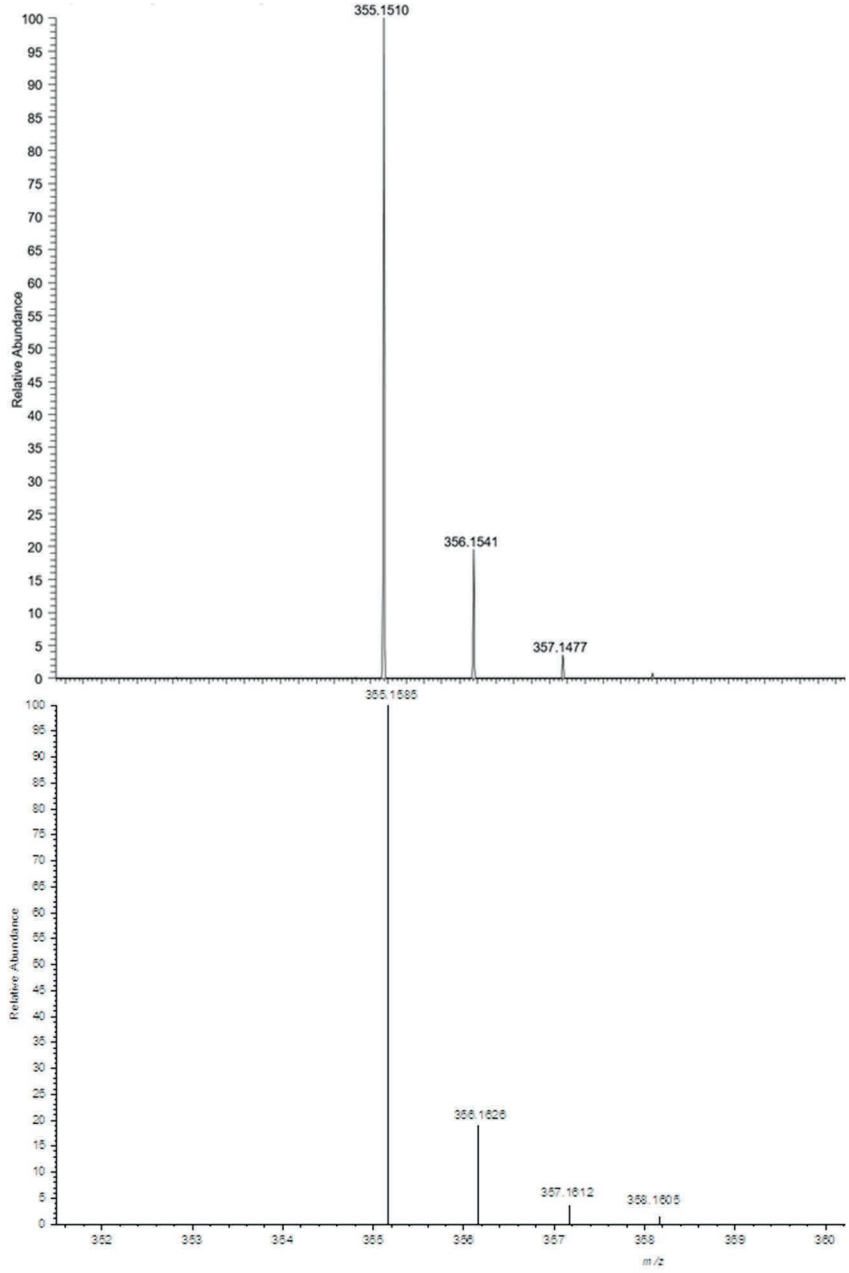

HRMS of compound alkylsulfonate benzaldehyde **AS** (top) and calculated isotopic pattern (bottom).

5.5.3 Rheology of trishydrazone hydrogelator formation

Oscillatory experiments were performed using a rheometer AR G2 from TA Instruments in a strain-controlled mode. The rheometer was equipped with a steel plate-and plate geometry of diameter 40 mm and a water trap. The temperature of the plates was controlled at 25 ± 0.2 °C. All the stock solutions were prepared in phosphate buffer 100 mM pH = 7.0. The total volume for each gelation experiment was 0.6 mL, adding 60 µL of the phosphate buffer, 120 µL of a 240 mM stock solution of the aldehyde **A**, 120 µL of a 40 mM stock solution of the acylhydrazide **H** and 300 µL of a 20 mM stock solution of the catalyst (aniline or 5-methylindoline). Thus each solution contains 8 mM acylhydrazide **H**, 48 mM aldehyde **A**, 10 mM catalyst. For uncatalyzed gels 300 µL of phosphate buffer was added instead of the catalyst stock solution. After stirring the vial by vortexing for 3 s, the gel was pipetted on the bottom plate of the rheometer and the upper plate was slowly rotated to equally spread the gel. The storage and loss moduli G' and G" were followed over time with the rheometer during the formation of the gel, setting up the instrument with a frequency of 1.0 Hz and under 0.1% strain. The measurements were stopped when no further increase of G' was observed. A frequency sweep was measured in the range 0.01-100 rad/s, confirming that the moduli are constant in the frequency range chosen and the strain sweep revealed that the applied strain percentage is in the linear strain regime.[2]

5.5.4 Inverted tube tests of catalytic hydrogelator formation

Inverted tube tests of catalytic trishydrazone hydrogelator formation (Gelation 5.1)

All the stock solutions were prepared in sodium phosphate buffer 100 mM pH = 7.0. The total volume for each gelation experiment was 0.2 mL in a 1.5 mL vial, adding 20 µL of the phosphate buffer, 40 µL of a 240 mM stock solution of the aldehyde **A**, 40 µL of a 40mM stock solution of the acylhydrazide **H** and 100 µL

of a 20 mM stock solution of the catalyst. Thus, each solution was containing 8 mM acylhydrazide **H**, 48 mM aldehyde **A**, 10 mM catalyst. For uncatalyzed gels 100 µL of phosphate buffer was added instead the catalyst stock solution. Each vial was stirred by vortexing for 3 seconds, capped, placed on a stable surface and left undisturbed for the selected time. The gelation of the uncatalyzed, aniline-catalyzed and 5-methylindoline-catalyzed sample was run in parallel, and the three vials were turned upsidedown simultaneously to evaluate the formation of the gel.

Inverted tube tests of catalytic trishydrazone hydrogelator formation (Gelation 5.2)

The 5-methylindoline catalyzed and the uncatalyzed gelation were carried in parallel in 1.5 mL vials. All the stock solutions were prepared in sodium phosphate buffer 100 mM pH = 7.0. To each vial 125 µL of a 480 mM stock solution of aldehyde **A**, 167 µL of a 60 mM stock solution of the acylhydrazide **H**, 208 µL of 24 mM stock solution of 5-methylindoline were added. Thus, 0.5 mL solution containing 20 mM acylhydrazide **H**, 120 mM aldehyde **A**, 10 mM catalyst was obtained. For uncatalyzed gels 208 µL of sodium phosphate buffer (100 mM pH = 7.0) was added instead the catalyst stock solution. The vials were capped, shaken by vortexing for 3 s, placed on a stable surface and left undisturbed for the selected time.

Inverted tube tests of catalytic trishydrazone hydrogelator formation with sulfonate aldehyde AS in phosphate buffer (Gelation 5.3)

The 5-methylindoline catalyzed and the uncatalyzed gelation were carried in parallel in 1.5 mL vials. All the stock solutions were prepared in sodium phosphate buffer 100 mM pH = 7.0. To each vial 125 µL of a 480 mM stock solution of aldehyde (aldehyde **A** with 30 mol % sulfonate-aldehyde **AS**), 167 µL of a 60 mM stock solution of the acylhydrazide **H**, 208 µL of 24 mM stock

solution of 5-methylindoline were added. Thus, 0.5 mL solution containing 20 mM acylhydrazide **H**, 120 mM aldehyde (aldehyde **A,** 30 mol % sulfonate-aldehyde **AS**), 10 mM catalyst was obtained. For uncatalyzed gels 208 µL of sodium phosphate buffer (100 mM pH = 7.0) was added instead the catalyst stock solution. The vials were capped, shaken by vortexing for 3 s, placed on a stable surface and left undisturbed for the selected time.

Table S1. Overview of the times for the trishydrazone hydrogelator formation with different compositions, concentrations and catalysts.

	Time for 5-methylindoline-catalyzed gelation (h)	**Time for aniline-catalyzed gelation (h)**	**Time for uncatalyzed gelation (h)**
Gelation 5.1	2.0	4.0	>8.0
Gelation 5.2	2.0	3.0	8.0
Gelation 5.3	1.5	-	6.0

5.5.5 Supplementary references

1. J. Boekhoven, J. M. Poolman, C. Maity, F. Li, L. van der Mee, C. B. Minkenberg, E. Mendes, J. H. van Esch and R. Eelkema, *Nat. Chem.*, 2013, **5**, 433-437.

2. J. M. Poolman, J. Boekhoven, A. Besselink, A. G. L. Olive, J. H. van Esch and R. Eelkema, *Nat. Protoc.*, 2014, **9**, 977-988.

3. D. A. Leigh and A. R. Thomson, *Tetrahedron*, 2008, **64**, 8411-8416.

4. O. Uzun, Y. Hu, A. Verma, S. Chen, A. Centrone and F. Stellacci, *Chem. Commun.*, 2008, 196-198.

5.5.6 Spectra overview

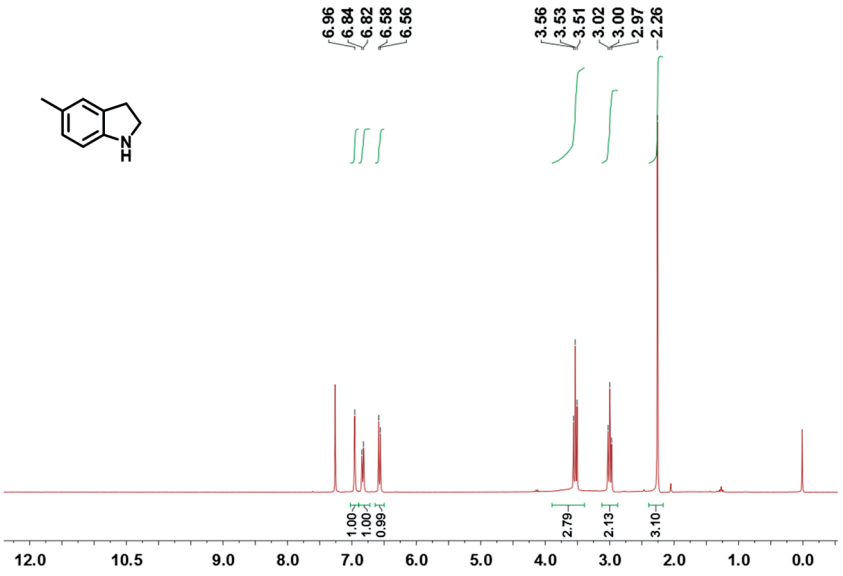

^{1}H NMR spectrum (300 MHz) of 5-methylindoline in $CDCl_3$.

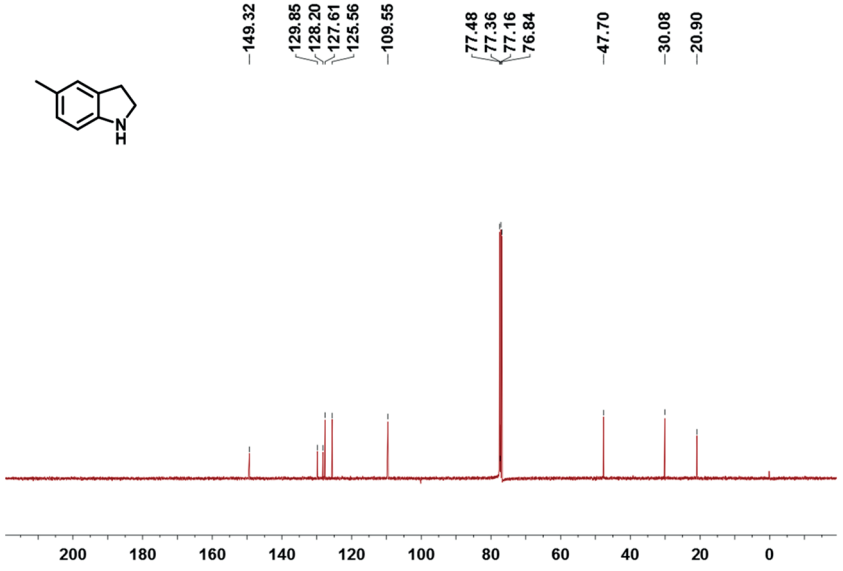

^{13}C NMR spectrum (75 MHz) of 5-methylindoline in $CDCl_3$.

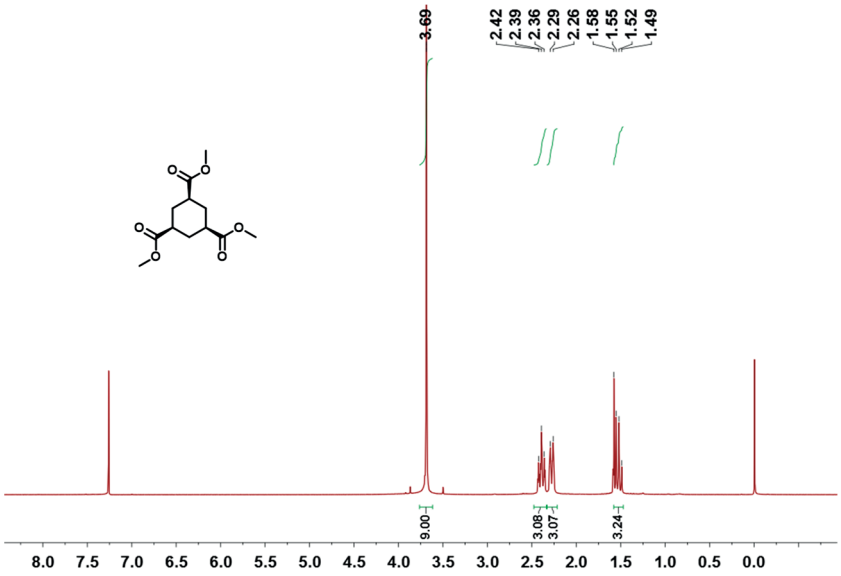

^{1}H NMR spectrum (400 MHz) of trimethyl-cyclohexane-1,3,5-tricarboxylate in $CDCl_3$.

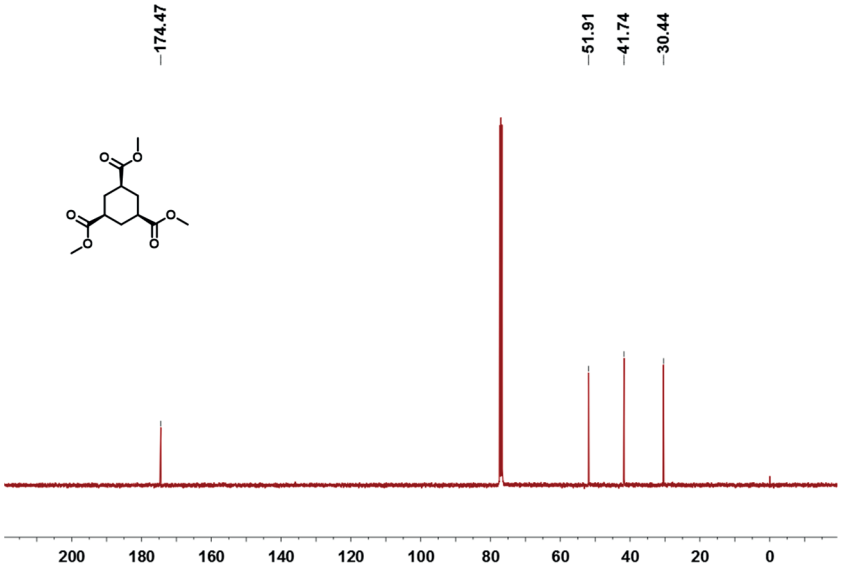

^{13}C NMR spectrum (101 MHz) of trimethyl-cyclohexane-1,3,5-tricarboxylate in $CDCl_3$.

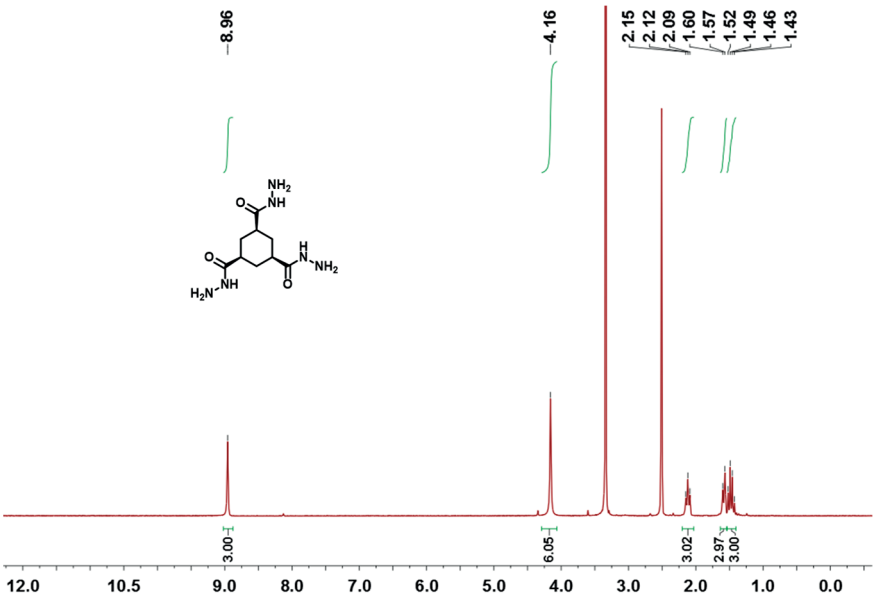

^{1}H NMR spectrum (400 MHz) of trishydrazide **H** in DMSO-d_6.

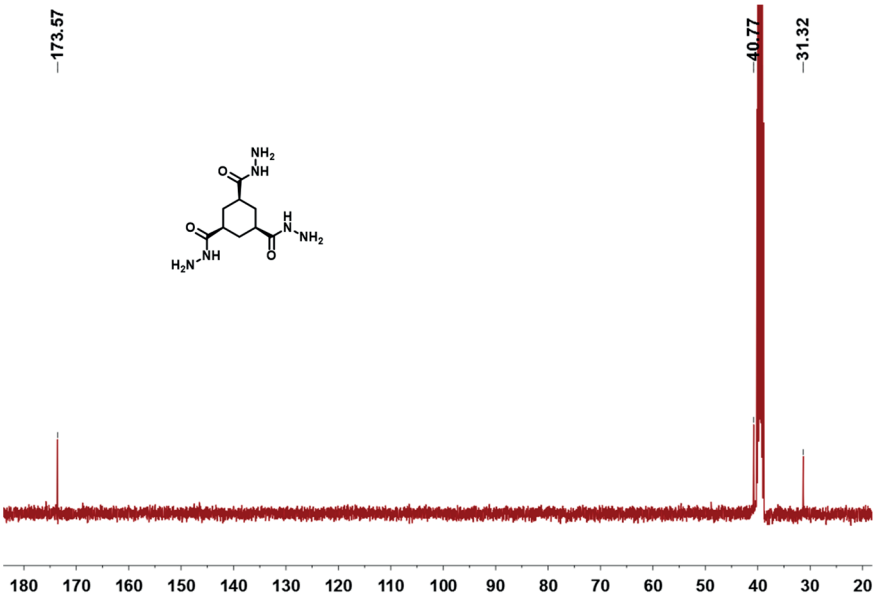

^{13}C NMR spectrum (101 MHz) of trishydrazide **H** in DMSO-d_6.

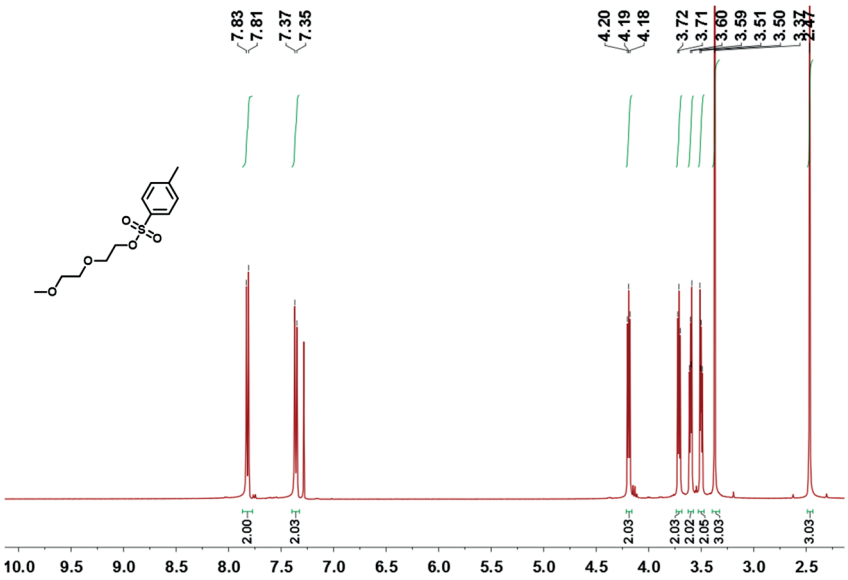

^{1}H NMR spectrum (400 MHz) of 2-(2-methoxyethoxy)ethyl 4-methylbenzenesulfonate in $CDCl_3$.

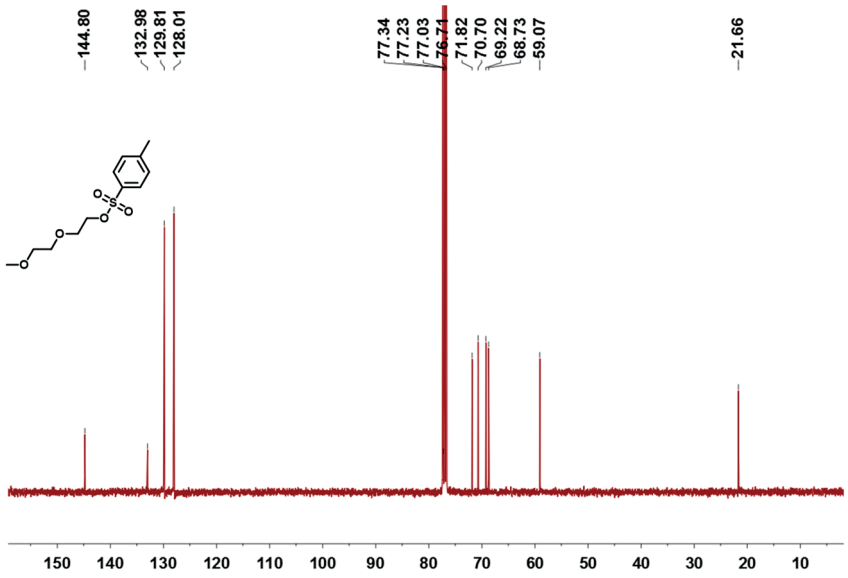

^{13}C NMR spectrum (400 MHz) of 2-(2-methoxyethoxy)ethyl 4-methylbenzenesulfonate in $CDCl_3$.

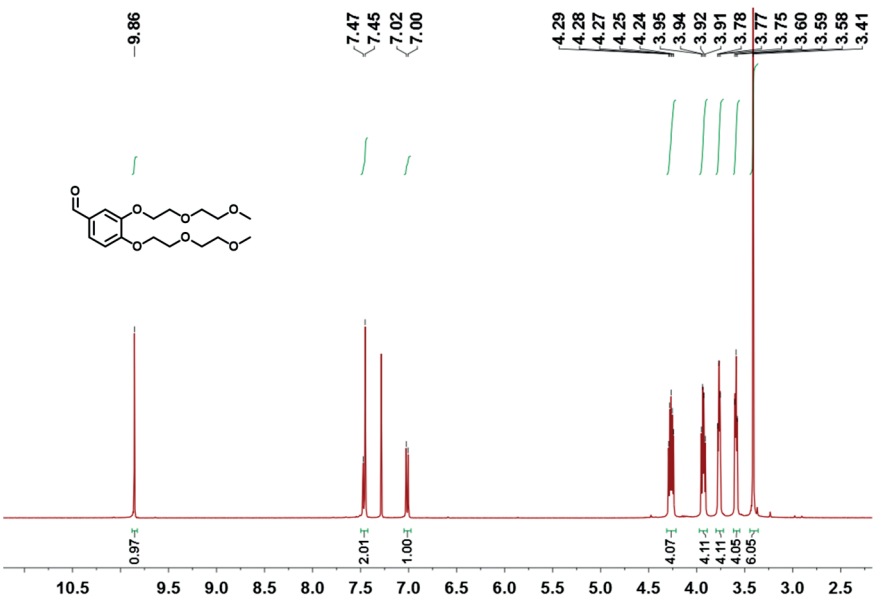

^{1}H NMR spectrum (400 MHz) of aldehyde **A** in $CDCl_3$.

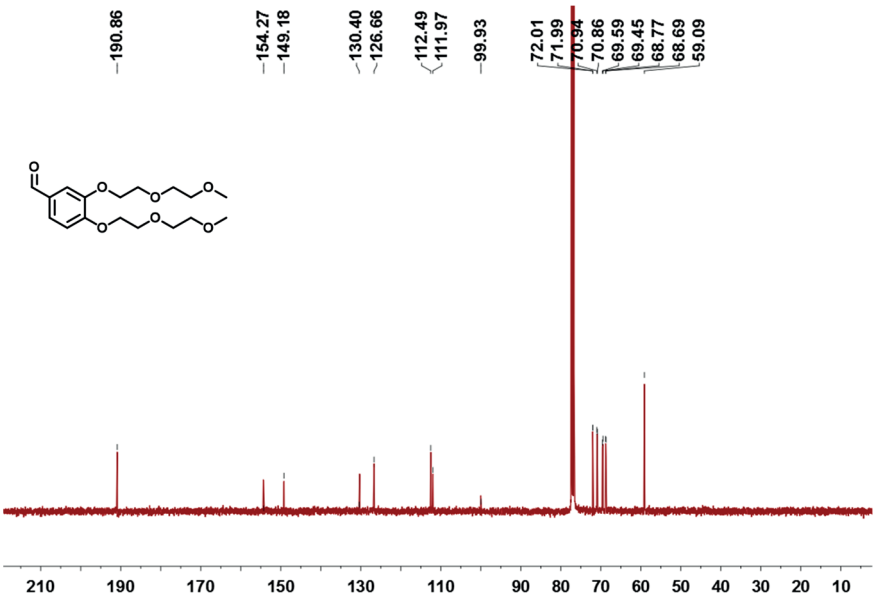

^{13}C NMR spectrum (400 MHz) of aldehyde **A** in $CDCl_3$.

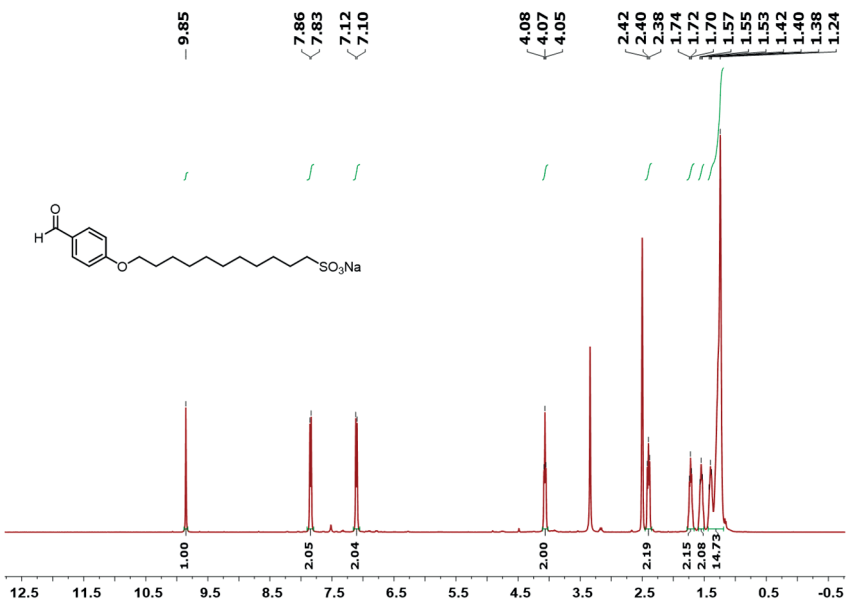

^{1}H NMR spectrum (400 MHz) of compound alkylsulfonate benzaldehyde **AS** in DMSO-d_6.

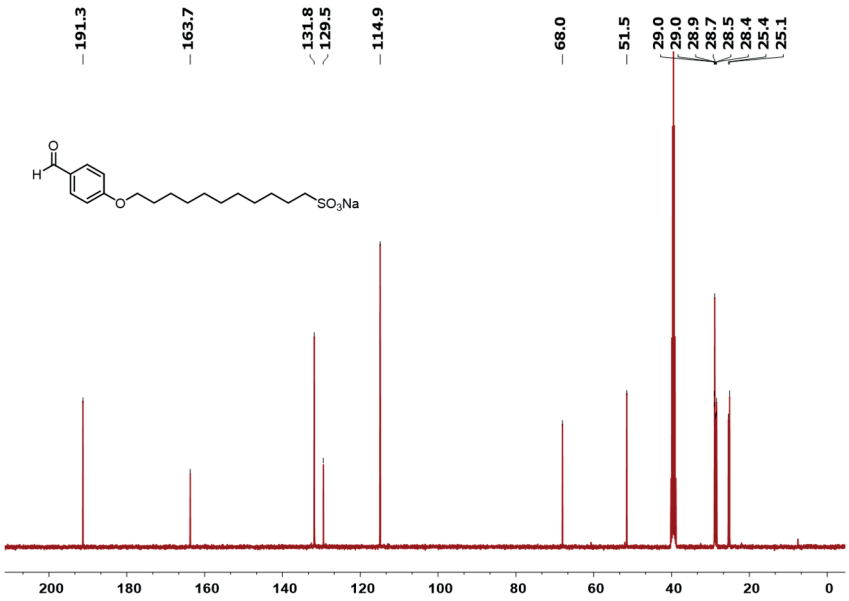

^{13}C NMR spectrum (101 MHz) of compound alkylsulfonate benzaldehyde **AS** in DMSO-d_6.

Chapter 6

Conclusions and Outlook

The main objective of the work described in this thesis is to use catalysis to control material behavior for responsive materials in drug delivery applications.

The thioether phenyl ester (Chapter 2) and carbamate (Chapter 4) functionality are designed to achieve hydrolysis as output only in presence of the oxidative input, establishing an oxidation-triggered cascade process. Installing logic gate mechanisms allows superior control over the performances of responsive materials. In particular, in thioether phenyl ester/carbamate-based materials the hydrolytic response leads to the disruption of the material matrix through molecular degradation. Materials with degradable behavior are widely used in drug delivery systems to obtain sustained and controlled drug release.[1] The easy derivatization of ester, carbamate and possibly carbonate moieties with the thioether phenyl group offers the possibility of implementing it as a linker in several types of ROS-responsive structures, such as cross-linked hydrogels, polymer-drug conjugates and prodrugs.[2-4] Moreover, the application of these systems in biological setting is favoured by the fact that the oxidation and hydrolysis proceed in neutral aqueous solution. Finally, the high cell viability data of the thioether phenyl ester based block copolymers presented in Chapter 2 and the safety data available for 4-(Methylthio)phenol suggest that this class of compounds could be safely used in drug delivery systems.[5]

The use of the organocatalyst reported in Chapter 3 and the peroxizymes presented in Chapter 4 dramatically accelerate the oxidation of the thioether with H_2O_2, achieving near complete material degradation in maximum five days in presence of 1.0 – 2.0 mM of H_2O_2. Considering that most polysulfide based materials require weeks to respond to these concentrations of oxidant,[6, 7] catalytic

strategies can be the key to reduce these timescales. Therefore, the combination of careful design of the material, combined with enzymes or organocatalysts to augment its sensitivity towards the oxidant, would be the ideal approach to achieve materials responsive to biologically relevant concentrations of H_2O_2.[8] Additionally, adaptive materials that depend on a catalyzed reaction could be programmed by simply changing the catalyst concentration.

Because of their frequent use in biotechnology, cytotoxicity data are usually available to establish if an enzyme can be safely used in drug delivery systems, while the toxicity of organocatalysts needs to be evaluated case by case. On the other hand, the versatility and easy modification of organocatalysts would allow to expand the toolbox of catalyzed reactions that can be used to control responsive materials. For example, building from the imine catalyst introduced in Chapter 3, further studies can focus on using different ketones and amines for the *in situ* catalysis of thioether oxidation with H_2O_2. Other organocatalysts, such as oxaziridines, flavins and flavinium salts can be considered to enhance oxidation-responsiveness,[9-11] after establishing that the presence of these organic compounds do not affect cargo encapsulation and stability of the material.

In general, the approach used for the research presented in this thesis is based on translating concepts traditionally belonging to chemistry into materials to realize potential targeted biomedical devices. In this regard, the hydrogels functionalized with alkylsulfonate groups described in Chapter 5 were prepared through the organocatalyzed formation of covalent bonds. These materials can be used for biomedical platforms against viral infections considering the virus-inhibition properties shown by other sulfonated materials.[12] However, performing viral inhibition assays in vitro and in vivo will be necessary to bring these devices towards relevant clinical application.

6.1 References

1. N. Kamaly, B. Yameen, J. Wu and O. C. Farokhzad, *Chem. Rev.*, 2016, **116**, 2602-2663.

2. H. Ye, Y. Zhou, X. Liu, Y. Chen, S. Duan, R. Zhu, Y. Liu and L. Yin, *Biomacromolecules*, 2019, **20**, 2441-2463.

3. M. Jiang, J. Mu, O. Jacobson, Z. Wang, L. He, F. Zhang, W. Yang, Q. Lin, Z. Zhou, Y. Ma, J. Lin, J. Qu, P. Huang and X. Chen, *ACS Nano*, 2020, **14**, 16875-16886.

4. C. Dong, Q. Zhou, J. Xiang, F. Liu, Z. Zhou and Y. Shen, *J. Controlled Release*, 2020, **321**, 529-539.

5. I. Piergentili, P. R. Bouwmans, L. Reinalda, R. W. Lewis, B. Klemm, H. Liu, R. M. de Kruijff, A. G. Denkova and R. Eelkema, *Polym. Chem.*, 2022, **13**, 2383-2390.

6. C. Zhao, J. Chen, R. Zhong, D. S. Chen, J. Shi and J. Song, *Angew. Chem. Int. Ed.*, 2021, **60**, 9804-9827.

7. K. M. Poole, C. E. Nelson, R. V. Joshi, J. R. Martin, M. K. Gupta, S. C. Haws, T. E. Kavanaugh, M. C. Skala and C. L. Duvall, *Biomaterials*, 2015, **41**, 166-175.

8. B. L. Allen, J. D. Johnson and J. P. Walker, *ACS Nano*, 2011, **5**, 5263-5272.

9. K. S. Williamson, D. J. Michaelis and T. P. Yoon, *Chem. Rev.*, 2014, **114**, 8016-8036.

10. A. A. Lindén, L. Krüger and J.-E. Bäckvall, *J. Org. Chem.*, 2003, **68**, 5890-5896.

11. P. Ménová, F. Kafka, H. Dvořáková, S. Gunnoo, M. Šanda and R. Cibulka, *Adv. Synth. Catal.*, 2011, **353**, 865-870.

12. V. Cagno, P. Andreozzi, M. D'Alicarnasso, P. Jacob Silva, M. Mueller, M. Galloux, R. Le Goffic, S. T. Jones, M. Vallino, J. Hodek, J. Weber, S. Sen, E.-R. Janeček, A. Bekdemir, B. Sanavio, C. Martinelli, M. Donalisio, M.-A. Rameix Welti, J.-F. Eleouet, Y. Han, L. Kaiser, L. Vukovic, C. Tapparel, P. Král, S. Krol, D. Lembo and F. Stellacci, *Nat. Mater.*, 2018, **17**, 195-203.

Summary

Living cells adapt to changes of their environment through a cascade of chemical reactions regulated by enzymes. Each cellular pathway contains a series of enzymes, which are capable of receiving and translating a specific chemical or physical signal into a biological response. Taking inspiration from nature, enzymatic mechanisms can be integrated or mimicked to install signal-response behavior in artificial materials. These systems undergo physical and mechanical change when a specific stimulus triggers a chemical transformation, which is pre-programmed in the material. This can be particularly interesting to realize drug delivery systems sensitive to signals overproduced by diseased cells, such as reactive oxygen species (ROS). Enzymes and organocatalysts can be implemented in the material matrix to facilitate the reactions integrated in the functional material. Control over the morphological properties of the materials can lead to complex functions, such as actuation, self-healing and targeted cargo release.

Chapter 2 describes an oxidation-sensitive polymer to obtain a targeted drug delivery and release system. Thioether phenyl esters are used to functionalize the hydrophobic block of an amphiphilic block copolymer. In aqueous buffer at pH 7.4, these surfactants form micelles with the ideal size for nanotherapeutics. The oxidation of thioether by H_2O_2, the most common ROS, triggers ester hydrolysis, turning the hydrophobic block into an hydrophilic acrylate anion block. The drastic change in polarity in the polymer causes eventually the disassembly of the micelles. After encapsulation of a fluorescent dye, Nile Red, the nanocarrier can release the cargo exclusively upon addition of H_2O_2. The release profile is dependent on the thioether/oxidant ratio, resulting in a system with a response directly influenced by the signal concentration. This makes these micelles a potential drug delivery system for ROS-responsive controlled and sustained drug release.

In order to enhance the responsiveness of the ROS-triggered micelles from **Chapter 2**, an organocatalyst capable to activate H_2O_2 is introduced in **Chapter 3**. Here, the formation of imines from trifluoroacetophenone and amino acid based catalysts in aqueous media is used to catalyze the disruption of thioether phenyl ester based micelles. With the addition of H_2O_2, the imine produces an activated peroxide to oxidize the thioether, causing then the hydrolysis of the nearby ester. The organocatalysis accelerates disassembly and cargo release of Nile Red-loaded micelles compared to the uncatalyzed micellar solution, even upon continuous addition of sub-millimolar concentrations of H_2O_2 that simulates the production in tissues. This outcome shows that organocatalysis can be a promising tool to increase the sensitivity of responsive materials.

In **Chapter 4**, first, a molecular model with thioether phenyl carbamate shows hydrolytic lability upon oxidation of the thioether moiety, demonstrating logic gate mechanism. Then, the functionalization of diphenylalanine with the thioether phenyl moiety leads to a low molecular weight amphiphilic compound that can form supramolecular gels in both mildly acidic and neutral aqueous solutions. The hydrogels have great stability for hours at 37 °C, while they turn into solution upon addition of H_2O_2 in stoichiometric amount to the thioether units. Two different peroxizymes, *Ci*VCPO for the hydrogel at pH 6.2 and r*Aae*UPO for the one at pH 7.0, are encapsulated in the gel matrix to achieve gel-sol transition with almost 10 times lower amount of oxidant for both formulations. Here, the main cause of gel collapse is the increased solubility of the sulfoxide against the thioether, with a minor contribute by the hydrolysis of the carbamate unit. All in all, enzyme catalysis demonstrates to be a valid strategy to decrease the response threshold of ROS-sensitive supramolecular hydrogels with possible applications in healthcare.

Chapter 5 reports hydrogels decorated with sulfonated fibers, which show potential for virus inhibition applications. Oligoethylene functionalized

benzaldehyde can react with the hydrazide groups of a cyclohexane-derived trishydrazide to obtain a trishydrazone that is able to assemble in water and form hydrogels. Before gelation occurs, adding alkylsulfonate benzaldehyde to the mixture allows its integration in the hydrazone bond of the supramolecular gelator, and therefore the functionalization of the final hydrogel fibers with alkylsulfonate chains. Catalysts, like acids and aniline, promote hydrazone bond formation and they can be used to tune the gelation kinetics, controlling gelation time and gel properties. Here, the use of indoline as catalyst forms the acylhydrazone two times faster than aniline under neutral aqueous conditions, thus achieving rapid formation of stable sulfonated gels. Organocatalysis can be useful to tune the formation and the properties of materials with potential antiviral effect, as well as to realize healthcare platforms with different medical purposes.

To conclude, in **Chapter 6** possible future developments of the systems investigated in the research presented in this thesis are discussed. Follow up studies and several strategies are proposed to bring these materials one step closer towards clinically relevant applications.

Samenvatting

Levende cellen kunnen zich aanpassen aan veranderingen in hun omgeving via een cascade van chemische reacties die worden gereguleerd door enzymen. Elke cellulaire route bevat een reeks van enzymen die in staat zijn een specifiek chemisch of fysisch signaal te ontvangen en om te zetten in een biologische reactie. Geïnspireerd door de natuur kunnen enzymatische mechanismen worden geïntegreerd of nagebootst om signaalresponsgedrag in kunstmatige materialen te installeren. Deze systemen ondergaan fysieke en mechanische veranderingen wanneer een specifieke stimulus een chemische transformatie teweegbrengt, die voorgeprogrammeerd is in het materiaal. Dit kan met name interessant zijn om systemen voor medicijnafgifte te realiseren die gevoelig zijn voor signalen die overmatig worden geproduceerd door zieke cellen, zoals reactieve zuurstofspecies (ROS). Enzymen en organokatalysatoren kunnen in de materiaalmatrix worden geïmplementeerd om de in het functionele materiaal geïntegreerde reacties te vergemakkelijken. Controle over de morfologische eigenschappen van de materialen kan leiden tot complexe functies, zoals beweging, zelfherstel en gerichte ladingafgifte.

Hoofdstuk 2 beschrijft een oxidatiegevoelig polymeer om een gericht medicijnafgiftesysteem te verkrijgen. Thioetherfenylesters worden gebruikt om het hydrofobe blok van een amfifiel blokcopolymeer te functionaliseren. In waterige buffer bij pH 7.4 vormen deze oppervlakteactieve stoffen micellen met de ideale grootte voor nanotherapeutica. De oxidatie van thioether door H_2O_2, de meest voorkomende ROS, veroorzaakt esterhydrolyse, waardoor het hydrofobe blok verandert in een hydrofiel acrylaatanionblok. De drastische verandering in polariteit in het polymeer veroorzaakt uiteindelijk het uiteenvallen van de micellen. Na inkapseling van een fluorescerende kleurstof, Nile Red, kan de nanodrager de lading uitsluitend vrijgeven door toevoeging van H_2O_2. Het afgifteprofiel is afhankelijk van de verhouding thioether/oxidant, wat resulteert

in een systeem met een respons die direct wordt beïnvloed door de signaalconcentratie. Dit maakt deze micellen tot een potentieel medicijnafgiftesysteem voor ROS-responsieve gecontroleerde en langdurige medicijnafgifte.

Om de responsiviteit van de ROS-getriggerde micellen uit **Hoofdstuk 2** te verbeteren, wordt in **Hoofdstuk 3** een organokatalysator geïntroduceerd die H_2O_2 kan activeren. Hier wordt de vorming van imines uit trifluoracetofenon en op aminozuren gebaseerde katalysatoren in waterige media gebruikt om de verstoring te katalyseren van op thioetherfenylester gebaseerde micellen. Met de toevoeging van H_2O_2 produceert het imine een geactiveerd peroxide om de thioether te oxideren, waardoor de nabijgelegen ester wordt gehydrolyseerd. De organokatalyse versnelt de demontage en ladingafgifte van Nile Red-geladen micellen in vergelijking met de niet-gekatalyseerde micellaire oplossing, zelfs bij continue toevoeging van submillimolaire concentraties van H_2O_2 die de productie in weefsels nabootst. Deze uitkomst laat zien dat organokatalyse een veelbelovend hulpmiddel kan zijn om de gevoeligheid van responsieve materialen te verhogen.

In **Hoofdstuk 4**, demonstreren we eerst het oxidatie-hydrolysemechanisme, aan de hand van een moleculair model met een thioetherfenylcarbamaatgroep. Vervolgens leidt de functionalisering van di(fenylalanine) met de thioetherfenylgroep tot een amfifiele verbinding met een laag molecuulgewicht die supramoleculaire gels kan vormen in zowel lichtzure als neutrale waterige oplossingen. De hydrogelen hebben een urenlange stabiliteit bij 37 °C, terwijl ze in oplossing gaan na toevoeging van H_2O_2 in een stoichiometrische hoeveelheid ten opzichte van de thioethereenheden. Twee verschillende peroxizymen, *Ci*VCPO voor oxidatie van de hydrogel bij pH 6.2 en r*Aae*UPO voor oxidatie bij pH 7.0, zijn ingekapseld in de gelmatrix om een gel-sol-overgang te bereiken met een bijna 10 keer lagere hoeveelheid oxidatiemiddel voor beide

formuleringen. Hier is de belangrijkste oorzaak voor het uiteenvallen van de gel, de verhoogde oplosbaarheid van het sulfoxide tegen de thioether, met een kleine bijdrage door de hydrolyse van de carbamaateenheid. Al met al blijkt enzymkatalyse een nuttige strategie te zijn om de responsdrempel van ROS-gevoelige supramoleculaire hydrogels te verlagen met mogelijke toepassingen in de gezondheidszorg.

Hoofdstuk 5 rapporteert hydrogelen gedecoreerd met gesulfoneerde groepen, die potentie hebben voor toepassingen voor virusremming. Oligoethyleen-gefunctionaliseerd benzaldehyde kan reageren met de hydrazidegroepen van een van cyclohexaan afgeleid trishydrazide om een trishydrazon te verkrijgen dat in water kan assembleren en hydrogelen kan vormen. Het toevoegen van alkylsulfonaatbenzaldehyde aan het mengsel leidt tot de integratie ervan in de hydrazonbinding van de supramoleculaire gelator, en daardoor de functionalisering van de uiteindelijke hydrogelvezels met alkylsulfonaatketens. Katalysatoren zoals zuren en aniline bevorderen de vorming van hydrazonbindingen en ze kunnen worden gebruikt om de geleringskinetiek af te stemmen, de geleertijd en geleigenschappen te regelen. Hier vormt het gebruik van indoline als katalysator het acylhydrazon twee keer sneller dan aniline onder neutrale waterige omstandigheden, waardoor een snelle vorming van stabiele gesulfoneerde gels wordt bereikt. Organokatalyse kan nuttig zijn om de vorming en de eigenschappen van materialen met een potentieel antiviraal effect af te stemmen, maar ook om zachte materialen met verschillende medische doeleinden te realiseren.

Tot slot worden in **Hoofdstuk 6** mogelijke toekomstige ontwikkelingen van de systemen die in het onderzoek gepresenteerd in dit proefschrift zijn onderzocht, besproken. Vervolgstudies en verschillende strategieën worden voorgesteld om deze materialen een stap dichter bij klinisch relevante toepassingen te brengen.

Acknowledgements

The PhD journey can be quite a roller coaster, balancing your daily life between the joy of the few successful experiments and the frustration of the many failed ones. Finally writing the acknowledgments makes me really reflect on these years, and it makes me realize how much I am glad for all the mistakes and the difficulties, because they, more than the successes, made the person and the professional that I am today. Of course, this personal growth was impacted to varying degrees by the people that accompany me along the way. Most of the work described in this thesis would not have been possible without collaborations, and the final result is the product of much help and support from others.

First, I would like to thank my supervisor and promotor, Rienk. Thank you for the opportunity to do the PhD in your group and to encourage me to supervise a MSc project during my first year on the topic of oxidation-triggered polymers. This objective led to the system that was mainly developed in this thesis. I greatly appreciate all the discussions that we had in these years and for the time you spent in the revisions and in the submission processes of my manuscripts. You were always available if I had questions and very timely in correcting my drafts, I also remember how much supportive you were when I had public talks. Jan, thank you for being my copromotor and for the appreciative comments of my thesis. I am grateful for the group activities, both the scientific discussions and the social gatherings, that you promoted. Frank, thank you for being in my committee and for the collaboration that led to Chapter 4 of this thesis. I am grateful for your advices about my future career. Antonia, I am glad for your guidance in working with micelles and for your warm encouragement. Sanzhong, I learned a lot from you and your group during my visit to Beijing in my first year of PhD. You and your students impressed me with your knowledge in catalysis and organic chemistry, as well as with your warm and generous

hospitality. Many thanks to Prof. Vermonden, Dr. Kieltyka, Prof. van der Veen, Prof. Picken and Prof. Grozema for assessing my thesis and for being part of my committee. Eduardo, Wolter, Marcel and Laura thank you for your suggestions during the ASM meetings. Gabrie, Alina and Valeria, I am thankful for our discussions and your counsel.

Stephen Eustace, thank you for taking care of the NMR and for being always willing to help with it, half of this thesis would not have been possible without it. We had a lot of fun at dinners and the Saturgays that you organized. Lloyd, I appreciated how much time you spent helping me with the semi-preparative HPLC and to make me feel welcome in the BOC labs. Thank you Liliana for the help with the UPLC and for inviting me at your birthday, it was a special evening! Robin, thanks for TEM and cryo-EM images of the micelles. Wiel, I really appreciated your help with the cryo-EM images of the hydrogels. Kristen, thanks for giving me access to the syringe pumps. Duco, thank you for trying to acquire some last minute SEM images for me. Your enthusiasm for your work and for helping others has always impressed me. Georgy, I am glad for your insights on experiments and on the publishing process. It was always fun chatting with you outside and hearing you singing in the corridors. I am very happy that your new position is still allowing you to cheer up the second floor of AS. Ida, our weekend breakfasts were an amazing way to release the pressure of these last two years, your support was truly special to me. Richard, thanks for the nice chats and for the advices on management and on future career perspectives. Veby, thank you for our chats, you were understanding and supportive in the serious talks, but very cheerful and funny in the light ones. Els, you always had a smile on when we met in the corridors and you quickly solved issues with lab access requests and package deliveries for me, thank you. Marcel, it was an honour to have such TV celebrity at our Thursday drinks. Sietse, you were promptly available for last minute questions and a great company during the

drinks (especially after some limoncello). Lars, thank you for taking the TU Delft profile picture that I also used in this thesis and for the many laughs during coffee breaks and afterwork drinks. Alexandra, you started during my last month at ASM, but I appreciated your organization in the lab and your advices on HPLC protocols. Xiaohui, I enjoyed talking about single-crystal XRD with you. Ben Norder, thank you for my first introduction on the rheometer. Tonny, thank you for your suggestions on the DMF disposal. I will always remember you for the chats during lunch and your positive attitude.

Sarah and Suellen thank you for being my paranymphs, which is the culmination of our PhD adventure as "hydrogen peroxide girls". I am very happy that we are here all defending almost at the same time. Suellen, you are so passionate about your work, staying long hours in the evening. Your drive in making better choices for the environment has encouraged me to be more mindful of many of my daily actions too. You were always there when I needed to vent or to confide in someone, thank you for being such a good friend. Sarah, I am impressed by your assertiveness at work and by your enthusiasm on the dancefloor. Thank you very much for all the help with the microscope, all the fun evenings and for being such a protective friend. Reece, thank you very much for unravelling to me the secrets of RAFT polymerization and DLS measurements. You were always willing to help and your methodical approach taught me a lot about lab protocols, but also about coffee making and beer brewing. Tobias, thanks for all the help to get me started in the lab during my first year and for the many BBQs and dinners in the following years. You and Robin are amazing hosts and the events at your place are memorable. Peggy, you gave a me a lot of tips in the lab, and the party is on when you are around. Hendrik, you were very welcoming when I first start in the group and your positivity has always been very contagious. Thank you all for the coffee breaks and for the load of fun that we had outside of work, all of you made this experience truly special.

Thomas, thank you for the peroxizymes and your assistance in their use. Huanhuan and Bing, thanks for performing the cytotoxicity assays for me. Yuntao and Mao, it was great to collaborate with you. Guotai, I am glad for our chats in the lab about work, but especially for the ones about the difficulties to live far away from the family. Bowen, thank you for your encouraging words during my first year. Mark, it was nice to share our interest in supramolecular gel. Susan, thanks for leaving me your fumehood when I started. Michelle, Jennifer and Mariano, thanks for your inputs during our collaboration. Juncheng, you are always smiling, keep this positivity towards the end of your PhD. Ardeshir, you are so cheerful, thank you for our coffee breaks together. Elmira, I will always remember our first trip to Scheveningen. Sahil, it was fun being neighbours at the DUWO accommodation, thanks for your help when I had to move. Anand, I appreciated your assistance with the rheometer. Benni and Anastasiia, we had nice chats in the NMR room. Cansel, Giovanna, Qian, Fanny, Matija, Vasu, Jos, Tomasz, Serhii, Emma, Angie, Kai, Fan, Yu, Nancy, Tamar, Gijs thanks for our time together at the ASM events. I am glad that I got the chance to supervise several students during my PhD, learning something from each of them. Luuk, you were a great student and I really appreciated your work attitude. Pepijn, I really enjoyed working with you, as well as sharing coffee and drinks during the breaks.

To my beloved “fioi”, Edo, Lara, Daniele, Jacopino, Jack, Rochi, Fili, Isa, Giups, Billy, Giulio and Andre, thank you for being my Little Italy in the Netherlands and for all the crazy moments that helped me to release the pressure of the week. Francesca, thanks for our amazing workshop in Tenerife and for our endless talks about PhD and after PhD life. Cate, I admire your strength and positivity, you always knew what to say to cheer me up. Veronica, thank you for being always there for me. Elisa, thank you for listening at my PhD dramas and being so

supportive. Ilaria, your joy has always been contagious, thanks for being so cheerful when we meet.

Finally, I would like to thank my family for their endless support and encouragement. It is not easy to be apart most of the time, but it is comforting to know that whenever I need you, you are a phone call apart. Mamma & Papo, I would have never get to this point of my education without your support. Thanks for teaching me the importance of hard work and commitment. Zia, thank you for listening at my endless PhD stories and for your supportive words. Zio, thank you for being such a reliable person, we can always count on you. Stefano and Linda, you were very encouraging about my choice of living and working abroad. To my grandparents, my great-uncle and my great-aunt, your strong work ethic influenced me deeply, even when you were not among us anymore. Nonna Maria, you were the strongest person that I ever known, I always could feel your love despite the language barrier. Ilaria, you are not only my sister, you are my best friend too. Thanks for keeping continuously in contact with endless WhatsApp chats about our daily lives and our career struggles. I don't think many people can be so close while being so far. Blake, I am very proud that you are getting out of the shell little by little. Thank you for helping mom and dad to get to the Netherlands for my defense. Lele, you are a lot of fun to have around, thanks for bringing many cheerful moments to our family.

Benj, you were my all-time "buddy" in and out the lab, but most importantly you are my main supporter, the one who always believes in me. The last four years would have not been the same without you and your constant help. A lot of the final result of this thesis, I own it to you, from ideas and scientific discussion to graphical designs and motivational speeches. I am extremely grateful for having shared the PhD journey with you and I am excited for what's to come next.

About the author

Irene Piergentili was born on 26th of April, 1993 in Rome, Italy. She obtained her Bachelor Degree in Chemistry at La Sapienza University of Rome in 2015. After graduating, she continued the same year with the Master programme in Organic and Biomolecular Chemistry at La Sapienza University. On March 2016, she won the Erasmus+ scholarship and she spent a semester at Dublin City University in Dublin, Ireland (September 2016-January 2017). She started as a research intern in the group of Prof. Rinaldo Marini Bettolo under the supervision of Dr. Francesca Leonelli in March 2017. During this internship, she carried a research focused on the use of organocatalysis in asymmetric synthesis. She obtained her M.Sc Degree *cum laude* on January 2018 defending the thesis entitled: "Study of the racemization of (+)-(*S*)-5-Methyl-Wieland–Miescher ketone under classical acetalization conditions". She started her PhD in the Advanced Soft Matter (ASM) group at TU Delf in August 2018 under the supervision of Dr. Rienk Eelkema and Prof. dr. Jan H. van Esch. Her research focused on the use of organocatalysis and enzymatic catalysis to control supramolecular materials for potential biomedical applications. Currently she is a postdoctoral researcher on light-responsive materials for eye-sight regeneration devices under the supervision of Jan van Hest at TU Eindhoven.

List of publications

- I. Piergentili, M. Cai, B. Klemm, B. Xu, S. Luo and R. Eelkema, Enhancing trigger sensitivity of nanocarriers through organocatalytic oxidant activation. *Cell Reports Physical Science* **2023**, DOI: 10.1016/j.xcrp.2023.101547.

- I. Piergentili, T. Hilberath, B. Klemm, F. Hollmann and R. Eelkema, Enhancing the ROS sensitivity of a responsive supramolecular hydrogel using peroxizyme catalysis. *Biomacromolecules* **2023**, 24 (7), 3184–3192.

- I. Piergentili, P. R. Bouwmans, L. Reinalda, R. W. Lewis, B. Klemm, H. Liu, R. M. de Kruijff, A. G. Denkova and R. Eelkema, Thioanisole ester based logic gate cascade to control ROS-triggered micellar degradation. *Polymer Chemistry* **2022**, 13, 2383-2390.

- B. Klemm, A. Roshanasan, I. Piergentili and R. Eelkema, Naked-eye thiol analyte detection via self-propagating amplified reaction cycle. *Journal of the American Chemical Society* **2023**, accepted.

- B. Klemm, R. W. Lewis, I. Piergentili and R. Eelkema, Temporally programmed polymer-solvent interactions using a chemical reaction network. *Nature Communications*, **2022**, 13, 6242.

- Y. Zhou, I. Piergentili, J. Hong, M. P. van der Helm, M. Macchione, Y. Li, S. Luo and R. Eelkema, Indoline catalyzed acylhydrazone/oxime condensation under neutral aqueous conditions. *Organic Letters*, **2020**, 22 (15), 6035–6040.

- F. Leonelli, I. Piergentili, G. Lucarelli, L. M. Migneco and R. Marini Bettolo, Unexpected racemization in the course of the acetalization of (+)-(S)-5-Methyl-Wieland–Miescher ketone with 1,2-ethanediol and TsOH under classical experimental conditions. *International Journal of Molecular Sciences*, **2019**, 20 (24), 6